University of Alberta

Synthesis and evaluation of an [^{18}F]-labelled antisense oligonucleotide as an imaging probe to measure cellular response to radiation therapy

by

Ingrid Koslowsky

A thesis submitted to the Faculty of Graduate Studies and Research
in partial fulfillment of the requirements for the degree of

Doctor of Philosophy

in

Pharmaceutical Sciences

Faculty of Pharmacy and Pharmaceutical Sciences

©Ingrid Koslowsky
Fall 2010
Edmonton, Alberta

Examining Committee

John Mercer, Faculty of Medicine
Supervisor

Steve McQuarrie, Faculty of Medicine
Supervisory Committee Member

Mavanur Suresh, Faculty of Pharmacy and Pharmaceutical Sciences
Committee Chair & Examiner

David Murray, Faculty of Medicine
Committee Member

Afsaneh Lavasanifar, Faculty of Pharmacy and Pharmaceutical Sciences
Committee Member

Michael Adam, Faculty of Chemistry, University of British Columbia
External Examiner

dedication

*to my father
Theodore Koslowsky*

*to whom I owe
my strong will to pursue my goals*

*I am proud of who he was
and what he aspired to be*

*I admire him for
his intense sense of integrity*

and his respect for others

Abstract

Antisense oligodeoxynucleotides (asODNs) show strong binding and high selectivity and can be constructed to recognize specific cellular targets such as gene regulated mRNA. Radiolabelled asODNs have the potential to image gene expression through mRNA targeting and could be a valuable tool in the early assessment of outcome to cancer treatment. We have explored the potential of *in vivo* imaging of p21 gene expression, using fluorine-18 labelled asODNs ([^{18}F]asODNs) and *in vitro* techniques, recognizing the relationship between the expression of this gene and resistance of cancer cells to radiation therapy. Radiolabelling of fully phosphorothioated, 20-mer ODNs was performed using the [^{18}F]-labelled prosthetic group, 4-*N*-[^{18}F]fluorobenzyl-2-bromoacetamide ([^{18}F]FBBA). [^{18}F]FBBA was first synthesized in an automated synthesis unit, resulting in a modest radiochemical yield. Methods to improve the yield were investigated using a metal catalyst-assisted borohydride exchange resin. Alkylation of [^{18}F]FBBA to ODN resulted in radiochemical yields of 40%. Cellular uptake and retention studies were performed in human carcinoma cells expressing p21$^{+/+}$ (HCT116) and the p21 knock-out cell line, 80S4, using both [^{18}F]-labelled antisense and random sequence ODNs. Nonradioactive FBBA-labelled ODNs were used to evaluate the antisense effectiveness and distribution of the FBBA-modified ODNs. *In vitro* studies demonstrated that FBBA did not interfere with the antisense effect of ODNs against *p21* mRNA; however, the probes required a transfection agent to observe an antisense effect. Cell fractionation studies with [^{18}F]ODNs revealed increasing accumulation of

liposome-transfected [^{18}F]asODN in the cytoplasm of HCT116 cells over time. A biocompatible spermine-grafted block copolymer (SP) was subsequently evaluated as a potential vector to improve the delivery of [^{18}F]asODN into cells. SP was shown to direct [F]-labelled ODNs to the cytoplasm, whereas naked [F]ODNs remained sequestered in vesicles, and liposome-transfected [F]ODNs localized mostly in the nucleus. Selective uptake and retention of [^{18}F]asODN was observed in p21$^{+/+}$ cells only when the probe was transfected with SP. Based on these studies, it can be concluded that [^{18}F]asODNs have the potential to image gene expression, however the focus may need to be directed to find an appropriate vector which can rapidly deliver [^{18}F]-labelled asODNs to the target tissue *in vivo*.

Acknowledgments

There are many people: professional colleagues, friends, and family, who deserve recognition. All have contributed to my goal of achieving my Doctorate, and I am sincerely thankful for their role in my success. The Faculty of Pharmacy allowed me to pursue my studies under a very flexible schedule, as did Diagnostic Imaging, Calgary, Alberta Health Services. Without the cooperation of both institutions, I would not have been able to achieve my goals. My family, in particular, my spouse Jack Sandford, was very patient and understanding, as I sacrificed my time with him over the past few years. Throughout my tenure as a graduate student Jack was, and remains, a stable foundation in my life and I am indebted to him for his unending love and support. A very big hug goes to my mother who, with her eternal optimism, purchased her dress for my convocation 2 year ago.

I would like to thank Dr. John Mercer, my Ph.D. supervisor and mentor for his guidance through the maze of graduate studies, and always lending an ear (as well as sage advice) throughout my studies. It has given me great pleasure to work under the direction of Dr. Mercer, and I hope that future research collaborations will be the fruit of this professional relationship.

Thank you to the other members of my Faculty of Pharmacy Ph.D. Committee, Dr. Steve McQuarrie and Dr. Mavanur Suresh. They offered advice and ensured that I did not deviate (too far) from my original plans. I am indebted to Joyce Johnson, Graduate Studies Coordinator for the Faculty of Pharmacy, who was instrumental in guiding me through the necessary steps of graduate studies.

I cannot adequately express how grateful I am for the professional and personal friendship that I have developed with Dr. Soraya Shahhosseini and Dr. Elisabeth von Guggenberg. I was very fortunate to find others with whom I could chat, in minute detail, about my research knowing that they fully understood the complexity of the work. The friendship that has developed is dearly cherished by me.

My sincere gratitude goes out to the Edmonton PET Center for providing me with resources to perform my research, as well as the social camaraderie that developed with the staff, post-doctoral fellows, research assistants, and graduate students. In particular, Dr John Wilson was an invaluable source of information, with his wealth of knowledge on cyclotrons and synthesis of $[^{18}F]$-labeled prosthetic groups. And he has such a great laugh!

I would like to thank Dr. Frank Wüst for taking the time to discuss my project with me, along with more philosophical aspects of radiopharmaceutical research. I trust our conversations will continue in the future, as partners in research as well as in friendship.

List of Abbreviations

ODN: oligodeoxynucleotide (oligonucleotide)
asODN: antisense oligonucleotide
rsODN: random sequence oligonucleotide

$[^{18}F]$asODN: $[^{18}F]$fluorine-labelled asODN
$[^{18}F]$FBA: 4-$[^{18}F]$fluorobenzylamine
$[^{18}F]$FBBA: 4-N-$[^{18}F]$fluorobenzyl-2-bromoacetamide
$[^{18}F]$FBN: 4-$[^{18}F]$fluorobenzonitrile
$[^{18}F]$ODN: $[^{18}F]$asODN and/or $[^{18}F]$rsODN
$[^{18}F]$rsODN: $[^{18}F]$fluorine-labelled rsODN
$[^{18}F]$SFB: succinimido 4-$[^{18}F]$fluorobenzoate
[F]asODN: nonradioactive [F]fluorine-labelled asODN
[F]asODN-Q: nonradioactive [F]asODN labelled with the fluorescent dye, Quasar 570
[F]ODN: [F]asODN and/or [F]rsODN
[F]ODN-Q: nonradioactive [F]asODN or [F]rsODN labelled with Quasar 570
[F]rsODN: nonradioactive [F]fluorine-labelled rsODN
[F]rsODN-Q: nonradioactive [F]rsODN labelled with Quasar 570

AOTF: acousto-optical tunable filter
ASU: automated synthesis unit
ATM: ataxia telengiectasia mutant
ATP: adenosine triphosphate
AUC: area under the curve
BER: borohydride exchange resin
CDK: cyclin-dependent kinase
CDKN1A: cyclin-dependent kinase inhibitor 1A
CIP1:   CDK-interacting protein 1
DAPI: 4',6-diamidino-2-phenylindole dihydrochloride
DMEM: Dulbecco's Modified Eagle medium
DMSO: dimethylsulfoxide
DNA: deoxynucleic acid
DO3A: 1,4,7-tris(carboxymethylaza)cyclododecane-10-azaacetyl
DOPE   1,2-dioleoyl-sn-glycero-3-phosphatidylethanolamine
DOTA: 1,4,7,10-tetraazacyclododecane-N,N′,N″,N‴-tetraacetic acid
DOTMA: N-[1-(2,3-dioleyloxy)propyl]-N,N,N-trimethylammonium chloride
DTPA: diethylenetriaminepentaacetic acid
EC: electron capture
EDTA: ethylenediamine tetraacetic acid
EGF: epidermal growth factor
FBA: 4-fluorobenzylamine
FBBA: 4-N-fluorobenzyl-2-bromoacetamide
FBN: 4-fluorobenzonitrile
FBS: fetal bovine serum
FDG: 2-$[^{18}F]$fluorodeoxyglucose
HD: Huntington's Disease
HRP: horse radish peroxidase
HYNIC: hydrazino nicotinamide

IGF:	insulin growth factor
IgG:	immunoglobulin G
K_{222}:	Kryptofix®222 (4,7,13,16,21,24-hexaoxa-1,10-diazabicyclo[8.8.8]hexacosane)
LiAlH$_4$:	lithium aluminum hydride
LNA:	locked nucleic acid
mAb:	monoclonal antibody
MAG3:	mercaptoacetyltriglycine
MFI:	median fluorescence intensity
MORF:	morpholino
mRNA:	messenger ribonucleic acid
NaBH$_4$:	sodium borohydride
NHS:	*N*-hydroxysuccinimide
NMR:	nuclear magnetic resonance
OMe:	2′-*O*-methyl RNA
PBS:	phosphate buffered saline
PCL:	polycaprolactone
PCR:	polymerase chain reaction
PEG:	poly(ethylene glycol)
PEI:	polyethyleneimine
PEO:	polyethylene oxide
PET:	positron emission tomography
PNA:	peptide nucleic acid
PO:	phosphodiester
PS:	phosphorothioate
PVDF:	polyvinylidene difluoride
RCP:	radiochemical purity
RME:	receptor mediated endocytosis
RP-HPLC:	reverse phase high pressure liquid chromatography
SDI1:	senescent cell-derived inhibitor 1
SDS:	sodium dodecylsulfonate
SDS-PAGE:	SDS polyacrylamide gel electrophoresis
siRNA:	small interfering RNA
SP:	poly(ethylene oxide)-poly(ε-caprolactone) spermine
SPECT:	single photon emission computed tomography
TfR:	transferrin receptor
THF:	tetrahydrofuran
TLC:	thin layer chromatography
TP:	tetraethylenepentamine
t_R:	retention time
WAF1:	wild-type p53 activated fragment 1
WGA:	wheat germ agglutinin conjugate

TABLE OF CONTENTS

LIST OF TABLES

LIST OF FIGURES

CHAPTER 1

The Development of Radiolabelled Antisense Oligonucleotides for Imaging Gene Expression

1.1   Introduction

The significant advances in imaging technology, exemplified by positron emission tomography (PET), have enabled the diagnostic imaging community to observe molecular/biochemical processes *in vivo* using noninvasive techniques. Molecular imaging with PET provides a sensitive means to identify, study, and diagnose the biological nature of disease early in and throughout its evolution, as well as providing information for development and assessment of therapies (1,2). Due to its superior sensitivity and resolving power PET imaging offers the potential to quantify biochemical/biomolecular disease processes *in vivo*. As the basis of disease ultimately lies in its genetic profile, imaging altered patterns of gene expression before, during, and/or after treatment with drug or radiation therapy can provide clues to the outcome of treatment well before changes are observed clinically. Central to this approach is messenger ribonucleic acid (mRNA), which is the critical intermediate molecule formed after a gene is activated, or 'expressed', and subsequently encodes a variety of proteins whose interactions in other biochemical pathways eventually manifest as clinical symptoms. Therefore, detection and quantification of mRNA is an important step in monitoring biochemical processes underlying specific diseases. Currently, gene expression profiling can be performed *in vitro* through the use of molecular biology tools which detect alterations in mRNA transcription (Northern blot, *in*

situ hybridization, microarrays, reverse transcriptase polymerase chain reaction) or translation/post-translational modification (Western blot, protein immunochemistry). However *in vitro* techniques require tissue samples, either obtained by biopsy or surgery. A noninvasive method for detecting changes in gene expression *in vivo* would be a welcome diagnostic tool to assist in effective chemo- and/or radiotherapeutic outcomes.

1.2   Oligonucleotides

1.2.1   Structure and Properties

Probes used in molecular biology to detect mRNA include antisense oligonucleotides that bind with high affinity and specificity to the target mRNA. Oligonucleotides (ODNs) are small, linear chains of nucleotides (or nucleobases), each unit consisting of a sugar molecule such as ribose (in RNA) or deoxyribose (in DNA), a phosphate group and one of four different nucleobases: cytosine (C), adenine (A), guanine (G), or thymine (T) (3). For RNA, the thymine is replaced with uracil (U). The backbone of the ODN consists of phosphodiester groups which form bridges between the 3′ and the 5′ carbons of the adjacent sugars conferring a 5′ → 3′ direction to the ODN chain (Figure 1-1).

The nucleobase is attached to carbon 1′ of the sugar. According to the Watson-Crick model, information that is coded by the sequence of nucleobases can be duplicated and read via a hybridization mechanism through the creation of 3 reversible hydrogen bonds between G and C, and 2 bonds between A and T (or U). Therefore two chains can hybridize with one another if their base sequences are complementary, i.e., a G on one chain faces a C on the opposite direction, or

an A faces a T (or U). Hybridization duplexes can be formed between two DNA chains, a DNA and RNA chain, two RNA chains or between oligonucleotides and DNA or RNA. Hybridization is a precise mechanism for the conservation and duplication of genetic information and transfer of this information via the transcription of DNA into messenger RNA (mRNA).
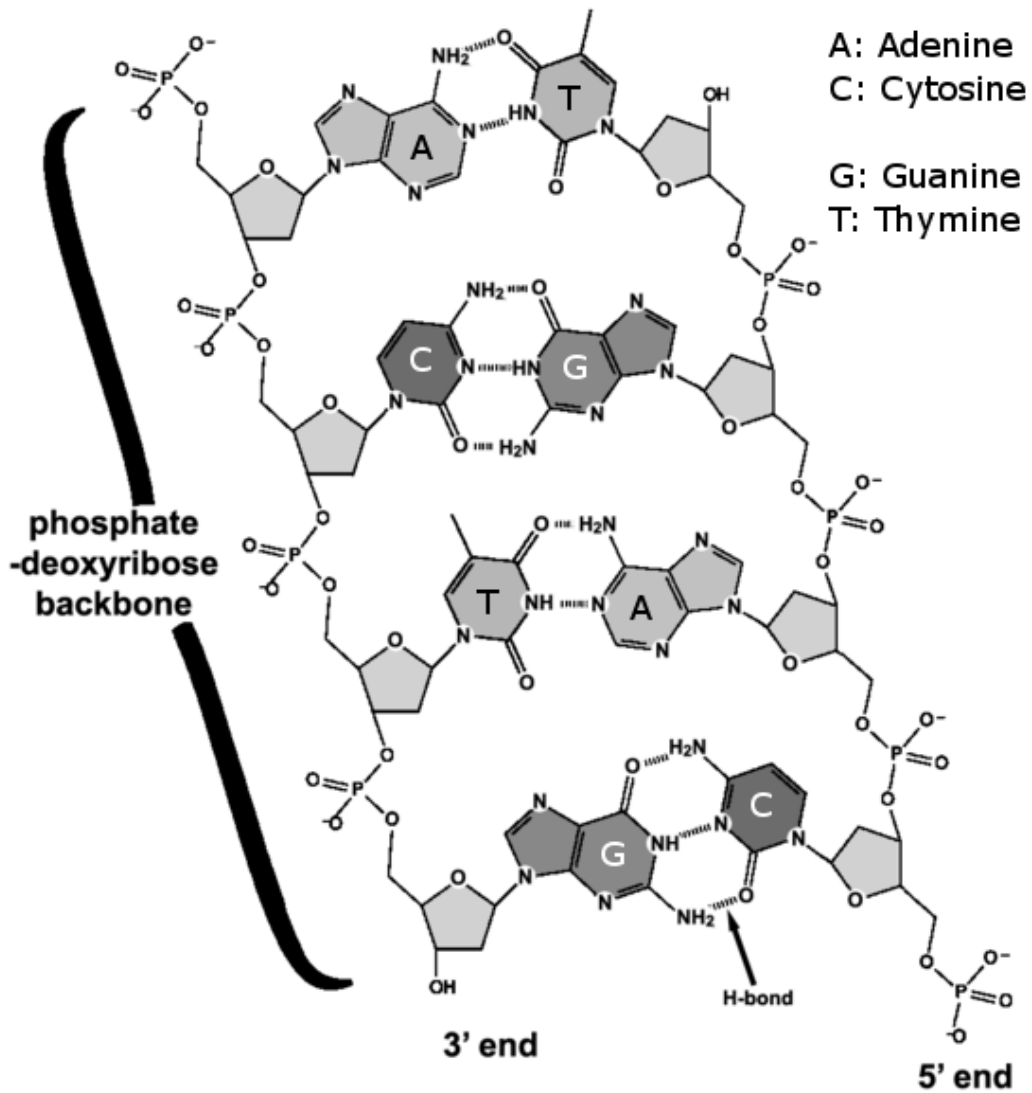
Figure 1-1 Structure of DNA (4)

1.2.2 Antisense oligonucleotides

ODNs that undergo Watson-Crick hybridization to the complementary or 'sense' portion of mRNA are termed 'antisense' oligonucleotides (asODNs). Successful hybridization within a cell leads to the inactivation of the mRNA by steric blockade or by RNase H activation and thus inhibits the translation into protein (Figure 1-2) (3). The minimum length of an asODN necessary to confer specificity to a particular mRNA has been estimated to be 13 nucleobases (13-mer) (5). The usual length of an ODN ranges from 13 to 25 nucleotides. Longer sequences are more difficult to import into the cells due to their size and their tendency to self-hybridize (6).

A variety of antisense probes have been synthesized and studied (6). Ribozymes are RNA molecules capable of cleaving mRNA molecules in a sequence-specific manner and have been studied for therapeutic applications. DNA-zymes are, generally, analogous to ribozymes in their ability to suppress translation of mRNA into protein, but are more biologically stable. Small interfering RNAs (siRNAs) are short, double-stranded RNA segments which become incorporated into RNA-induced silencing complexes and bind to the mRNA of interest. This causes mRNA degradation and leads to specific 'gene silencing'. ODNs have been designed to recognize double-stranded DNA through Hoogsten-base pairing leading to the formation of a triple helix (7). In addition, ODNs have been investigated to modify aberrant expression patterns of alternatively spliced mRNAs, which have been implicated in the development and progression of numerous diseases (8).
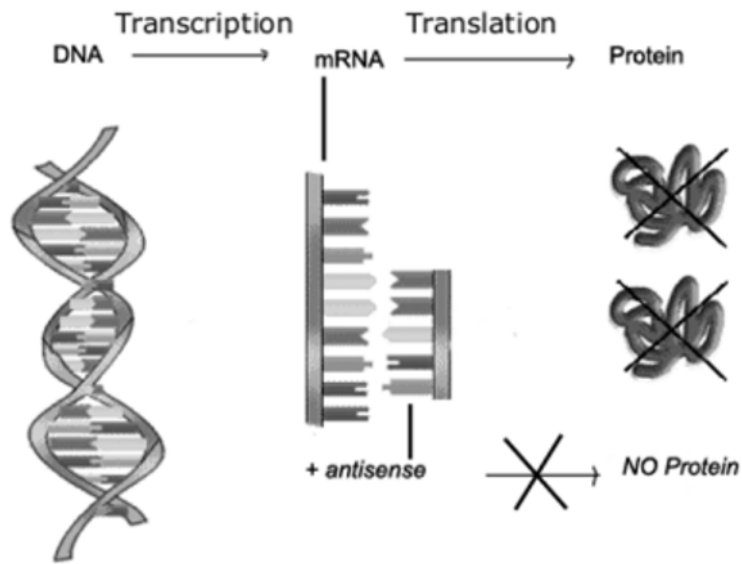
Figure 1-2 Antisense mechanism of oligonucleotides. The antisense oligonucleotide hybridizes with its complementary mRNA thus blocking mRNA translation into protein (3)

1.2.3 Chemical modification of oligonucleotides

The use of 'natural' ODNs, i.e., those ODNs with the phosphodiester-deoxyribose backbone found in native DNA, would be the most desirable molecules for targeting mRNA as they are designed to optimize duplex formation between the antisense molecule and the RNA. Unfortunately, the phosphodiester (PO) linkage is rapidly degraded by exo-and endonucleases in serum, resulting in a plasma half-life of less than 20 minutes (9). In an attempt to decrease the rate and extent of degradation, a large number of ODNs have been synthesized which introduce changes to the sugar-phosphate backbone, or the nucleobases. These modifications have been extensively reviewed in the literature (5,10-13). Examples of ODN modifications are illustrated in Figure 1-3 (13).

1st Generation

Phosphorothioate DNA (PS)

2nd Generation

2'-O-methyl RNA (OMe)   2'-O-methoxy-ethyl RNA (MOE)

3rd Generation

Peptide nucleic acid (PNA)

N3'-P5'-Phosphoroamidate (NP)

2'-fluoro-arabino nucleic acid (FANA)

Locked nucleic acid (LNA)

Morpholino phosphoroamidate (MF)

Cyclohexene nucleic acid (CeNA)

Tricyclo-DNA (tcDNA)
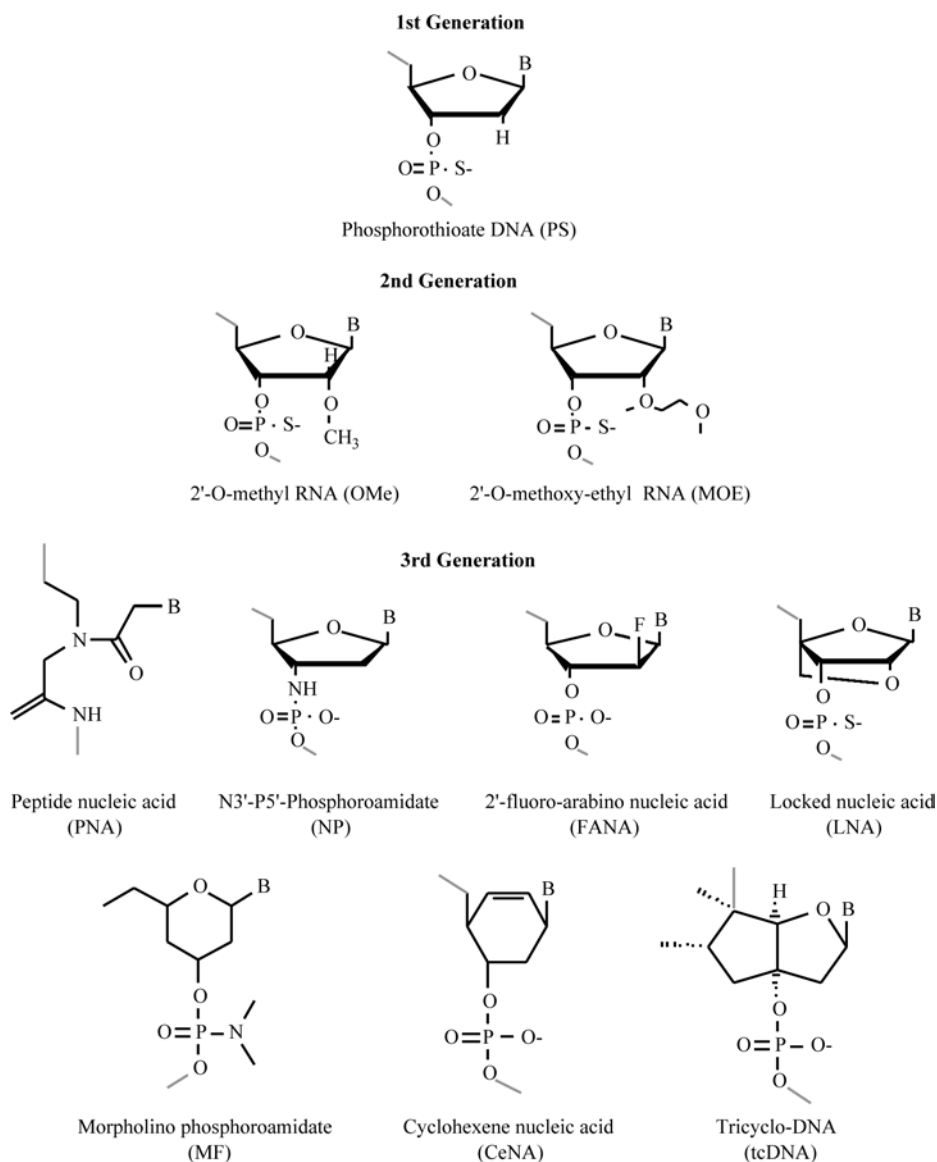
Figure 1-3 Modifications of oligonucleotide analogues. 'B' represents any one of the bases cytosine, adenine, thymine, or guanine (13)

1.2.3.1 Phosphorothioated oligonucleotides: 1st generation oligonucleotides

The most common modification of the native phosphodiester ODN is the replacement of the non-bridging oxygen with a sulfur atom and is referred to as a phosphorothioate (PS) linkage. PS-ODNs are considered 'first generation ODNs' and are the most widely studied asODNs because of their nuclease stability and ease of synthesis (10).

PS-ODNs are anionic complexes: the negative charge can hinder the passage of the ODN through the plasma membrane of the cell due to the electrostatic repulsion from the negatively charged cell surface. However they display a high affinity for certain cell surface proteins, particularly heparin-binding proteins including platelet-derived growth factor, vascular endothelial growth factor, and epidermal growth factor (EGF) receptor which are expressed on the cell surface membrane (14). The negatively charged PS-ODNs also bind to plasma proteins *in vivo* resulting in reduced plasma clearance as observed in pharmacokinetic studies (15). Binding to extracellular plasma proteins could, however, contribute to toxicity, especially if delivered in doses intended to provide a therapeutic effect.

1.2.3.2 Modified oligonucleotides: 2nd and 3rd generation oligonucleotides
The need to improve stability, decrease protein binding, and improve intracellular access of antisense probes has produced second and third generation ODNs (Figure 1-3). Modifications to the ODN typically involve the backbone of the oligonucleotide resulting in anionic internucleoside linkages (e.g. phosphoroamidate), uncharged linkages (e.g. methylphosphonate), and isosteric moieties (e.g. guanidine bridge) (5,13). Synthetic DNA-analogues with modifications in the sugar backbone have also been synthesized, such as 2′-O-methyl (OMe) RNA and locked nucleic acids (LNA). Radical structural changes have resulted in the development of peptide-nucleic acids (PNA) where the entire sugar-phosphate backbone of the DNA is replaced by a 2-aminoethylglycine based polyamide structure. Morpholine can also replace the backbone resulting in

7

the chiral 'morpholinos' (MORF) (5,13). These alterations significantly impact the pharmacokinetics and stability of the ODN. For example, the neutrally charged ODNs, such as PNAs and MORFs, exhibit lower protein binding, faster plasma clearance and higher renal elimination, as opposed to that observed with PS-ODNs, which demonstrate both renal and hepatic clearance. However cellular accumulation remains low with neutrally charged ODNs and they demonstrate less ability to cross the plasma membrane than PS-ODNs (16).

1.3   Radiolabelled probes developed for antisense imaging

Molecular imaging using PET or single photon emission computed tomography (SPECT) requires additional modifications to the ODN to link the radionuclide in such a manner that the radiolabelled ODN retains its antisense activity and remains stable *in vivo*. An abundant array of radiolabelled ODNs have been studied in cell culture and *in vivo*, and generally fall into 2 categories: chelation of a radiometal (e.g. [99m]Tc, ^{111}In, ^{68}Ga, ^{64}Cu) to the antisense ODN, usually via a 6-carbon linker; or labelling with a prosthetic group carrying a radiohalogen (e.g. [125]I, ^{123}I, [76]Br, ^{18}F) (17). Tables 1-1 and 1-2 contain a representation of radiolabelled, modified ODNs which have been developed and studied *in vitro* and *in vivo*, respectively. The Hnatowich group have exhaustively investigated the potential of antisense imaging using ^{99m}Tc-labelled hydrazino nicotinamide (HYNIC), mercaptoacetylglycine (MAG$_3$), or *N*-hydroxysuccinimide (NHS) conjugated to PS-ODNs, MORFs, and LNAs, and have demonstrated specificity of the ^{99m}Tc-labelled asODNs to the selected mRNA target (18-22). ^{111}In-labelled ODNs are synthesized through chelation with diethylenetriaminepentaacetic acid

(DTPA) (or similar chelate), which has been previously conjugated to the ODN (23). Using this approach, Dewanjee *et al* (24) and Wang *et al* (25) each visualized uptake of ^{111}In-labelled asODNs in animal tumour models 24 h after i.v. injection using SPECT imaging.

Chelation chemistry has also been employed for labelling ODNs with PET radionuclides such as ^{68}Ga and [64]Cu. For example, Tian *et al* reported positive tumour uptake with PET imaging after injection of ^{64}Cu-labelled PNA directed toward *K-ras* mRNA in AsPC1 pancreatic xenografts (26) and *CCND1* mRNA in human MCF7 estrogen receptor positive breast cancer xenografts (27). Roivainan *et al* (28) and Lendvai *et al* (29) have used ^{68}Ga to label PO-, mono PS-, and mono OMe-asODNs directed to mRNA expressed by the K-*ras* oncogene. The modifications did not interfere with sense:antisense hybridization *in vitro*. However the modifications to the ODN dramatically influenced its pharmacokinetics with rapid and complete degradation of the native ODN within 2 h, rapid plasma clearance and high renal uptake of the OMe-modified ODN, and prolonged plasma clearance, with high kidney and moderate liver uptake with the PS-ODNs (28,29).

None of the available PET radiometals has optimal radionuclide characteristics for routine clinical PET imaging, due to short half-lives, and high β^+ energy (Table 1-3) (30). Some emit additional γ-radiation and β^- energy as well (e.g. [64]Cu), all of which results in increased radiation doses for human clinical application.

1.4 [^{18}F]Fluoride

Of the 4 most common positron emitting radionuclides produced in a cyclotron (^{15}O, ^{13}N, ^{11}C, ^{18}F), ^{18}F is the only radionuclide suitable for labelling ODNs. The most obvious reason is its physical half life: ^{18}F has a half-life of 110 min which is of sufficient length to perform radiochemical syntheses of moderate complexity before the radionuclide decays. As a positron emitter, ^{18}F emits a β^+ particle with a maximum energy (E_{max}) of 0.635 MeV. This is the lowest energy exhibited by the positron emitting radionuclides typically used in molecular imaging (Table 1-3). ^{18}F is a pure β^+ emitter, i.e., ^{18}F does not emit other particulate or electromagnetic radiation, a characteristic common with other positron emitting radionuclides. Radiation emitted through other forms of decay degrades the resolution of the image and contribute to the radiation dose to the patient. A pure positron emitter, such as ^{18}F, with a lower β^+ energy allows imaging studies to be repeated without an unacceptable radiation dose to the patient.

The technology for producing and isolating ^{18}F and providing it in a form suitable for organic radiosynthesis is now well developed. Typically production of ^{18}F is via proton bombardment of stable [^{18}O]-enriched water by the nuclear reaction ^{18}O(p,n)^{18}F using a medical cyclotron. The [^{18}F]fluoride anion-containing water is transferred to a quaternary methylammonium column previously conditioned with potassium carbonate. Pre-conditioning of the column is necessary to replace the chloride anion with the more weakly bound carbonate anion. Subsequent application of fluorinated ^{18}O-water to the column traps the fluoride ion by displacement of the carbonate ion. The fluoride ion is eluted from the cartridge

with a solution containing both potassium carbonate and the cryptand, Kryptofix-222 (K_{222}). K_{222} acts as a phase transfer catalyst which sequesters the potassium cation inside its core leaving the 'naked' fluoride ion outside the core and in a reactive state (31). Thus, K_{222} enhances the solubility and nucleophilicity of ^{18}F in organic solvents. To improve reactivity of the fluoride ion, residual water molecules are removed with successive azeotropic evaporations using anhydrous acetonitrile (32).

1.5 [^{18}F]-labelled prosthetic groups for labelling oligonucleotides

A wide variety of [^{18}F]-labelled prosthetic groups have been developed for the labelling of biomolecules, and several reviews on the topic have been published (33-35). Most [^{18}F]-prosthetic groups, that are compatible for conjugation with ODNs and have been produced in high yields with high specific activity, are prepared via nucleophilic substitution of small aromatic compounds containing a strong electron withdrawing group such as a nitro or halogen, or sulphonic acid ester such as mesylate, tosylate, or trimethylammonium triflate in the *ortho* or *para* position (31-33). These [^{18}F]fluorophenyl intermediates can be synthesized in high yield (31) and can be further derivatized to form a large variety of synthons capable of reacting with biomolecules carrying a protic function such as a thiol, amino or hydroxyl group (33). For example, the synthesis of the [^{18}F]-prosthetic group, 4-*N*-[^{18}F]fluorobenzyl-2-bromoacetamide ([^{18}F]FBBA) is a 4-step reaction involving (a) preparation of the K[^{18}F]-cryptand, (b) labelling of the benzonitrile triflate, (c) reduction of the nitrile to the radiofluorinated benzylamine, and (d) condensation with bromoacetyl bromide (Figure 1-4A).

Using automated synthesis, typical decay-corrected yields of 20 to 30% have been reported (36,37). Purified [18F]FBBA is subsequently conjugated to the modified ODN containing a thiol group on either the 3′- or 5′-end (Figure 1-4B).

de Vries *et al* recently compared the synthesis of various alkyl and aromatic [18F]-labelled prosthetic groups, including [18F]FBBA, and their efficacy in labelling ODNs (36). Although the alkyl groups could be produced in relatively high yields, the highest yield of radiolabelled ODNs was found with the [18F]-labelled aromatic synthons.

A

B
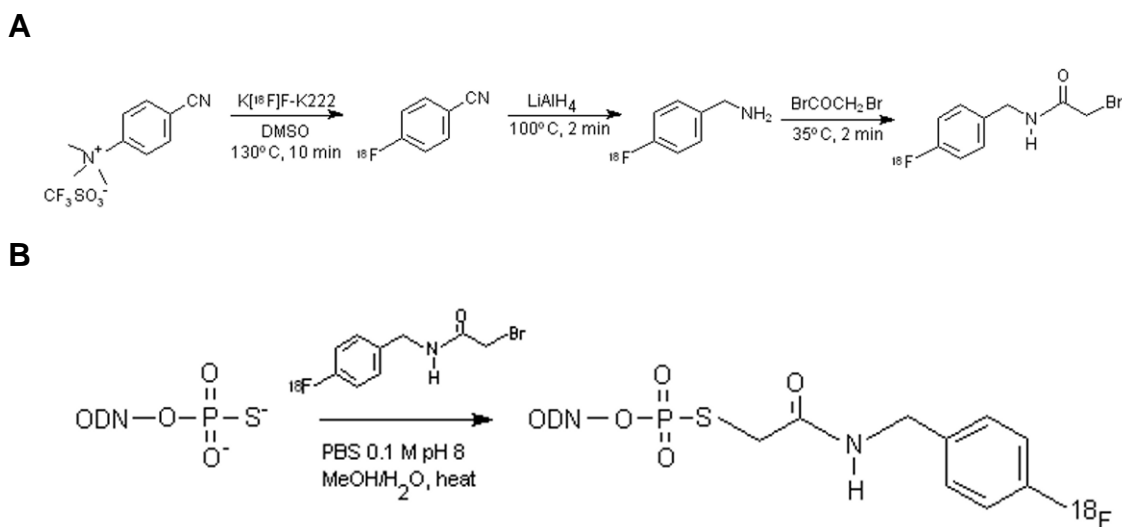
Figure 1-4 Schema for the radiolabelling of oligonucleotides (ODN) with the prosthetic group [18F]FBBA: (A) synthesis of [18F]FBBA from the triflate precursor; (B) radiolabelling of ODN with [18F]FBBA

The group from Orsay, France has been, by far, the most prolific in reporting the radiolabelling and *in vivo* pharmacokinetics of [18F]-labelled ODNs using [18F]FBBA. [18F]FBBA has been used to label the 3′-monophosphorothioated end of a native phosphodiester ODN (17), a fully phosphorothioated ODN, 2′-*O*-methyl-modified RNA, or hybrid phosphodiester methylphosphonate ODN

(15,37), the 5´-phosphorothioated 2´-*O*-methyl-modified RNA (38), 3´- or 5´-labelled RNA and DNA spiegelmers (39,40), and PNAs (41,42). Typical uncorrected (i.e. not decay-corrected) yields of approximately 4 to 5% of [^{18}F]FBBA-labelled ODNs were obtained. A related bromoacetamide, *N*-[3-(2-[^{18}F]fluoropyridin-3-yloxy)-propyl]-2-bromoacetamide, has also been used to label monophosphorothioated ODNs, modified RNAs (43), as well as siRNAs (44,45).

Pharmacokinetic studies of [^{18}F]FBBA-labelled ODNs in healthy male baboons demonstrated differences in the biodistribution and clearance between the various modified ODNs (15). Competitive hybridization assays were performed to demonstrate that the [^{18}F]-labelled synthon did not affect the ODN's capacity to hybridize with its complementary sequence. However, these studies did not include an *in vivo* tumour model to confirm targeting ability of the injected [^{18}F]-labelled ODNs.

Very few reports exist describing cellular accumulation and efflux studies with [^{18}F]-labelled asODNs. In 2004, de Vries *et al* reported the synthesis and evaluation of an [^{18}F]asODN directed against the enzyme nitric oxide synthase (iNOS) mRNA in cytokine stimulated DLD-1 colon carcinoma cells (46). Overexpression of iNOS mRNA stimulates overproduction of NO which contributes to the deleterious effects observed in chronic bowel inflammation. The fully phosphorothioated asODN was radiolabelled with [^{18}F]FBBA via a hexylthiol linker at 120°C for 30 minutes at pH 8.0 with a resulting specific activity of 1 to 13 GBq/µmol. Cellular accumulation studies with naked and

liposome-transfected [^{18}F]asODNs demonstrated no statistically significant difference in uptake or efflux of the [^{18}F]asODN between cytokine stimulated and control cells. iNOS expression also did not influence the efflux of the radiolabelled ODNs within the 2 h time period studied. The authors suggested that the long length of the ODNs selected (20 to 24 nucleobases) allowed hybridization to mismatched sequences in the PCR assay. As yet, no reports of *in vivo* imaging with [^{18}F]asODN directed to a specific target in an animal tumour model have been described in the literature.

1.6   Mechanism of uptake of oligonucleotides

There are no ODN specific binding sites on the cell surface, and therefore ODNs generally have difficulty traversing the cell membrane. Internalization probably follows non-specific binding to one or more cell-surface proteins followed by active transport into the cell (47). In cell culture, cells internalize the ODN in a saturable, size-dependent manner, which in turn depends on environmental conditions, such as temperature, the structure and concentration of the ODN, and the cell line (48). Both energy-dependent (receptor-mediated endocytosis (RME) and adsorptive pinocytosis), and energy-independent mechanisms (fluid phase pinocytosis) have been documented in various cell cultures (49). RME involves internalization of an ODN which has become bound to a receptor via a ligand, whereas adsorptive pinocytosis implies direct, but nonspecific binding to the cell surface membrane. According to Lebedeva *et al*, adsorptive pinocytosis is the major mechanism by which naked ODNs are internalized (50). Endocytosis involves the inward folding of the plasma

membrane around the ODN-membrane complex (51). The plasma membrane is pinched off to form 'early endosomes' whose internal pH is ~6. Two sets of endosomes can be distinguished: early endosomes are located near the plasma membrane whereas late endosomes, with an internal pH of ~5.5, are found near the nucleus. Acidification is the major energy-driven event during endocytosis with the gradual shift in pH triggering specific processes. The late endosomes fuse with lysosomes to form secondary lysosomes. This is followed by hydrolysis of the contents.

Clathrin-coated vesicles play a major role in the uptake of macromolecules which can bind to receptors such as the transferrin receptor (TfR), the EGF receptor, and the platelet-derived growth factor receptor (51). In this form of endocytosis the vesicles shed their clathrin coat and fuse with early endosomes. This form of uptake usually results in intra-lysosomal hydrolysis of the endocytosed material.

A clathrin-independent mechanism also exists via uptake by the caveolae which are flask-shaped, non-coated plasma membrane invaginations. They are implicated in transcytosis and endocytosis of blood components and are especially abundant in endothelial and epithelial cells. Since endocytosis via caveolae often circumvents intra-lysosomal destruction, the exploration of ligands for this transcytosis could lead to new drug delivery strategies. Rejman *et al* have reported that the type of endocytosis employed by the cell is dependent on the size of the complex with smaller particles (< 200 nm) being taken up by the clathrin-dependent method and larger particles (> 500 nm) by the caveolae method (52).

Thus, larger ODN particles may avoid lysosomal degradation if targeted to this pathway.

Both adsorptive and fluid-phase pinocytosis are unspecific in the substances that are transported i.e. the cell takes in surrounding fluids, including all solutes present. Uptake of ODNs appears to be related to the ODN concentration: at low concentrations, internalization occurs via energy-dependent mechanisms whereas at high ODN concentrations the non-specific pinocytotic processes take precedence (49).

1.7 Vehicles for delivery of radiolabelled oligonucleotides

Many studying the delivery of ODNs for therapeutic use argue that a delivery vehicle is not needed for the asODN to exert its antisense effect. Lebedeva refers to several studies providing positive results with naked ODNs in the treatment of colitis, leukemia, melanoma, hepatocellular carcinoma and hepatitis B in murine and duck animal models (50). Studies to evaluate therapeutic efficacy employ higher doses of asODN, and often the injection of asODNs is repeated over a series of days. The higher amounts of antisense ODN saturate both the energy dependent and independent plasma membrane binding sites with some probe escaping degradation. Also, the mode of systemic delivery may differ for therapeutic administrations of asODNs.

For diagnostic imaging studies, picomolar amounts of radiolabelled asODN are administered in a single i.v. injection. The probe generally needs to reach the target tissue rapidly, with high plasma clearance to reduce background radiation. Upon reaching the target cell membrane, the radiolabelled asODNs would likely

be transported across the membrane by adsorptive pinocytosis with only a few ODNs escaping endosomal encapsulation. Indeed, most cell culture studies have demonstrated low and slow accumulation of probe in the cell. For example, Zhang *et al* showed that naked ^{99m}Tc-labelled asODNs selectively accumulated in ACHN cells (a human renal adenocarcinoma cell line) over 24 h as compared with the radiolabelled control ODN (53). While the *in vitro* results are promising, Hnatowich and others maintain that for radiolabelled asODNs to become useful probes of gene expression, an improvement in cellular delivery is required (18,54,55).

Most evaluations of radiolabelled asODNs in cell culture have utilized a liposomal vector, not to evaluate the liposome as a potential transfection agent, but to ascertain the probe's targeting ability in an ideal environment. However, the conditions that prevail in an *in vitro* environment (serum-free media, short incubation times, lack of scavengers such as macrophages, single cell colonies) differ greatly from those in an *in vivo* environment (51). Few reports exist which evaluate transfection agents for the *in vivo* delivery of radiolabelled ODNs for diagnostic purposes. Vectors that have been investigated for the delivery of radiolabelled ODNs include lipid formulations, polycations, bispecific monoclonal antibodies, and cell penetrating peptides. Table 1-4 contains a list delivery vectors which have been assessed as potential asODN transfection agents *in vivo*.

1.7.1 Liposomes

One of the most common vectors used for drug delivery are the first generation of vectors: liposomes. Liposomes are colloid vesicles consisting of an aqueous compartment enclosed in a bilayer of phospholipids and cholesterol (6) and can be engineered to yield a specific size, surface charge, and composition. Liposomes transport ODNs by entrapping the ODN inside the aqueous core, or complexing the ODN to the phospholipid lamellae. Entry into the cell has been shown to occur through the clathrin-mediated endocytosis (56).

Cationic lipids have been shown to enhance encapsulation efficiency of ODNs due to their ability to cause condensation of a polyanionic ODN by electrostatic interaction with the liposome (51). Due to their positive charge the cationic liposomes have a high affinity for cell membranes. The addition of a 'helper molecule', such as DOPE (1,2-dioleoyl-sn-glycero-3-phosphatidylethanolamine), assists in membrane perturbation and fusion. The endosomal membrane destabilization allows ODNs to escape from the endosomes by leaking into the cytoplasm (57). Unfortunately, the positive global charge of the nucleic acid-lipid complex (lipoplex) may result in its inactivation due to non-specific binding with anionic serum proteins. Another drawback is that lipoplexes tend to aggregate *in vivo* and are rapidly engulfed by macrophages resulting in uptake of the materials in the lung and liver. This could lead to pulmonary toxicity and cytotoxicity to phagocytic macrophages (6).

The commercially available cationic liposome Lipofectamine™ has been investigated as a transfection agent for the *in vivo* delivery of an antisense ODN directed against *c*-myc-mRNA, which is over-expressed in colon carcinoma.

Zheng *et al* reported an uptake of 13.5% liposome-entrapped ^{99m}Tc-labelled asODN in the tumour 2 hours post injection in biodistribution studies (58). In addition to higher uptake in the liver and lungs, significant uptake was observed in the stomach. An approximate 2-fold increase in radioactivity was observed in the tumour versus the contralateral side of the abdomen. Unfortunately, no control asODN or tumour model was used in this experiment to confirm specificity of the ^{99m}Tc-labelled asODN to the target.

A negatively charged liposome may prove to be an attractive alternative to the cationic liposome as safety of these lipids has been demonstrated (6). Tavitian *et al* have described the use of an anionic lipid for the delivery of ^{18}F-labelled ODNs (59). The liposome was prepared by mixing three molecules of different charge: DOPE (neutral), cardiolipin (anionic) and GLB43, a monocationic phospholipid. The mixture was dissolved in ethanol and water. Immediately prior to i.v. injection into baboons, the vesicles were mixed with an ^{18}F-labelled ODN. The level of ODN incorporation was 94%. Radio-HPLC analysis of the plasma showed that 5 to 10% of the lipoplex injected was detected unchanged in plasma up to 60 minutes after injection. In comparison, only radioactive metabolites could be detected 30 minutes after 'naked' ODN was injected, i.e., no intact ^{18}F-labelled ODN was observed Although the 'area under the curve' (AUC) and clearance rate of the naked ODN and the anionic lipoplex did not differ, the volume of distribution and terminal half-life of the anionic lipoplex increased significantly suggesting that the lipoplex was able to penetrate the tissues. PET images showed higher accumulation in the lungs, spleen, and brain as compared

to the naked ODN or the cationic lipoplex. The use of this anionic vector in cell culture or in an *in vivo* tumour model has yet to be reported.

1.7.2   Bispecific monoclonal antibodies

Another approach for delivery of antisense molecules into the cell is to use vectors which can be targeted to specific proteins on the cell surface. An example is the use of a monoclonal antibody (mAb) as a transport vector. Lee *et al* used this method to view gene expression *in vivo* in a transgenic mouse model of Huntington's disease (HD) (60). A PNA targeting the HD gene was modified by the attachment of a biotin molecule on the amino terminus, with the radioiodine (^{125}I) attached to a tyrosine molecule on the carboxyl terminus. The targeting vector was composed of a conjugate of recombinant streptavidin and an anti-mouse mAb to the TfR receptor. Binding of the mAb-streptavidin-biotin-^{125}I-PNA complex to TfR, which is expressed on the membranes of the blood brain barrier *and* the brain cell, resulted in the transcytosis of the complex across both membranes. The results provided evidence of selective sequestration of the sequence-specific HD-PNA in the brains of the transgenic mice relative to the brain uptake in mice of a control PNA. Conjugation of the ^{125}I-PNA to the targeting vector did not affect hybridization of the PNA to the target HD mRNA even though conjugation dramatically increased the molecular size of the imaging agent.

1.7.3   Polycations

Polycations such as polyethyleneimine (PEI) are promising carriers due to their ability to increase the transfection efficiency of lipid-based polynucleotide

carriers and to protect DNA and RNA against degradation. Rejman *et al* showed that polycations utilize caveolae-mediated endocytosis to gain entry into the cell, and are released from endosomes through intrinsic endosomolytic activity often referred to as the 'proton-sponge' mechanism (56). The amino groups of the polycation become protonated as the proton pump in the endosomal membrane transports protons into the endosome. This is followed by the passive influx of counterions, such as chloride ions, which leads to water influx and vesicle destabilization, with subsequent release of the endocytosed material into the cytoplasm. As polycations are very efficient DNA-condensing agents, the ODN-PEI complex remains protected: there is evidence that these complexes can enter the nucleus (61).

Two transfectors, jetPEI™ (a linear PEI polymer) and Neophectin™ (a liposome containing a modified cationic cardiolipin) were recently compared in their ability to target mdr1 mRNA using an antisense PS-ODN (62). The transfectors were chosen based on earlier *in vitro* studies which demonstrated that these agents were non-toxic and exhibited rapid pharmacokinetics with no evidence of entrapment in vesicles. Biodistribution studies in KB-G2 tumour-bearing mice exhibited higher blood levels with the ^{99m}Tc-labelled asODN when transfected with either transfection agent as compared with the naked radiolabelled asODN. However, tumour-to-blood ratios were 2 to 3 times higher with the naked asODN versus the liposome or PEI transfected ODNs at 6 and 24 hours post injection. The liver, spleen, and lung uptake were significantly higher with the transfected agents. The

authors proposed that the transfector-to-ODN ratio may not have been optimized for *in vivo* use resulting in suboptimal tumour uptake.

A disadvantage of PEIs is that the polymer can be cytotoxic and can induce apoptosis in cells (6). The toxicity and transfection efficiency appear to be related to its molecular weight. Attempts to reduce the cytotoxicity include the use of low-molecular weight PEI, or the synthesis of PEI with copolymers such as linear poly(ethylene glycol) (PEG). PEG has been used for the formulation of stealth liposomes. PEGylation prevents the opsonization and recognition of the vesicles by the phagocytic cells of the reticuloendothelial system (RES) (6), thus reducing nonspecific interactions of the complexes in the blood. In addition, modification of the complex surface with appropriate amounts of PEG does not block ligand mediated internalization (63).

Copolymers of PEI and hydrophilic PEG have been synthesized by Fischer *et al* to compare the *in vivo* distribution and pharmacokinetics of a naked 20-mer double-stranded ODN with the ODN complexed to a 25-kDa PEI, a low molecular weight 2.7-kDa PEI, or a PEGylated high molecular weight PEI in BALB/c mice (64). A double-labelling technique was employed to simultaneously follow the distribution of both complex components. The polymers were radioactively labelled with ^{125}I and the ODNs with [γ-^{32}P]ATP. Complexation with the low and high molecular weight PEI polymers increased the uptake into the liver and spleen as compared with the naked ODN, which was rapidly excreted through the kidneys. Similar organ distribution profiles for ^{125}I and ^{32}P were observed suggesting that the ODN-polymer complex remained intact. In

contrast, the PEGylated compound exhibited slower uptake into the RES system. However dissociation between the PEGylated PEI and ODN was evident. The authors suggested that modification of the PEG shell to stabilize the complex could result in improved pharmacokinetics.

The use of PEG has been studied to modify the uptake of aptamers into tumours. Hicke *et al* compared the distribution of a ^{99m}Tc-labelled aptamer, with and without PEG as a linker, to a target protein, tenascin-C (65). Tenascin-C is a large molecular weight protein that is over-expressed in many types of cancers and has been linked to angiogenesis. They hypothesized that inserting PEG between the chelate and the aptamer might increase the hydrophilicity of the metabolic product and thus alter the biodistribution. Biodistribution studies in *nu/nu* mice bearing human glioblastoma tumours demonstrated that addition of a PEG$_{3,400}$ linker dramatically reduced hepatobiliary clearance and increased renal clearance. However, tumour uptake of the PEGylated aptamer was slightly less than with the non-PEGylated compound.

1.7.4   Cell Penetrating Peptides

Another interesting development in the search for an efficient *in vivo* transfector is the discovery of the Tat protein. An 11 amino acid arginine-rich peptide belonging to the RNA binding domain of Tat has been shown to cross plasma membranes (66). Thus it is possible that antisense ODNs could be internalized when conjugated to Tat. Zhang *et al* investigated the influence of Tat on the accumulation of ^{99m}Tc-labelled antisense ODNs in cell culture (67). The addition of Tat significantly increased the accumulation of antisense ODN, and an

antisense effect was suggested through the ODNs ability to hybridize with mRNA. Cellular accumulation was attributed solely to its function as a cationic carrier as no difference in uptake between scrambled and antisense ODNs was observed.

More recently, Nakamura *et al* compared the cellular uptake of ^{99m}Tc-labelled PO- and PS-ODNs *in vitro* and *in vivo*, using 3 biotinylated carriers: Tat peptide, a polyarginine peptide and cholesterol. Streptavidin acted as a linker between the carrier and 3'-biotin labelled ODN (68). The cellular accumulation of ^{99m}Tc-labelled PS-ODN was more than an order of magnitude higher than with the ^{99m}Tc-labelled PO-ODN regardless of the carrier used. Between 30 and 40% of the Tat and cholesterol ^{99m}Tc-PS-ODNs accumulated in the cell by 23 h, as compared with carrier free ^{99m}Tc-PS-ODN which demonstrated an uptake of approximately 25% over the same time period. *In vivo* biodistribution studies demonstrated higher uptake of the ^{99m}Tc-PS-ODN streptavidin-Tat and ^{99m}Tc-PS-ODN streptavidin-cholesterol at 6 h but no difference at 18 h. The higher uptake of ^{99m}Tc-PS-ODN versus ^{99m}Tc-PO-ODN *in vivo* was attributed to plasma protein binding rather than the presence of streptavidin in the nanoparticles (69).

Other cell penetrating peptides have been designed for the delivery of drugs. Tian *et al* designed a ^{99m}Tc-peptide-PNA-peptide chimera to bind to the *MYC* mRNA in the MCF7 breast cancer cell line (70), ,in which elevated levels of Myc protein are observed due to overexpression of *MYC* mRNA, The antisense PNA probe showed a higher tumour-to-blood and tumour-to-muscle ratio than the mismatched probe or the PNA-free probe. *In vivo* images in mice implanted with

the MCF7 estrogen receptor positive tumour cell line, clearly show uptake of radioactivity in the flank containing the tumour, with the maximum intensity observed 12 h post injection. In contrast, the tumour was not visible with the mismatched and PNA-free controls. A similar probe directed to *CCND1* cancer gene has also been reported by the same group (71). More recently, Zhang *et al* used a ^{99m}Tc-labelled MORF conjugated to a Tat peptide via a N_2S_2 linker to investigate uptake of the probe directed to the type-I regulatory subunit α of cAMP-dependent protein kinase A (RIα) mRNA in ACHN cells (72). Within 12 minutes, nearly 20% of the added radioactivity was associated with the cells; by 120 min, accumulation had reached 35%. In contrast, less than 1% of the radioactivity was associated with the cells when the MORF ODN without Tat was incubated with the cells. *In vivo* studies have not yet been published using this particular probe and carrier.

1.8   Use of transfectors versus delivery of naked oligonucleotides *in vivo*

In vivo imaging studies have been published which have reported encouraging results using radiolabelled antisense ODNs without a carrier (24,25,28,65). The choice of the ligand binding the radionuclide to the ODN may be an important determinant in the biodistribution of naked ODNs. Zhang *et al* demonstrated that the biodistribution of ODNs in mice varied with the ^{99m}Tc chelate. Also, the cellular accumulation in tissue culture of radiolabelled antisense ODN was strongly influenced by the chelator (73). Therefore, modification of an ODN, by introduction of a linker and chelating agent, appears to confer stability to the

ODN complex, alter its pharmacokinetics, and protect it from endosomal degradation.

Promising reports of gene expression imaging using naked ^{111}In-labelled ODNs have been published. For example, Dewanjee *et al* described the uptake of ^{111}In-labelled PS-asODNs directed to *c-myc* oncogene in mammary tumour-bearing BALB/C mice (24). A tumour-to-blood ratio of 2.5 to 3 was observed at all time points up to 72 h post injection. In contrast, the sense probe showed very little uptake in the tumour over the same time period. The images were obtained 24 to 48 h after i.v. injection. Wang *et al* also demonstrated uptake of ^{111}In-labelled PS-asODN in EGF induced MDA-MB-468 cells 48 h after i.v. injection (25). However with evidence of endosomal entrapment of naked ODNs in cell culture studies, it is unclear how radiolabelled asODNs in an animal model could avoid similar entrapment.

1.9 Cellular senescence and its role in cancer

The gene, p21, is located on chromosome 6 at location 6p21.2, and is also referred to as cyclin-dependent kinase inhibitor 1A (*CDKN1A*), wild-type p53 activated fragment 1 (*WAF1*), cyclin-dependent kinase (CDK)-interacting protein 1 (*CIP1*), or senescent cell-derived inhibitor 1 (*SDI1*). This 21-kDa protein controls the cell cycle checkpoints cyclin A/CDK-2, cyclin B/CDK-1, cyclin D1, and cyclin E, all of which have been implicated in the control of the G1/S and G2/M transition in mammals (74-76) . It is responsible for cell growth arrest when a cell is damaged, and allows time for the cell to repair itself prior to returning to the cell cycle. Exposure to ionizing radiation causes the upregulation or expression of p21 via

the ataxia telengiectasia mutant (ATM) protein which activates p53, often referred

to as the tumour suppressor or apoptosis gene (Figure 1-5), via phosphorylation.

Phosphorylation of p53 subsequently induces transcriptional activation of a

number of p53–responsive genes. Depending on the state of the genotoxic injury,

activation of the p53 pathway promotes (a) survival by coordinating DNA repair

with activation of the G1/S and G2/M checkpoints, (b) apoptosis, or (c) p21-

directed premature cellular senescence, or 'accelerated' senescence (76-80).
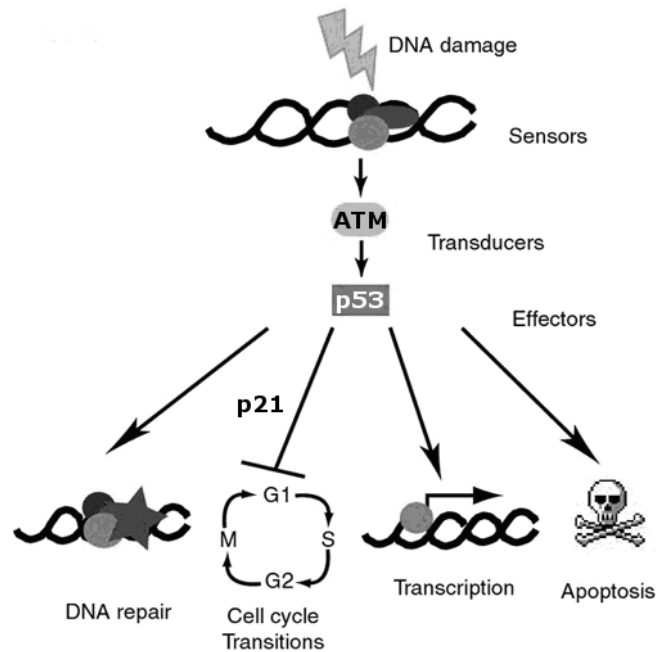
Figure 1-5   Responses triggered by ionizing radiation in human cells with a functional p53 signaling pathway.   Arrows indicate stimulation and T-shaped lines indicate inhibition (75).

It is unclear whether the induction of accelerated senescence in cancerous tissue

after radiation therapy translates, clinically, to a beneficial treatment outcome.

Induction of a senescent phenotype by anticancer drugs has been shown to

contribute to successful treatment (81). However, a critical feature of senescent

cells is that they remain metabolically active, and can act as 'feeder' cells by communicating with neighbouring surviving and arrested cells through the secretion of tumour-promoting factors, such as proinflammatory cytokines (82). It has been proposed that senescent cells can, through this chemical communication, stimulate and protect the proliferation of surviving tumour cells (83,84). In addition, senescent cells with unrepaired DNA may escape arrest by forming multi-nucleated/polyploid giant cells which can proliferate via the nuclear budding process, neosis. These progeny can eventually develop into highly metastatic cells (85,86). Blocking p21 expression has been shown to increase radiosensitivity of some cell lines as opposed to those cells with intact p21 expression (87). Based on these observations, it is plausible that cellular senescence could be considered a negative predictor of treatment outcome.

1.10 p21 and antisense oligonucleotides

The use of asODNs as molecular probes to explore the relationship between premature senescence and *p21* expression in cell culture has been reported by a number of groups (87-91). Poluha *et al* showed that PS-asODNs directed to the 3′-end, the initiation codon, or the middle of the coding region of *p21* mRNA, exhibited an equally effective ability to inhibit cell cycle arrest in the neuroblastoma cell line, SH-SY5Y (90). Ohtsuba *et al* witnessed continuous growth in A431 cells upon incubation of the cells with an asODN directed to the 5′-region of *p21* mRNA in human squamous carcinoma cell line, A431 (89). Sak *et al* demonstrated that radiation-induced G2 arrest was decreased, and radiation-induced apoptosis was increased in NSCLC cells when p53-responsive pathways

were blocked via PS-asODNs targeting *p53* or *p21* mRNA (87). Tian *et al* demonstrated an antisense dose dependent inhibition of p21 protein expression in p21$^{+/+}$ human colon carcinoma (HCT116) cells which had previously been exposed to 10 Gy of γ-radiation (91). Kokunai *et al* also demonstrated increased apoptosis in radioresistant glioma cells after treatment of the cells with p21-directed asODNs (92). Thus asODNs directed toward p21 appear to be effective inhibitors of cellular senescence in a variety of tumour cell lines.

The potential of p21 asODN as an imaging agent of *p21* mRNA was described by Wang *et al* in 2003 who evaluated an ^{111}In-labelled PS-asODN for imaging EGF-induced p21 expression in MDA-MB-468 breast cancer xenografts (25). In this study, *in vivo* SPECT imaging of tumour-bearing mice were obtained 48 h post i.v. injection of the ^{111}In-labelled probe. Localization of radioactivity was clearly observed in EGF-induced tumours. No tumour uptake was observed in the control tumours (i.e. no EGF induction). The tumour-to-blood ratio of the antisense probe reached 4.9 as opposed to the 2.1 for the random sequence probe in EGF induced tumours or the antisense probe in non-EGF induced tumours. Biodistribution studies demonstrated a 2-fold higher tumour:blood ratio of ^{111}In-labelled asODNs in EGF-induced cells versus controls; however, the actual uptake was modest at 0.32% of the injected dose per gram tumour (as compared with uptake of the random sequence of 0.21%). Although the *in vivo* data imply specificity of the probe for the target tissue, doubt remains as to whether the naked radiolabelled asODNs truly reflect antisense hybridization, or merely sequestration in endosomal vesicles.

1.11 Hypothesis

Radiofluorinated antisense oligonucleotides, due to their specificity towards mRNA targets, can be used to noninvasively visualize and quantitatively evaluate upregulated p21 expression with PET in patients undergoing radiation therapy.

1.12 Objectives

The objectives of this thesis are:

- to prepare a radiofluorinated asODN directed to *p21* mRNA;

- to demonstrate that the addition of the [^{18}F]-labelled prosthetic group does not interfere with the ability of the asODN to bind with *p21* mRNA;

- to evaluate the cellular accumulation of [^{18}F]asODN *in vitro* using a tumour cell line which is known to express p21 (p21$^{+/+}$) upon induction with ionizing radiation against two controls: a radiolabelled random sequence ODN, and a p21 deficient cell line (p21$^{-/-}$); and

- to evaluate a polyamide block copolymer as a potential delivery vector of [^{18}F]ODNs *in vitro*.

1.13 Experimental Overview

[^{18}F]FBBA was synthesized, based on previously described methods, using an automated synthesis unit. The prosthetic group was subsequently conjugated to 20-mer fully phosphorothioated antisense ODN, directed to *p21* mRNA, and a random sequence ODN. Both [^{18}F]-labelled and nonradioactive [F]-labelled probes were used to evaluate the specificity and localization of the (radio)fluorinated asODN to *p21* mRNA   in cell culture. The nonradioactive

[F]asODN was evaluated for its antisense ability to confirm that addition of a prosthetic group did not interfere with hybridization to *p21* mRNA . The probes were transfected into cells as naked and liposome-transfected probes to evaluate their ability to accumulate in p21$^{+/+}$-expressing cells over time. The cellular accumulation, localization, and specificity of (radio)fluorinated ODNs was further evaluated in both p21$^{+/+}$ and p21$^{-/-}$-expressing cell lines using ODNs transfected with a polyamine block copolymer.

Table 1-1 Cell culture studies with modified radiolabelled oligonucleotides

ODN	Radiolabelled chelate or prosthetic group	mRNA target	Cell culture	Method of transfection	Ref
15-mer PS antisense and sense	^{111}In-DTPA	Mdr1	P388S P388R	naked; liposome	(23)
24-mer PS antisense	[18F]FBBA	iNOS	DLD-1	naked; liposome	(46)
20-mer PS antisense and sense	^{99m}Tc-MAG$_3$	Mdr1	KB-G2 KB-G1 KB-31	naked; liposome	(93)
28-mer PS antisense, sense, and random	^{99m}Tc-MAG$_3$	RIα	ACHN	naked	(53)
15-mer PS antisense and sense	^{99m}Tc-MAG$_3$	RIα; c-myc	ACHN MDA-MB-231	naked; cationic liposome	(94)
18-mer PS antisense and sense	^{99m}Tc-HYNIC	RIα	ACHN	naked; Tat peptide	(67)
15-mer LNA antisense and sense	^{99m}Tc-MAG$_3$	RIα	ACHN	naked; liposome	(20)
18-mer MORF antisense and sense	^{99m}Tc-N$_2$S$_2$	RIα	ACHN	naked; Tat peptide	(72)
25-mer MORF antisense and sense	^{99m}Tc-MAG$_3$	Survivin	MCF7	HIV-Tat peptide; polyA; cholesterol; + streptavidin nanoparticles	(69)
15-mer PO antisense and sense	^{99m}Tc-HYNIC	c-myc	TGR-1 HO15.19	naked	(95)

Table 1-2 *In vivo* studies with naked radiolabelled oligonucleotides

mRNA target	ODN	Radiolabelled chelate or prosthetic group	Tumour Cell line	Animal model	*In vivo* studies	Ref
no specific target	25-mer 3′-mono-PS spiegelmers of RNA and DNA	[18F]FBBA		rat baboon	autoradiography PET	(40)
SFFV (Friend erythroleukemia virus)	18-mer PO, PS, OMe	[18F]FBBA		baboon	PET	(15)
c-myc	15-mer PO and mono PS; antisense, sense	111In-DTPA-isothiocyanate	P388	mouse	SPECT	(24)
asialo-glycoprotein receptor	10-mer PNA	[18F]FBBA		rat	biodistribution	(42)
no specific target	22-mer PO, PS, mixed PO-PS	99mTc-HYNIC		mouse	SPECT	(96)
GFAP	25-mer PS; antisense, mismatch, sense	[11C]ethylketene	C6-glioma	rat	autoradiography	(97)
Streptavidin-mAB-TfR	Biotinylated PNA	125I		mouse	autoradiography	(60)
K-ras	17-mer PO, PS, and OMe; antisense and sense	68Ga-DOTA	A549 BxPC-3	rat	autoradiography PET	(29) (28)
Chromogranin A	6, 12, 20, 30-mer; PS; 30-mer; PS , PO	*N*-succinimidyl 4-[76Br]bromobenzoate		rat	autoradiography; biodistribution	(98) (99)
Chromogranin A	20-mer LNA-DNA mixmer; antisense, mismatched, sense	68Ga-DOTA		rat	autoradiography; biodistribution	(100)
hTERT	18-mer PS ; antisense, sense	99mTc-MAG3	MCF-7	mouse	SPECT	(101)
c-myc	15- and 18-mer PO; antisense, sense	99mTc-MAG3		rabbit	SPECT; biodistribution	(102)
cMORF-coupled beads	15-mer MORF, PNA	99mTc-MAG3		mouse	SPECT	(103)
'sense' PNA-coupled beads	15-mer PNA	99mTc-MAG3		mouse	SPECT	(104)
p21	18-mer PS antisense	111In-DTPA	MDA-MB-468	mouse	SPECT	(25)
RIα	18-mer PS	99mTc HYNIC 99mTc MAG3 99mTc DTPA	ACHN	mouse	biodistribution	(73)

Table 1-3 Physical characteristics of radionuclides used for positron emission tomography (30,105)

Radioisotope	Half-life	β^+ E_{max} (MeV)	Max range in water (mm)	Remarks
Carbon-11	20.4 min	0.960	3.9	
Nitrogen-13	10.0 min	1.20	5.1	
Oxygen-15	2.03 min	1.73	8.0	
Fluorine-18	109.8 min	0.634	2.3	
Gallium-68	68 min	1.90	8.9	88% β^+ decay 22% EC*
Copper-61	3.3 h	1.215 (52%)	5.1	62% β^+ 38% EC
Copper-64	12.7 h	0.653	2.4	18% β^+ 42% EC 40% β^-
Iodine-124	4.2 days	1.54 (50%) 2.14 (50%)	6.9 10	23% β^+ 77% EC High energy γ-rays: 602, 772, 1691 keV
Bromine-76	16.2 h	3.94	20.2	55% β^+ 45% EC Multiple β^+ branching

*EC: electron capture decay

Table 1-4 *In vivo* studies of carrier-mediated radiolabelled oligonucleotides

mRNA target	ODN	Radiolabelled chelate or prosthetic group	Tumour Cell line	Delivery vector	Animal model	*In vivo* study	Ref
c-myc	15-mer mono-PS; antisense	^{99m}Tc-HYNIC	LS-174-T	liposome	mouse	SPECT biodistribution	(58)
mdr1	20-mer PS; antisense	^{99m}Tc-MAG$_3$	KB-G2	linear PEI; cationic liposome	mouse	biodistribution	(62)
mdr1	18-mer PO, PS; antisense	^{99m}Tc-MAG$_3$	KB-G2 KB-G1 TCO-1	Tat peptide; polyA; biotinylated cholesterol	mouse	biodistribution	(68)
RIα	25-mer MORF; antisense and sense	^{99m}Tc-MAG$_3$	SUM179	biotinylated Tat peptide; polyA;	mouse	biodistribution	(106)
c-myc CCND1 K-ras	12-mer PNA antisense: PNA-peptide control: PNA mismatch	^{99m}Tc-peptide [64]Cu –N$_2$S$_2$ ^{64}Cu-DO3A	MCF-7 AsPC1	IGF1 peptide; peptide mismatch	mouse	SPECT PET biodistribution	(26,27)
unr	18-mer PNA; antisense, mismatch	^{64}Cu-DOTA	MCF-7	4-lysine permeation peptide	mouse	PET	(107)
GFAP; CAV	Biotinyl-lysine PNA	^{111}In-DTPA	RG2	Streptavidin-mAB to TfR receptor	rat	biodistribution	(108)
HIV	18-mer PO	[^{18}F]FBBA		anionic and cationic liposomes	baboon	PET	(59)

1.14 References

(1) Phelps ME. Positron emission tomography provides molecular imaging of biological processes. Proc.Natl.Acad.Sci.U.S.A. 2000;97(16):9226-9233.

(2) Britz-Cunningham SH, Adelstein SJ. Molecular targeting with radionuclides: state of the science. J.Nucl.Med. 2003 Dec;44(12):1945-1961.

(3) Tavitian B. In vivo imaging with oligonucleotides for diagnosis and drug development. Gut 2003;52(SUPPL. 4).

(4) Google Image Result for http://faculty.ksu.edu.sa/aak/Pictures. Accessed 2/24/2010, 2010.

(5) Haberkorn U, Mier W, Eisenhut M. Scintigraphic imaging of gene expression and gene transfer. Curr.Med.Chem. 2005;12(7):779-794.

(6) Patil SD, Rhodes DG, Burgess DJ. DNA-based therapeutics and DNA delivery systems: a comprehensive review. AAPS J. 2005 Apr 8;7(1):E61-77.

(7) Opalinska JB, Gewirtz AM. Nucleic-acid therapeutics: basic principles and recent applications. Nat.Rev.Drug Discov. 2002 Jul;1(7):503-514.

(8) Thierry AR, Abes S, Resina S, Travo A, Richard JP, Prevot P, et al. Comparison of basic peptides- and lipid-based strategies for the delivery of splice correcting oligonucleotides. Biochim Biophys Acta 2006;1758:364-374.

(9) Urbain JL. Sense, antisense, and common sense. J.Nucl.Med. 2001 Nov;42(11):1670-1672.

(10) Sahu NK, Shilakari G, Nayak A, Kohli DV. Antisense technology: A selective tool for gene expression regulation and gene targeting. Curr.Pharm.Biotechnol. 2007;8(5):291-304.

(11) Kurreck J. Antisense technologies. Improvement through novel chemical modifications. Eur.J.Biochem. 2003 Apr;270(8):1628-1644.

(12) Lendvai G, Estrada S, Bergström M. Radiolabelled oligonucleotides for imaging of gene expression with PET. Curr.Med.Chem. 2009;16(33):4445-4461.

(13) Duatti A. In vivo imaging of oligonucleotides with nuclear tomography. Curr. Drug Targets 2004;5(8):753-760.

(14) Lebedeva I, Stein CA. Antisense oligonucleotides: Promise and reality. Annu. Rev. Pharmacol. Toxicol. 2001;41:403-419.

(15) Tavitian B, Terrazzino S, Kühnast B, Marzabal S, Stettler O, Dollé F, et al. In vivo imaging of oligonucleotides with positron emission tomography. Nat.Med. 1998;4(4):467-470.

(16) Lysik MA, Wu-Pong S. Innovations in oligonucleotide drug delivery. J.Pharm.Sci. 2003;92(8):1559-1573.

(17) Kuhnast B, Dolle F, Terrazzino S, Rousseau B, Loc'h C, Vaufrey F, et al. General method to label antisense oligonucleotides with radioactive halogens for pharmacological and imaging studies. Bioconjugate Chem. 2000;11(5):627-636.

(18) Hnatowich DJ, Nakamura K. Antisense targeting in cell culture with radiolabeled DNAs - A brief review of recent progress. Ann.Nucl.Med. 2004;18(5):363-368.

(19) Nakamura K, Fan C, Liu G, Gupta S, He J, Dou S, et al. Evidence of antisense tumor targeting in mice. Bioconjugate Chem. 2004;15(6):1475-1480.

(20) Zhang Y, He J, Liu G, Venderheyden J, Gupta S, Rusckowski M, et al. Initial observations of ^{99m}Tc labelled locked nucleic acids for antisense targeting. Nucl.Med.Commun. 2004;25(11):1113-1118.

(21) Nakamura K, Kubo A, Hnatowich DJ. Antisense targeting of P-glycoprotein expression in tissue culture. J.Nucl.Med. 2005;46(3):509-513.

(22) Li Y, Tan T, Zheng J, Zhang C. Anti-sense oligonucleotide labeled with technetium-99m using hydrazinonictinamide derivative and N-hydroxysuccinimidyl S-acetylmercaptoacetyltriglycline: A comparison of radiochemical behaviors and biological properties. World J.Gastroenterol. 2008;14(14):2235-2240.

(23) Bai J, Yokoyama K, Kinuya S, Shiba K, Matsushita R, Nomura M, et al. In vitro detection of mdr1 mRNA in murine leukemia cells with 111In-labeled oligonucleotide. Eur.J.Nucl.Med.Mol.Imaging 2004;31(11):1523-1529.

(24) Dewanjee MK, Ghafouripour AK, Kapadvanjwala M, Dewanjee S, Serafini AN, Lopez DM, et al. Noninvasive imaging of *c-myc* oncogene messenger RNA with indium-111-antisense probes in a mammary tumor-bearing mouse model. J.Nucl.Med. 1994;35(6):1054-1063.

(25) Wang J, Chen P, Mrkobrada M, Hu M, Vallis KA, Reilly RM. Antisense imaging of epidermal growth factor-induced p21[WAF-1/CIP-1] gene expression in MDA-MB-468 human breast cancer xenografts. Eur.J.Nucl.Med.Mol.Imaging 2003;30(9):1273-1280.

(26) Tian X, Chakrabarti A, Amirkhanov NV, Aruva MR, Zhang K, Mathew B, et al. External imaging of CCND1, MYC, and KRAS oncogene mRNAs with tumor-targeted radionuclide-PNA-peptide chimeras. Ann. New York Acad. Sci. 2005;1059:106-144.

(27) Tian X, Aruva MR, Zhang K, Shanthly N, Cardi CA, Thakur ML, et al. PET imaging of *CCND1* mRNA in human MCF7 estrogen receptor positive breast cancer xenografts with oncogene-specific [^{64}Cu]chelator-peptide nucleic acid-IGF1 analog radiohybridization probes. J.Nucl.Med. 2007;48(10):1699-1707.

(28) Roivainen A, Tolvanen T, Salomäki S, Lendvai G, Velikyan I, Numminen P, et al. ^{68}Ga-labeled oligonucleotides for in vivo imaging with PET. J.Nucl.Med. 2004;45(2):347-355.

(29) Lendvai G, Velikyan I, Bergstrom M, Estrada S, Laryea D, Valila M, et al. Biodistribution of ^{68}Ga-labelled phosphodiester, phosphorothioate, and 2'-*O*-methyl phosphodiester oligonucleotides in normal rats. Eur.J.Pharm.Sci. 2005 Sep;26(1):26-38.

(30) Serdons K, Verbruggen A, Bormans GM. Developing new molecular imaging probes for PET. Methods 2009 Jun;48(2):104-111.

(31) Miller PW, Long NJ, Vilar R, Gee AD. Synthesis of ^{11}C, ^{18}F, ^{15}O, and ^{13}N radiolabels for positron emission tomography. Angew.Chem.Int.Ed Engl. 2008;47(47):8998-9033.

(32) Elsinga PH. Radiopharmaceutical chemistry for positron emission tomography. Methods 2002 Jul;27(3):208-217.

(33) Coenen HH. Fluorine-18 labeling methods: Features and possibilities of basic reactions. Ernst Schering Res.Found.Workshop 2007(62):15-50.

(34) Dollé F. [^{18}F]fluoropyridines: From conventional radiotracers to the labeling of macromolecules such as proteins and oligonucleotides. Ernst Schering Res.Found.Workshop 2007(62):113-157.

(35) Wester HJ, Schottelius M. Fluorine-18 labeling of peptides and proteins. Ernst Schering Res.Found.Workshop 2007(62):79-111.

(36) De Vries EFJ, Vroegh J, Elsinga PH, Vaalburg W. Evaluation of fluorine-18-labeled alkylating agents as potential synthons for the labeling of oligonucleotides. Appl.Radiat.Isot. 2003;58(4):469-476.

(37) Kuhnast B, Dolle F, Vaufrey F, Hinnen F, Crouzel C, Tavitian B. Fluorine-18 labeling of oligonucleotides bearing chemically-modified ribose-phosphate backbones. J.Label.Compd.Radiopharm. 2000;43(8):837-848.

(38) Kuhnast B, Hinnen F, Boisgard R, Tavitian B, Dollé F. Fluorine-18 labelling of oligonucleotides: Prosthetic labelling at the 5´-end using the *N*-(4-[^{18}F]fluorobenzyl)-2-bromoacetamide reagent. J.Label.Compd.Radiopharm. 2003;46(12):1093-1103.

(39) Kuhnast B, Klussmann S, Hinnen F, Boisgard R, Rousseau B, Fürste JP, et al. Fluorine-18- and iodine-125-labelling of spiegelmers. J.Label.Compd.Radiopharm. 2003;46(13):1205-1219.

(40) Boisgard R, Kuhnast B, Vonhoff S, Younes C, Hinnen F, Verbavatz J, et al. In vivo biodistribution and pharmacokinetics of ^{18}F-labelled Spiegelmers: A new class of oligonucleotidic radiopharmaceuticals. Eur.J.Nucl.Med.Mol.Imaging 2005;32(4):470-477.

(41) Kuhnast B, Dolle F, Tavitian B. Fluorine-18 labeling of peptide nucleic acids. J.Label.Compd.Radiopharm. 2002;45(1):1-11.

(42) Hamzavi R, Dolle F, Tavitian B, Dahl O, Nielsen PE. Modulation of the pharmacokinetic properties of PNA: Preparation of galactosyl, mannosyl, fucosyl, *N*-acetylgalactosaminyl, and *N*-acetylglucosaminyl derivatives of aminoethylglycine peptide nucleic acid monomers and their incorporation into PNA oligomers. Bioconjugate Chem. 2003;14(5):941-954.

(43) Kuhnast B, De Bruin B, Hinnen F, Tavitian B, Dollé F. Design and synthesis of a new [^{18}F]fluoropyridine-based haloacetamide reagent for the labeling of oligonucleotides: 2-bromo-*N*-[3-(2-[^{18}F]fluoropyridin-3-yloxy)propyl]acetamide. Bioconjugate Chem. 2004;15(3):617-627.

(44) Viel T, Kuhnast B, Hinnen F, Boisgard R, Tavitian B, Dollé F. Fluorine-18 labelling of small interfering RNAs (siRNAs) for PET imaging. J.Label.Compd.Radiopharm. 2007;50(13):1159-1168.

(45) Viel T, Boisgard R, Kuhnast B, Jego B, Siquier-Pernet K, Hinnen F, et al. Molecular imaging study on in vivo distribution and pharmacokinetics of modified small interfering RNAs (siRNAs). Oligonucleotides 2008;18(3):201-212.

(46) De Vries EFJ, Vroegh J, Dijkstra G, Moshage H, Elsinga PH, Jansen PLM, et al. Synthesis and evaluation of a fluorine-18 labeled antisense oligonucleotide as a potential PET tracer for iNOS mRNA expression. Nucl.Med.Biol. 2004;31(5):605-612.

(47) Hnatowich DJ. Antisense and nuclear medicine. J.Nucl.Med. 1999;40(4):693-703.

(48) Loke SL, Stein CA, Zhang XH, Mori K, Nakanishi M, Subasinghe C, et al. Characterization of oligonucleotide transport into living cells. Proc.Natl.Acad.Sci.U.S.A. 1989 May;86(10):3474-3478.

(49) Yakubov LA, Deeva EA, Zarytova VF, Ivanova EM, Ryte AS, Yurchenko LV, et al. Mechanism of oligonucleotide uptake by cells: involvement of specific receptors? Proc.Natl.Acad.Sci.U.S.A. 1989 Sep;86(17):6454-6458.

(50) Lebedeva I, Benimetskaya L, Stein CA, Vilenchik M. Cellular delivery of antisense oligonucleotides. Eur.J.Pharm.Biopharm. 2000;50(1):101-119.

(51) Bartsch M, Weeke-Klimp AH, Meijer DKF, Scherphof GL, Kamps JAAM. Cell-specific targeting of lipid-based carriers for ODN and DNA. J.Liposome Res. 2005;15(1-2):59-92.

(52) Rejman J, Oberle V, Zuhorn IS, Hoekstra D. Size-dependent internalization of particles via the pathways of clathrin- and caveolae-mediated endocytosis. Biochem.J. 2004 Jan 1;377(Pt 1):159-169.

(53) Zhang Y, Wang Y, Liu N, Zhu Z-, Rusckowski M, Hnatowich DJ. In vitro investigations of tumor targeting with 99mTc-labeled antisense DNA. J.Nucl.Med. 2001;42(11):1660-1669.

(54) Hnatowich DJ, Nakamura K. The influence of chemical structure of DNA and other oligomer radiopharmaceuticals on tumor delivery. Curr.Opin.Mol.Ther. 2006 Apr;8(2):136-143.

(55) Lewis MR, Jia F. Antisense imaging: And miles to go before we sleep? J.Cell.Biochem. 2003;90(3):464-472.

(56) Rejman J, Bragonzi A, Conese M. Role of clathrin- and caveolae-mediated endocytosis in gene transfer mediated by lipo- and polyplexes. Mol.Ther. 2005 Sep;12(3):468-474.

(57) Dias N, Stein CA. Antisense oligonucleotides: basic concepts and mechanisms. Mol.Cancer.Ther. 2002 Mar;1(5):347-355.

(58) Zheng J, Tan T. Antisense imaging of colon cancer-bearing nude mice with liposome-entrapped 99m-technetium-labeled antisense oligonucleotides of *c-myc* mRNA. World J.Gastroenterol. 2004;10(17):2563-2566.

(59) Tavitian B, Marzabal S, Boutet V, Kühnast B, Terrazzino S, Moynier M, et al. Characterization of a synthetic anionic vector for oligonucleotide delivery using *in vivo* whole body dynamic imaging. Pharm.Res. 2002;19(4):367-376.

(60) Lee HJ, Boado RJ, Braasch DA, Corey DR, Pardridge WM. Imaging gene expression in the brain in vivo in a transgenic mouse model of Huntington's disease with an antisense radiopharmaceutical and drug-targeting technology. J.Nucl.Med. 2002 Jul;43(7):948-956.

(61) Brunner S, Furtbauer E, Sauer T, Kursa M, Wagner E. Overcoming the nuclear barrier: cell cycle independent nonviral gene transfer with linear polyethylenimine or electroporation. Mol.Ther. 2002 Jan;5(1):80-86.

(62) Nakamura K, Wang Y, Liu X, Kubo A, Hnatowich DJ. Influence of two transfectors on delivery of ^{99m}Tc antisense DNA in tumor-bearing mice. Mol.Imaging Biol. 2006;8(3):188-192.

(63) Ogris M, Steinlein P, Carotta S, Brunner S, Wagner E. DNA/polyethylenimine transfection particles: influence of ligands, polymer size, and PEGylation on internalization and gene expression. AAPS PharmSci 2001;3(3):E21.

(64) Fischer D, Osburg B, Petersen H, Kissel T, Bickel U. Effect of poly(ethylene imine) molecular weight and pegylation on organ distribution and pharmacokinetics of polyplexes with oligodeoxynucleotides in mice. Drug Metab.Dispos. 2004 Sep;32(9):983-992.

(65) Hicke BJ, Stephens AW, Gould T, Chang YF, Lynott CK, Heil J, et al. Tumor targeting by an aptamer. J.Nucl.Med. 2006 Apr;47(4):668-678.

(66) Vives E, Brodin P, Lebleu B. A truncated HIV-1 Tat protein basic domain rapidly translocates through the plasma membrane and accumulates in the cell nucleus. J.Biol.Chem. 1997 Jun 20;272(25):16010-16017.

(67) Zhang Y, Liu C, Liu N, Flores GF, He J, Rusckowski M, et al. Electrostatic binding with Tat and other cationic peptides increases cell accumulation of ^{99m}Tc-antisense DNAs without entrapment. Mol.Imaging Biol. 2003;5(4):240-247.

(68) Nakamura K, Wang Y, Liu X, Kubo A, Hnatowich DJ. Cell culture and xenograft-bearing animal studies of radiolabeled antisense DNA-carrier nanoparticles with streptavidin as a linker. J.Nucl.Med. 2007;48(11):1845-1852.

(69) Wang Y, Nakamura K, Liu X, Kitamura N, Kubo A, Hnatowich DJ. Simplified preparation via streptavidin of antisense oligomers/carriers nanoparticles showing improved cellular delivery in culture. Bioconjugate Chem. 2007;18(4):1338-1343.

(70) Tian X, Aruva MR, Qin W, Zhu W, Sauter ER, Thakur ML, et al. Noninvasive molecular imaging of MYC mRNA expression in human breast

cancer xenografts with a [99mTc]peptide-peptide nucleic acid-peptide chimera. Bioconjug.Chem. 2005 Jan-Feb;16(1):70-79.

(71) Tian X, Aruva MR, Qin W, Zhu W, Duffy KT, Sauter ER, et al. External imaging of CCND1 cancer gene activity in experimental human breast cancer xenografts with 99mTc-peptide-peptide nucleic acid-peptide chimeras. J.Nucl.Med. 2004 Dec;45(12):2070-2082.

(72) Zhang YM, Tung CH, He J, Liu N, Yanachkov I, Liu G, et al. Construction of a novel chimera consisting of a chelator-containing Tat peptide conjugated to a morpholino antisense oligomer for technetium-99m labeling and accelerating cellular kinetics. Nucl.Med.Biol. 2006 Feb;33(2):263-269.

(73) Zhang Y, Liu N, Zhu Z, Rusckowski M, Hnatowich DJ. Influence of different chelators (HYNIC, MAG$_3$ and DTPA) on tumor cell accumulation and mouse biodistribution of technetium-99m labeled to antisense DNA. Eur.J.Nucl.Med. 2000;27(11):1700-1707.

(74) Harper JW, Adami GR, Wei N, Keyomarsi K, Elledge SJ. The p21 Cdk-interacting protein Cip1 is a potent inhibitor of G1 cyclin-dependent kinases. Cell 1993 Nov 19;75(4):805-816.

(75) Mirzayans R, Murray D. Cellular senescence: implications for cancer therapy. In: Garvey RB, editor. New research on cell aging Hauppauge, NY: Nova Science Publishers, Inc; 2007. p. 1-64.

(76) Jänicke RU, Sohn D, Essmann F, Schulze-Osthoff K. The multiple battles fought by anti-apoptotic p21. Cell Cycle 2007;6(4):407-413.

(77) Mazzatti DJ, Lee Y, Helt CE, O'Reilly MA, Keng PC. p53 modulates radiation sensitivity independent of p21 transcriptional activation. Am.J.Clin.Oncol.Cancer Clin.Trials 2005;28(1):43-50.

(78) Belka C. The fate of irradiated tumor cells. Oncogene 2006;25(7):969-971.

(79) Wendt J, Radetzki S, Von Haefen C, Hemmati PG, Güner D, Schulze-Osthoff K, et al. Induction of p21[CIP/WAF-1] and G2 arrest by ionizing irradiation impedes caspase-3-mediated apoptosis in human carcinoma cells. Oncogene 2006;25(7):972-980.

(80) Mirzayans R, Scott A, Cameron M, Murray D. Induction of accelerated senescence by γ radiation in human solid tumor-derived cell lines expressing wild-type TP53. Radiat.Res. 2005;163(1):53-62.

(81) Schmitt CA, Fridman JS, Yang M, Lee S, Baranov E, Hoffman RM, et al. A senescence program controlled by p53 and p16^{INK4a} contributes to the outcome of cancer therapy. Cell 2002 5/3;109(3):335-346.

(82) McBride WH, Chiang C, Olson JL, Wang C, Hong J, Pajonk F, et al. A sense of danger from radiation. Radiat.Res. 2004;162(1):1-19.

(83) Waldman T, Zhang Y, Dillehay L, Yu J, Kinzler K, Vogelstein B, et al. Cell-cycle arrest versus cell death in cancer therapy. Nat.Med. 1997;3(9):1034-1036.

(84) Roninson IB, Broude EV, Chang BD. If not apoptosis, then what? Treatment-induced senescence and mitotic catastrophe in tumor cells. Drug Resist.Updat. 2001 Oct;4(5):303-313.

(85) Mirzayans R, Murray D. Pharmacological modulation of p53 function in cancer therapy. Curr.Signal Transduction Ther. 2008;3(3):183-194.

(86) Elmore LW, Di X, Dumur C, Holt SE, Gewirtz DA. Evasion of a single-step, chemotherapy-induced senescence in breast cancer cells: implications for treatment response. Clin.Cancer Res. 2005 Apr 1;11(7):2637-2643.

(87) Sak A, Wurm R, Elo B, Grehl S, Pöttgen C, Stüben G, et al. Increased radiation-induced apoptosis and altered cell cycle progression of human lung cancer cell lines by antisense oligodeoxynucleotides targeting p53 and p21$^{WAF1/CIP1}$. Cancer Gene Ther. 2003;10(12):926-934.

(88) Crescenzi E, Palumbo G, De Boer J, Brady HJM. Ataxia telangiectasia mutated and p21^{CIP1} modulate cell survival of drug-induced senescent tumor cells: Implications for chemotherapy. Clin.Cancer Res. 2008;14(6):1877-1887.

(89) Ohtsubo M, Gamou S, Shimizu N. Antisense oligonucleotide of *WAF1* gene prevents EGF-induced cell-cycle arrest in A431 cells. Oncogene 1998;16(6):797-802.

(90) Poluha W, Poluha DK, Chang B, Crosbie NE, Schonhoff CM, Kilpatrick DL, et al. The cyclin-dependent kinase inhibitor p21^{WAF1} is required for survival of differentiating neuroblastoma cells. Mol.Cell.Biol. 1996;16(4):1335-1341.

(91) Tian H, Wittmack EK, Jorgensen TJ. p21$^{WAF1/CIP1}$ antisense therapy radiosensitizes human colon cancer by converting growth arrest to apoptosis. Cancer Res. 2000 Feb 1;60(3):679-684.

(92) Kokunai T, Urui S, Tomita H, Tamaki N. Overcoming of radioresistance in human gliomas by p21$^{WAF1/CIP1}$ antisense oligonucleotide. J.Neurooncol. 2001 Jan;51(2):111-119.

(93) Liu X, Nakamura K, Wang Y, Wang Y, Liu G, He J, et al. Initial mechanistic studies of antisense targeting in cells. J.Nucl.Med. 2006 Feb;47(2):360-368.

(94) Zhang YM, Rusckowski M, Liu N, Liu C, Hnatowich DJ. Cationic liposomes enhance cellular/nuclear localization of ^{99m}Tc-antisense oligonucleotides in target tumor cells. Cancer Biother.Radiopharm. 2001 Oct;16(5):411-419.

(95) Stalteri MA, Mather SJ. Hybridization and cell uptake studies with radiolabelled antisense oligonucleotides. Nucl.Med.Commun. 2001 Nov;22(11):1171-1179.

(96) Hnatowich DJ, Mardirossian G, Fogarasi M, Sano T, Smith CL, Cantor CR, et al. Comparative properties of a technetium-99m-labeled single-stranded natural DNA and a phosphorothioate derivative in vitro and in mice. J.Pharmacol.Exp.Ther. 1996 Jan;276(1):326-334.

(97) Kobori N, Imahori Y, Mineura K, Ueda S, Fujii R. Visualization of mRNA expression in CNS using ^{11}C-labeled phosphorothioate oligodeoxynucleotide. Neuroreport 1999 Sep 29;10(14):2971-2974.

(98) Wu F, Yngve U, Hedberg E, Honda M, Lu L, Eriksson B, et al. Distribution of ^{76}Br-labeled antisense oligonucleotides of different length determined ex vivo in rats. Eur.J.Pharm.Sci. 2000;10(3):179-186.

(99) Wu F, Lendvai G, Yngve U, Eriksson B, Långström B, Bergström M. Hybridisation of [^{76}Br]-labelled antisense oligonucleotides to Chromogranin A mRNA verified by RT-PCR. Nucl.Med.Biol. 2004;31(8):1073-1078.

(100) Lendvai G, Velikyan I, Estrada S, Eriksson B, Långström B, Bergström M. Biodistribution of ^{68}Ga-labeled LNA-DNA mixmer antisense oligonucleotides for rat chromogranin-A. Oligonucleotides 2008;18(1):33-49.

(101) Liu M, Wang RF, Zhang CL, Yan P, Yu MM, Di LJ, et al. Noninvasive imaging of human telomerase reverse transcriptase (hTERT) messenger RNA with ^{99m}Tc-radiolabeled antisense probes in malignant tumors. J.Nucl.Med. 2007 Dec;48(12):2028-2036.

(102) Qin G, Zhang Y, Cao W, An R, Gao Z, Li G, et al. Molecular imaging of atherosclerotic plaques with technetium-99m-labelled antisense oligonucleotides. Eur.J.Nucl.Med.Mol.Imaging 2005 Jan;32(1):6-14.

(103) Mang'era KO, Liu G, Yi W, Zhang Y, Liu N, Gupta S, et al. Initial investigations of ^{99m}Tc-labeled morpholinos for radiopharmaceutical applications. Eur.J.Nucl.Med. 2001 Nov;28(11):1682-1689.

(104) Mardirossian G, Lei K, Rusckowski M, Chang F, Qu T, Egholm M, et al. In vivo hybridization of Technetium-99m-labeled peptide nucleic acid (PNA). J.Nucl.Med. 1997;38(6):907-913.

(105) Laforest R, Liu X. Cascade removal and microPET imaging with 76Br. Phys.Med.Biol. 2009 Mar 21;54(6):1503-1531.

(106) Wang Y, Liu X, Nakamura K, Chen L, Rusckowski M, Hnatowich DJ. In vivo delivery of antisense MORF oligomer by MORF/carrier streptavidin nanoparticles. Cancer Biother.Radiopharm. 2009 Oct;24(5):573-578.

(107) Sun X, Fang H, Li X, Rossin R, Welch MJ, Taylor JS. MicroPET imaging of MCF-7 tumors in mice via unr mRNA-targeted peptide nucleic acids. Bioconjug.Chem. 2005 Mar-Apr;16(2):294-305.

(108) Suzuki T, Wu D, Schlachetzki F, Li JY, Boado RJ, Pardridge WM. Imaging endogenous gene expression in brain cancer in vivo with ^{111}In-peptide nucleic acid antisense radiopharmaceuticals and brain drug-targeting technology. J.Nucl.Med. 2004 Oct;45(10):1766-1775.

CHAPTER 2

Automated Radiosynthesis of *N*-(4-[^{18}F]Fluorobenzyl)-2-Bromoacetamide: an F-18-Labelled Reagent for the Prosthetic Radiolabelling of Oligonucleotides

A version of this chapter has been published in the Journal of Labelled Compounds and Radiopharmaceuticals, August 2008, by I. Koslowsky, S. Shahhosseini, J. Wilson, and J. Mercer.

The work presented in this chapter was carried out by I. Koslowsky with technical assistance from S. Shahhosseini.

2.1 Introduction

Following the first reported radiolabelling of an antisense oligonucleotide (asODN) in 1994 (1), there has been active interest in radiolabelling these biological molecules for imaging gene expression. asODNs are short pieces of single stranded DNA or RNA, typically 13 to 25 nucleobases in length, with a sugar-phosphate backbone. The native phosphodiester backbone can be modified with various functional groups to increase the stability of the ODNs *in vivo* (2). An asODN with a specific nucleotide sequence has the ability to hybridize with its complementary 'sense' mRNA which, in therapeutic concentrations, can inhibit specific gene expression. From a diagnostic/clinical perspective, ODNs can be tagged with a radioactive probe in order to detect upregulated gene expression in various diseases, such as cancer. Our specific interest is to use ODNs as probes to measure early cellular response to drug or radiation treatment. This would be an invaluable tool for clinicians as it offers prognostic information regarding the success (or failure) of treatment, and ultimately, on patient outcome. The enhanced detection and resolution that is available with positron emission tomography (PET) has encouraged the development of PET labelled oligonucleotides. A variety of synthetic methods have been described for the labelling of ODNs with [^{18}F]fluoride. Pan *et al* (3) reported the direct labelling of a native (phosphodiester) ODN with 5′-deoxy-5′-[^{18}F]-*O*-methylthymidine. Using a hexylamine linker ODNs have also been labelled with 4-([^{18}F]]fluoromethyl)phenyl isothiocyanate (4), *N*-succinimidyl 4-[^{18}F]fluorobenzoate (5,6), and the photosensitive compound, 3-azido-5-

nitrobenzyl-[^{18}F]fluoride (7). Toyokuni *et al* (8) synthesized an [^{18}F]-labelled maleimide agent for conjugation to ODNs containing a 5′-hexylthiol linker. de Vries *et al* (9,10) investigated a number of ^{18}F-labelled alkylating agents for their ability to radiolabel a monophosphorothioated nucleotide and a hexylthiol-reactive ODN. Their investigations included the alkylating agent *N*-(4-[^{18}F]fluorobenzyl)-2-bromoacetamide, the synthesis of which was originally described by Dollé *et al* in 1997 (11). Use of *N*-(4-[^{18}F]fluorobenzyl)-2-bromoacetamide has since been extensively reported by the Orsay group and has been used to label the 3′-monophosphorothioated end of a native phosphodiester ODN (12), a fully phosphorothioated ODN, 2′O-methyl-modified RNA, or hybrid phosphodiester methylphosphonate ODN (13,14); the 5′-phosphorothioated 2′O-methyl-modified RNA (15); 3′- or 5′ labelled RNA and DNA spiegelmers (16,17); and peptide nucleic acids (18-20). A related bromoacetamide reagent has also been described by this group for the labelling of monophosphorothioated ODNs, modified RNAs (21), and small interfering RNAs (22).

The first step in the synthesis of *N*-(4-[^{18}F]fluorobenzyl)-2-bromoacetamide is the nucleophilic substitution reaction of [^{18}F]fluoride anion with a trimethylanilinium precursor. Thus all reactions in this multi-step synthesis require the manipulation of radioactivity. High activities of [^{18}F]fluoride must be employed at the start of the synthesis in order to obtain a sufficient amount of radiolabelled oligonucleotide for biological studies. The issues of radiation safety and the complexity of the synthesis make it an ideal candidate for remote automated preparation using robotic systems or automated synthesis units (ASUs). The

intent of this work was to modify a commercially available ASU (General Electric TRACERlab Fx_{FDG}) for the synthesis of *N*-(4-[^{18}F]fluorobenzyl)-2-bromoacetamide as described in the literature.

2.2   Materials and Methods

2.2.1   General

Chemicals. Chemicals were purchased from Sigma-Aldrich (St. Louis, MO, USA) or Caledon Lab (Georgetown, ON, Canada) and were used without further purification. [^{18}F]fluoride was produced in-house using the Edmonton PET Center Cyclotron Facility.

Fully phosphorothioated, 20-mer oligonucleotides were purchased from the University Core DNA Services, Calgary, Canada: an antisense oligonucleotide complementary to the 3′-untranslated region of human *p21^{WAF1}* mRNA with the sequence 5′-TGT.CAT.GCT.GGT.CTG.CCG.CC-3′ (23) and a random sequence oligonucleotide sequence (5′-CCG.GTG.AAC.GAG.CGA.GCA.CA-3′) (24). The above oligonucleotides, with *N*-(4-fluorobenzyl)-2-bromoacetamide substituted in the 5′ position, were synthesized by the University Core DNA Services for use as reference compounds. Mass spectra and HPLC retention times for fluorinated and nonfluorinated ODNs are provide in Table 2-1.

Analytical methods. Thin layer chromatography (TLC) was performed using MK6F Silica Gel 60Å, 250 µm plates (Whatman, UK) and visualized under u.v. illumination at 254 nm. Heptane:ethyl acetate, 50:50 was used as the mobile phase for all TLC analyses. Radio-TLC was performed with an AR-2000 imaging scanner (Bioscan Inc, Washington, DC). Radio-TLC results were

compared with corresponding TLC of nonradioactive reference compounds. The concentration of ODN was determined by u.v. spectroscopy at 260 nm using a Beckman DU 7400 spectrophotometer. Reverse phase high pressure liquid chromatography (HPLC) analyses and purifications were performed with a Beckman Coulter Inc system consisting of a Model 168 Diode Array u.v. module, 254nm; a Model 126 analytical dual pump; a radioactivity detector (Ortec, TN): ACE *Mate*™ Single Channel Analyzer; and a Whatman Partisil 10 ODS-3, 9.4 x 50 mm column (Whatman, UK) with guard column.

2.2.2 Chemistry

The method of Dollé *et al* (11) was utilized for the synthesis of the nonradioactive, fluorinated reference compound, *N*-(4-fluorobenzyl)-2-bromoacetamide as well as synthesis of the precursor **(1)** with the exception that *N*-(4-fluorobenzyl)-2-bromoacetamide was recrystallized in cyclohexane (37% yield). TLC and NMR spectra were in agreement with that published earlier (11).

2.2.3 Radiochemistry

2.2.3.1 *Synthesis of N-(4-[^{18}F]fluorobenzyl)-2-bromoacetamide ([^{18}F]-4)*

Aqueous [^{18}F]fluoride (4 to 15.3 GBq) was transferred to a GE TRACERlab FX$_{FDG}$ automated synthesis unit (GE Healthcare, WS) and loaded onto a preconditioned Chromafix 30-PS-HCO$_3$ cartridge, (Machery-Nagel, Germany). The ^{18}F was then eluted into the reaction vessel (reactor 1) with the Kryptofix® eluant (Figure 2-2, V1) consisting of 16 mg of Kryptofix®222 (4,7,13,16,21,24-hexaoxa-1,10-diazabicyclo[8.8.8]hexacosane) and 2.7 mg of potassium carbonate in 0.8 mL of a 77.5%/22.5% mixture of acetonitrile and water. The solvent was

co-evaporated with 0.8 mL acetonitrile (Figure 2-2, V2) at 55°C over 6 minutes with a stream of nitrogen and reduced pressure. The contents were then heated to 95°C under full vacuum to remove residual water. The precursor (Figure 2-2, V3) was transferred to the reaction vessel (10 mg in 0.8 mL anhydrous DMSO) and the reaction proceeded at 130°C for 10 minutes. The temperature was reduced to 40°C followed by transfer of the mixture to a preconditioned Sep-Pak Plus® C18 cartridge (Waters Corp, MA) with 10 mL water (Figure 2-2, V5). The cartridge was partially dried with nitrogen for 3 minutes. Residual water in reactor 1 was azeotropically removed with 1 mL toluene (Figure 2-2, V4) at 150°C for 2 minutes. 4-[^{18}F]fluorobenzonitrile (**[^{18}F]-2**) was then eluted from the C18 cartridge with 6 mL of anhydrous THF (Figure 2-2, V6) through a series of drying columns consisting of a 2.5 g sodium sulphate cartridge (International Sorbent Technology Inc, UK) followed by a column containing 4 g of ground molecular sieves (4 Å). The mixture was allowed to interact with the molecular sieves for 4 to 6 minutes before transferring the material via a SepPak silica cartridge (Waters Corp, MA) to reactor 2 containing 1 mL of a 1 M solution of LiAlH$_4$ in THF. Reduction of the nitrile group proceeded at 100°C for 2 minutes. The reaction mixture was cooled to 50°C and the solvent removed under reduced pressure and nitrogen. Water (400 µL; Figure 2-2, V7) was subsequently added to destroy the lithium aluminum complex followed by the addition of a 1:100 dilution of bromoacetyl bromide in methylene chloride (1 mL) (Figure 2-2, V9). The reaction proceeded for 2 minutes at 35°C. Methylene chloride (5 mL)

(Figure 2-2, V8) was added and the soluble components were dispensed through a 1 µm glass fibre filter (Waters, MA) into a vented, 10 mL vial.

The clear, colourless **[¹⁸F]-4** reaction mixture was concentrated to dryness under low heat and a stream of nitrogen. The residue was redissolved in methanol, reserving an aliquot for radio-TLC analysis, and the remainder purified with the following HPLC gradient system: acetonitrile 5% (*aq*) to 95% over 20 minutes; flow rate: 6 mL/min; retention time (t_R): 13.3 minutes. The centre fraction of the peak representing **[¹⁸F]-4** was collected to avoid the collection of non radioactive side products formed during synthesis (t_R: 15.4 min) as well as unreacted reagents such as bromoacetyl bromide (t_R: 10 min) and concentrated to dryness using azeotropic distillation under a gentle stream of nitrogen. Radio-TLC of the reaction mixture was performed before and after purification by HPLC. The occasional sample of purified **[¹⁸F]-4** was analyzed by RP-HPLC to verify radio-TLC results. The samples were co-spotted with non-radioactive *N*-(4-fluorobenzyl)-2-bromoacetamide (R_f 0.4).

2.2.3.2 Radiolabelling of oligonucleotide (ODN)

Lyophilized ODN (148 nmol, 1 mg) was reconstituted with 1 mL of phosphate buffered saline (PBS) 0.1 M, pH 8 mixed with methanol, 1:1 (v/v) and added to **[¹⁸F]-4**. The mixture was heated in a vented vial at 120°C for 30 minutes. The volume of the reaction mixture was maintained by the addition of 0.5 to 1 mL of 50% methanol midway through the reaction. Unreacted **[¹⁸F]-4** was separated from the radiolabelled ODN with a NAP™-10 column (GE Healthcare, UK). The ODN was eluted with 1.5 mL PBS 0.01 M, pH 7.2. No further purification was

performed. The concentration of ODN in the eluate was determined by u.v. spectroscopy at 260 nm. Analysis of the mixture was performed with radio-TLC (R$_f$ [^{18}F]ODN: 0.0; **[^{18}F]-4**: 0.4) and by HPLC using the following gradient system: Triethylammonium acetate 0.1 M, pH 7/acetonitrile, 95/5 to 90/10 over 3 minutes, followed by 90/10 to 75/25 over 7 minutes, with a washout phase of 50/50 for 10 minutes; flow rate: 6 mL/min; retention time: 14.6 to 14.9 minutes. The [^{18}F]ODNs eluted with the same retention time as the non-radioactive, fluorinated ODNs (Table 2-1).

2.3   Results

2.3.1   *Chemistry*

2.3.1.1   Synthesis of N-(4-[^{18}F]fluorobenzyl)-2-bromoacetamide ([^{18}F]-4)

The multi-step synthesis of **[^{18}F]-4** reported by Dollé *et al* (11) (Figure 2-1) was adapted to permit automation using the TRACERlab Fx$_{FDG}$ ASU. This ASU incorporates two separate reaction trains, each designed for the synthesis of 2-[^{18}F]fluorodeoxyglucose (FDG). Both reaction trains and reactors were required for the preparation of **[^{18}F]-4**. A schematic diagram of the ASU modified for this synthesis is illustrated in Figure 2-2.

The synthesis of 4-[^{18}F]fluorobenzonitrile (**[^{18}F]-2**) was achieved by displacement of the quaternary ammonium leaving group of the precursor 4-cyano-*N,N,N*-trimethylanilinium trifluoromethanesulfonate (**1**) with [^{18}F]fluoride at elevated temperature in dimethyl sulfoxide (DMSO). Previous reports have used different reaction conditions for the synthesis of **[^{18}F]-2**. Dollé *et al* (11) heated the precursor for 20 minutes at 120°C resulting in a yield of 60 to 85%. Kuhnast *et al*

(13) performed the reaction at 180°C for 20 minutes with similar yields. As 165°C is the maximum temperature to which the reactors in this ASU can be heated, the synthesis of [¹⁸F]-2 was performed at two temperatures, 130°C and 160°C, for 10 or 20 minutes to determine the optimum temperature for this reaction. As seen in Figure 2-3, no difference in radiochemical purity (RCP) as determined by radio-thin layer chromatography (radio-TLC) or yield was observed when varying the temperature or length of reaction. Decay corrected radiochemical yields (with respect to [^{18}F]fluoride ion at end of bombardment and prior to the transfer of [^{18}F]-2 to the C18 Sep-Pak cartridge) varied widely but typically ranged between 40 and 50%. However, fewer nonradioactive side products were observed by thin layer chromatography at 254 nm at the lower temperature (130°C) and shorter reaction time and these could be removed via Sep-Pak purification or ultimately by reverse phase HPLC (RP-HPLC) purification of [^{18}F]-4. Therefore the reaction conditions of 130°C for 10 minutes were chosen for the synthesis of [^{18}F]-2. Upon completion of this step, water was added to reactor 1 to transfer the reaction mixture containing [^{18}F]-2 to a C18 Sep-Pak cartridge. The cartridge was washed with additional water (via reactor 1) to remove unreacted reagents and water-soluble side products.

The following step, i.e. the conversion of the nitrile group of [^{18}F]-2 to the amine of [^{18}F]-3, utilizes lithium aluminum hydride (LiAlH$_4$), and thus requires anhydrous conditions. Reactor 1 acts as a conduit for the transfer of anhydrous tetrahydrofuran (THF) and is used for the elution of [^{18}F]-2 from the C18 Sep-Pak cartridge to reactor 2. Thus, toluene was used to azeotropically remove residual

water from reactor 1 prior to the elution of **[^{18}F]-2** with THF. Residual water in the tubing and on the Sep-Pak cartridge was removed by passing the reaction mixture through a series of drying columns. The transfer of activity from reactor 1 to reactor 2 resulted in the largest loss of radioactivity (based on readings from radioactivity detectors located under the reactors) with approximately 17 to 38% of the original activity transferred to reactor 2. Losses depended in part on the radiochemical yield of **[^{18}F]-2** (a higher yield reduced the amount of unreacted [^{18}F]fluoride in the waste with more **[^{18}F]-2** transferred to the drying cartridges), and in part on product retention on the molecular sieve drying column and cartridges. Decreasing the amount of molecular sieves or eliminating the sodium sulphate or silica cartridges increased the amount of radioactivity transferred to reactor 2, however residual water carried into the reactor likely consumed a portion of the reducing agent, LiAlH$_4$, and ultimately resulted in a lower RCP and yield of **[^{18}F]-4**.

In the conversion of **[^{18}F]-2** to 4-[^{18}F]fluorobenzylamine (**[^{18}F]-3**) reaction temperatures of 120°C to 140°C were reported by Kuhnast *et al* (13,15). In our system lower temperatures were used to prevent losses of volatile **[^{18}F]-2**. Trial reactions at longer reaction times and/or lower temperatures gave inconsistent results and did not improve the RCP or yield of **[^{18}F]-4**. The use of powdered, dry LiAlH$_4$ was generally observed to produce lower yields of **[^{18}F]-4** versus commercially available LiAlH$_4$ solution in THF. This may be due to inefficient mixing of powdered LiAlH$_4$ with the reaction mixture. The final step, the condensation with 2-bromoacetyl bromide, was quantitative. With the above

modifications, a mean radiochemical purity of 80% of **[^{18}F]-4** was achieved with decay corrected radiochemical yields (before HPLC purification) ranging from 3 to 18% with a synthesis time of 1 hour. The **[^{18}F]-4** reaction mixture was purified by RP-HPLC and a centre cut of the radioactive peak representing **[^{18}F]-4** was collected. A mean decay corrected yield of 3.8% (n = 9) was achieved after purification. Typically, 100 to 200 MBq of purified **[^{18}F]-4** could be obtained for radiolabelling ODNs from starting [^{18}F]fluoride of 10 GBq.

2.3.1.2 *Radiolabelling of oligonucleotide (ODN)*

Preliminary experiments have resulted in radiochemical yields of 36% (as determined by the fraction of radioactivity in the ODN reaction mixture eluted as [^{18}F]-labelled ODN) when the reaction was carried out at atmospheric pressure in a vented vial. Lower yields and additional side products were observed when the reaction was performed in a sealed vial. The use of a Sephadex G-25 DNA grade mini-column for purification negated the need for HPLC and provided a rapid purification with less loss of radioactivity. The disadvantage of purification with this method, however, is that unreacted ODN is co-eluted with the radiolabelled product resulting in lower specific activity. Preliminary results show similar yields of [^{18}F]ODN with 0.5 to 1 mg of ODN. Reducing the amount of starting material would improve the specific activity assuming that the yields remain the same. Currently, specific activities of 1.1 GBq/µmol (at end of synthesis) have been attained using the above method.

2.4   Discussion

The multi-step synthesis of [^{18}F]-4 is challenging to perform using commercial ASUs designed for simpler syntheses. The synthesis of [^{18}F]-4 as described in the literature cannot be performed in a single reaction vessel and synthesis units designed for clinically used products such as [^{18}F]FDG typically do not have 2 reaction trains. Thus these units are not designed to transfer materials in and out of the same vessel. Nor are sufficient reagent vessels available for a multi-step synthesis. A scrupulous cleaning or drying step of the reaction vessel may also be required between steps in a synthesis. This complicates the possibility of reusing a reactor. The TRACERlab FX$_{FDG}$ synthesis unit is unique in that it contains 2 reactors which can be interconnected, with minor modifications, between the Sep-Pak cartridge and reactor 2. The challenge in the use of this ASU for the synthesis of [^{18}F]-4 is the difficulty in eliminating water from [^{18}F]-2 prior to its transfer to reactor 2 containing LiAlH$_4$, as well as the losses of radioactivity with each transfer. For example, the transfer from reactor 1 to reactor 2 often resulted in the loss of up 75% of the radioactivity. Also, purification of [^{18}F]-4 by RP-HPLC adds time to the total synthesis as well as loss of product. Use of a normal phase HPLC system could improve the yield of purified [^{18}F]-4 simply due to the faster removal of the organic mobile phase solvents as compared with those used in RP-HPLC. Modular research synthesis units for complex syntheses should allow improved flexibility in the synthetic design and allow more efficient transfer of solutions and reagents. Purification with an HPLC directly attached to the modular ASUs also reduces loss of product.

2.5 Conclusion

Regardless of the limitations stated above, sufficient N-(4-[^{18}F]fluorobenzyl)-2-bromoacetamide can be produced in ASUs designed for clinical products to permit radiolabelling of ODNs for our ongoing investigations with gene expression imaging in biological models.

2.6 References

(1) Dewanjee MK, Ghafouripour AK, Kapadvanjwala M, Dewanjee S, Serafini AN, Lopez DM, et al. Noninvasive imaging of *c-myc* oncogene messenger RNA with indium-111-antisense probes in a mammary tumor-bearing mouse model. J.Nucl.Med. 1994;35(6):1054-1063.

(2) Haberkorn U, Mier W, Eisenhut M. Scintigraphic imaging of gene expression and gene transfer. Curr.Med.Chem. 2005;12(7):779-794.

(3) Pan D, Gambhir SS, Toyokuni T, Iyer MR, Acharya N, Phelps ME, et al. Rapid synthesis of a 5'-fluorinated oligodeoxy-nucleotide: A model antisense probe for use in imaging with positron emission tomography (PET). Bioorg.Med.Chem.Lett. 1998;8(11):1317-1320.

(4) Hedberg E, Långström B. Synthesis of 4-([^{18}F]fluoromethyl)phenyl isothiocyanate and its use in labelling oligonucleotides. Acta Chem.Scand. 1997;51(12):1236-1240.

(5) Hedberg E, Långström B. ^{18}F-labelling of oligonucleotides using succinimido 4-[^{18}F]fluorobenzoate. Acta Chem.Scand. 1998;52(8):1034-1039.

(6) Li J, Trent JO, Bates PJ, Ng CK. Labeling G-rich oligonucleotides (GROs) with N-succinimidyl 4-[^{18}F]fluorobenzoate (S^{18}FB). J.Label.Compd.Radiopharm. 2006;49(14):1213-1221.

(7) Lange CW, VanBrocklin HF, Taylor SE. Photoconjugation of 3-azido-5-nitrobenzyl-[^{18}F]fluoride to an oligonucleotide aptamer. J.Label.Compd.Radiopharm. 2002;45(3):257-268.

(8) Toyokuni T, Walsh JC, Dominguez A, Phelps ME, Barrio JR, Gambhir SS, et al. Synthesis of a new heterobifunctional linker, *N*-[4-(aminooxy)butyl]maleimide, for facile access to a thiol-reactive ^{18}F-labeling agent. Bioconjugate Chem. 2003;14(6):1253-1259.

(9) de Vries EFJ, Vroegh J, Elsinga PH, Vaalburg W. Evaluation of fluorine-18-labeled alkylating agents as potential synthons for the labeling of oligonucleotides. Appl.Radiat.Isot. 2003;58(4):469-476.

(10) de Vries EF, Vroegh J, Dijkstra G, Moshage H, Elsinga PH, Jansen PL, et al. Synthesis and evaluation of a fluorine-18 labeled antisense oligonucleotide as a potential PET tracer for iNOS mRNA expression. Nucl.Med.Biol. 2004 Jul;31(5):605-612.

(11) Dolle F, Hinnen F, Vaufrey F, Tavitian B, Crouzel C. A general method for labeling oligodeoxynucleotides with ^{18}F for *in vivo* PET imaging. J.Label.Compd.Radiopharm. 1997;39(4):319-330.

(12) Kuhnast B, Dolle F, Terrazzino S, Rousseau B, Loc'h C, Vaufrey F, et al. General method to label antisense oligonucleotides with radioactive halogens for pharmacological and imaging studies. Bioconjugate Chem. 2000;11(5):627-636.

(13) Kuhnast B, Dolle F, Vaufrey F, Hinnen F, Crouzel C, Tavitian B. Fluorine-18 labeling of oligonucleotides bearing chemically-modified ribose-phosphate backbones. J.Label.Compd.Radiopharm. 2000;43(8):837-848.

(14) Tavitian B, Terrazzino S, Kühnast B, Marzabal S, Stettler O, Dollé F, et al. *In vivo* imaging of oligonucleotides with positron emission tomography. Nat.Med. 1998;4(4):467-470.

(15) Kuhnast B, Hinnen F, Boisgard R, Tavitian B, Dollé F. Fluorine-18 labelling of oligonucleotides: Prosthetic labelling at the 5'-end using the *N*-(4-[^{18}F]fluorobenzyl)-2-bromoacetamide reagent. J.Label.Compd.Radiopharm. 2003;46(12):1093-1103.

(16) Boisgard R, Kuhnast B, Vonhoff S, Younes C, Hinnen F, Verbavatz J-, et al. In vivo biodistribution and pharmacokinetics of ^{18}F-labelled Spiegelmers: A new class of oligonucleotidic radiopharmaceuticals. Eur.J.Nucl.Med.Mol.Imaging 2005;32(4):470-477.

(17) Kuhnast B, Klussmann S, Hinnen F, Boisgard R, Rousseau B, Fürste JP, et al. Fluorine-18- and iodine-125-labelling of spiegelmers. J.Label.Compd.Radiopharm. 2003;46(13):1205-1219.

(18) Kuhnast B, Dolle F, Tavitian B. Fluorine-18 labeling of peptide nucleic acids. J.Label.Compd.Radiopharm. 2002;45(1):1-11.

(19) Kuhnast B, Hinnen F, Hamzavi R, Boisgard R, Tavitian B, Nielsen PE, et al. Fluorine-18 labelling of PNAs functionalized at their pseudo-peptidic backbone for imaging studies with PET. J.Label.Compd.Radiopharm. 2005;48(1):51-61.

(20) Hamzavi R, Dolle F, Tavitian B, Dahl O, Nielsen PE. Modulation of the pharmacokinetic properties of PNA: Preparation of galactosyl, mannosyl, fucosyl, *N*-acetylgalactosaminyl, and *N*-acetylglucosaminyl derivatives of aminoethylglycine peptide nucleic acid monomers and their incorporation into PNA oligomers. Bioconjugate Chem. 2003;14(5):941-954.

(21) Kuhnast B, De Bruin B, Hinnen F, Tavitian B, Dollé F. Design and synthesis of a new [^{18}F]fluoropyridine-based haloacetamide reagent for the labeling of

oligonucleotides: 2-bromo-*N*-[3-(2-[^{18}F]fluoropyridin-3-yloxy)propyl]acetamide. Bioconjugate Chem. 2004;15(3):617-627.

(22) Viel T, Kuhnast B, Hinnen F, Boisgard R, Tavitian B, Dollé F. Fluorine-18 labelling of small interfering RNAs (siRNAs) for PET imaging. J.Label.Compd.Radiopharm. 2007;50(13):1159-1168.

(23) Poluha W, Poluha DK, Chang B, Crosbie NE, Schonhoff CM, Kilpatrick DL, et al. The cyclin-dependent kinase inhibitor p21*WAF1* is required for survival of differentiating neuroblastoma cells. Mol.Cell.Biol. 1996;16(4):1335-1341.

(24) Tian H, Wittmack EK, Jorgensen TJ. p21[WAF1/CIP1] antisense therapy radiosensitizes human colon cancer by converting growth arrest to apoptosis. Cancer Res. 2000 Feb 1;60(3):679-684.

Table 2-1   Mass spectrometry and HPLC analyses of 20-mer oligonucleotide

Sequence	Calc Mass [M]	Major peak observed	HPLC t_R (min)
5′-ps-TGT.CAT.GCT.GGT. CTG.CCG.CC	6477.2	6475.2	13.8
5′-FBBA-ps-TGT.CAT.GCT.GGT. CTG.CCG.CC	6642.4	6643.7	14.6
5'-ps-CCG.GTG.AAC.GAG.CGA.GCA.CA	6562.3	6561.2	13.7
5'-FBBA-ps-CCG.GTG.AAC.GAG.CGA.GCA.CA	6727.5	6733.2	14.4

*fully phosphorothioated oligonucleotides
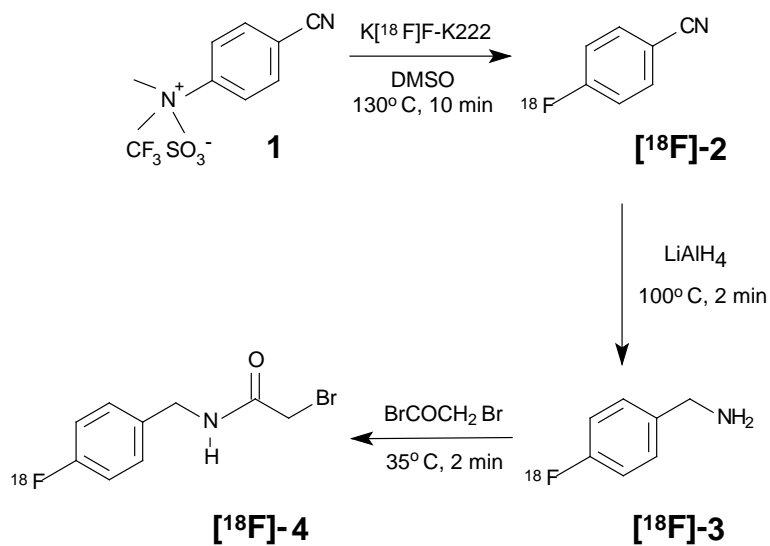
Figure 2-1   Synthesis of *N*-(4-[^{18}F]fluorobenzyl)-2-bromoacetamide ([^{18}F]-4)
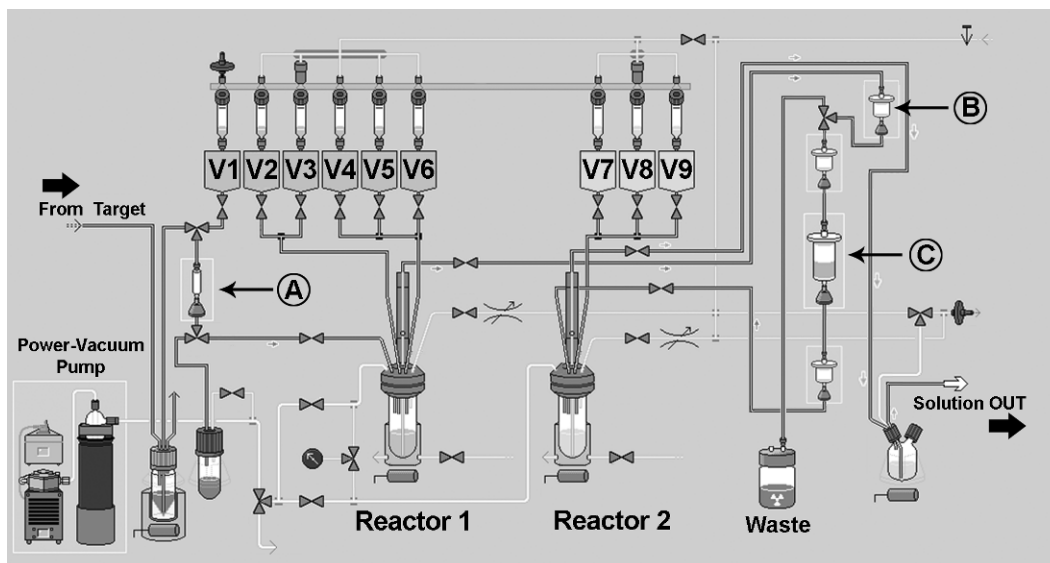
Figure 2-2 Schematic diagram of the reaction train for the synthesis of [^{18}F]-4 using the GE TRACERlab FX$_{FDG}$ ASU. The content of the reagent vessels is as follows: **V1**: 0.8 mL Kryptofix eluant; **V2**: 0.8 mL acetonitrile; **V3**: 10 mg 4-cyano-*N,N,N*-trimethylanilinium trifluoromethanesulfonate in 0.8 mL DMSO (anhydrous); **V4**: 1 mL toluene; **V5**: 10 mL water; **V6**: 6 mL anhydrous THF; **V7**: 400 µL water; **V8**: 5 mL methylene chloride; **V9**: 10 µL bromoacetyl bromide 1.0 M solution diluted to 1 mL of methylene chloride; **A**: ion exchange column for loading [^{18}F]fluoride; **B**: C18 cartridge; **C**: drying columns consisting of sodium sulphate cartridge (top), ground molecular sieves (centre), and silica cartridge (bottom).
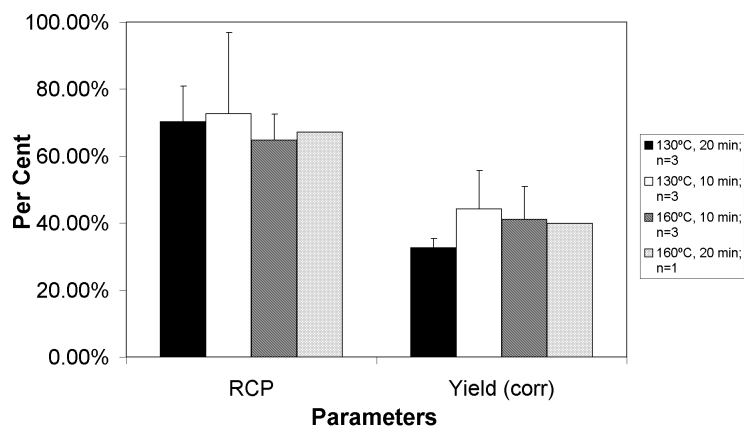
Figure 2-3 Effect of temperature and reaction time on the radiochemical purity (RCP) and yield (corrected for decay) in the synthesis of [^{18}F]-2. No significant difference in the RCP and yield was observed between syntheses performed at 130°C or 160°C at 10 or 20 minutes.

CHAPTER 3

Improved Synthesis of 4-[^{18}F]Fluorobenzylamine - a Useful Building Block in ^{18}F Radiochemistry

This chapter is based on the manuscript 'Synthesis and application of 4-[^{18}F]fluorobenzylamine: A versatile building block for the preparation of PET radiotracers', accepted for publication in Org. Biomol. Chem., and authored by I. Koslowsky, J. Mercer, and F. Wuest

The work presented in this chapter was carried out by I. Koslowsky

3.1 Introduction

Technological advances in positron emission tomography (PET) have reached a level of sophistication that allows researchers to realize the goal of imaging intracellular biochemical processes (i.e. molecular imaging) *in vivo.* This advancement has expanded the interest in developing positron-emitting [^{18}F]-labelled biomolecules which can be utilized in PET to observe and quantitate aberrant biochemical processes of disease. [^{18}F]-labelled asODNs, for example, have the potential to provide diagnostic information on the progress of a particular disease by visualizing and quantifying upregulated gene expression. This can lead to improved clinical diagnosis and treatment planning.

The direct radiolabelling of biological molecules with ^{18}F is not always suitable because of the harsh reaction conditions, such as the use of aprotic solvents and high temperatures. Therefore, small reactive [^{18}F]-labelled prosthetic groups (or synthons) are first synthesized and purified prior to further reaction with the biomolecules. These prosthetic groups are designed for facile labelling of macromolecules such as peptides, proteins, and ODNs, which have been modified with a hexylthiol or hexylamine linker conaining the sulphur or amine nucleophile, respectively. The subsequent alkylation of the biomolecules can then proceed under milder reaction conditions.

The radiochemistry involved in the development of such probes has a number of unique characteristics that provide challenges to the routine preparation of PET radiopharmaceuticals:

- Half Life considerations: for a [^{18}F]-labelled probe to be useful for imaging with PET, the probe should be synthesized rapidly before the probe decays. [^{18}F] has a relatively short physical half-life of 110 min; therefore long, complex syntheses of [^{18}F]-labelled prosthetic groups are not possible.   The synthesis of many [^{18}F]-labelled synthons can be performed within 60 min. However, methods are constantly sought to shorten the length of a synthesis in order to reduce losses due to decay.

- Requirement for multistep synthesis: [^{18}F]-labelled prosthetic groups differ in the complexity of their radiosynthesis and labelling yield, however their synthesis generally involves several steps, the first of which is preparation of a reactive [^{18}F] anion, followed by heating with an alkyl or aromatic compound containing a good leaving group.   The intermediate radiofluorinated compound is further converted to the desired [^{18}F]-labelled prosthetic group through an additional one or two steps, followed, typically, by HPLC purification. Multi-step syntheses usually involve multiple transfers of the reaction mixture and separation of radioactive and nonradioactive byproducts between steps, which results in the loss of radioactivity and leads to a lower yield.

- Need for remote handling: the [^{18}F]-labelled prosthetic group is performed under automation since relatively high amounts of radioactivity are needed at the start of the synthesis to allow for losses as described above.   The automated synthesis units are housed in lead-shielded hot cells, which reduce the radiation exposure from the high energy gamma emission of positron

emitters (511 kev) to the researcher. All reagents (except for [18F]fluoride, which is loaded remotely from the cyclotron) must be preloaded into the units. The synthesis is followed remotely with limited capability to alter/modify the synthesis once it is in progress. Therefore, all steps must be optimized and validated in advance to ensure a successful synthesis.

- Stoichiometry: in large scale synthesis a controlled stoichiometry is used with the purpose of providing sufficient reactants to drive the product toward a maximum yield. On occasion, this requires several fold molar excess of one or more of the reactants relative to the final product formed. In radiosynthesis, at high specific activity, the non-radioactive reactants will be in vast excess relative to the radioactive element or compound. Reaction rate kinetics depend on reagent concentrations and thus the very low concentration of the radiolabelled component will generally change the reaction rate compared with large scale synthesis.

Despite these challenges, a variety of [18F]-labelled prosthetic groups have been synthesized in reasonable yields for the labelling of proteins, peptides, and DNA-like probes (1,2) The [18F]fluorophenyl prosthetic groups, such as succinimido 4-[18F]fluorobeznoate ([18F]SFB) (3-5), 3-azido-5-nitro-benzyl[18F]fluoride (6), and 4-[18F]fluorobenzyl-2-bromoacetamide ([18F]FBBA) (7,8) tend to be produced in higher yields, and have been shown to label biomolecules more efficiently than the radiofluorinated alkyl prosthetic groups (9). More recently, [18F]-labelled pyridines, have also been shown to label ODNs readily and with high specific activity and reasonable yield (10-12).

The [18F]fluorophenyl compound, 4-[18F]fluorobenzylamine ([18F]FBA), is a versatile prosthetic group that is able to label biomolecules, such as ODNs. The standard method of synthesis of [18F]FBA is by the initial formation and subsequent nitrile reduction of 4-[18F]fluorobenzonitrile ([18F]FBN) (Figure 3-1). Haradahira *et al* (13) synthesized [18F]FBA with a reported yield of 39 to 49%. They were able to radiolabel prostaglandins with this prosthetic group targeting the glutathione S-conjugate export pump which plays a role in multi-drug tumour resistance. More recently, the synthesis of [18F]-labelled folic acid using [18F]FBA was described for the imaging of tumours which overexpress the folate receptor (14). The formation of [18F]FBA is also an important intermediate step in the synthesis of [18F]-labelled prosthetic groups such as [18F]FBBA. [18F]FBBA has been shown to successfully radiolabel DNA-type probes such as modified oligonucleotides and peptide nucleic acids (7,8,15-18), and automated synthesis of this compound has been reported, albeit with relatively low yields of 3 to 18% (19).

The reduction of the intermediate [18F]FBN to obtain the final [18F]FBA product was initially performed using borane dimethyl sulfide (13) but the superior reduction obtained with lithium aluminum hydride (LiAlH$_4$) has led to the general adoption of this reducing agent for most syntheses of [18F]FBA. There are, however, 2 significant drawbacks in using LiAlH$_4$ in these syntheses. Firstly, LiAlH$_4$ effectively reduces fluoroaryl nitriles only under strict anhydrous conditions. These conditions are particularly difficult to maintain in automated synthesis units where the transfer of reagents through common lines compromises

the anhydrous conditions required to ensure the quantitative reduction of the nitrile group. The use of molecular sieves and sodium sulfate drying cartridges, and flushing the lines with drying solvents, have been attempted to improve the yield (9,19). Secondly, the formation of aluminum salts during the reduction can create problems in a synthesis unit as transfer of the [^{18}F]FBA reaction mixture can clog the transfer lines in the unit. A more forgiving method for the reduction step which tolerates the presence of water would be a welcome improvement in the synthesis of [^{18}F]FBA.

Sodium borohydride (NaBH$_4$) is a more water tolerant reducing agent, but is incapable of reducing nitriles when used alone. However, it has been shown that in the presence of aqueous solutions of the metal catalysts nickel (Ni), cobalt (Co(II)) and copper (Cu(II)), sodium borohydride readily reduces nitrile groups through the formation of metal borides *in situ* followed by the release of hydrogen. Using the metal catalyst cobalt (II) chloride and NaBH$_4$, Osby *et al* reported that benzylamine could be produced in high yield from benzonitrile (20). More recently, Khurana *et al* demonstrated that high yields of benzylamine could be obtained in 5 min when incubated with nickel chloride and sodium borohydride in anhydrous ethanol at ambient temperature (21).

In this work we report on the improved synthesis of FBA utilizing a solid-phase approach to nitrile reduction. Using a NaBH$_4$ impregnated resin, FBN is rapidly and quantitatively reduced in the presence of catalytic quantities of transition metals to form FBA within a few minutes at ambient temperature.

3.2 Materials and Methods

3.2.1 Materials

Chemicals were purchased from Sigma-Aldrich (St. Louis, MO, USA) or Caledon Lab (Georgetown, ON, Canada) and were used without further purification. The required [^{18}F]fluoride was produced with a TR19/9 cyclotron (Advanced Cyclotron Systems, Burnaby, Canada) via the $^{18}O(p,n)^{18}F$ nuclear reaction using enriched [^{18}O]water (Rotem Inc, Topsfield, MA, USA). The synthesis of the precursor, 4-cyano-*N,N,N*-trimethylanilinium trifluoromethanesulfonate was performed as described previously (22).

3.2.2 Analytical methods

Thin layer chromatography (TLC) was performed using MK6F Silica Gel 60Å, 250 µm plates (Whatman, UK) visualized under u.v. illumination at 254 nm. Heptane:ethyl acetate, 50:50 was used as the mobile phase for all TLC analyses. Radio-TLC was performed with an AR-2000 imaging scanner (Bioscan Inc, Washington, DC). Radio-TLC results were compared with corresponding TLC of nonradioactive reference compounds.

3.2.3 Synthesis of borohydride exchange resin (BER)

BER was prepared as reported by Sim *et al* (23). To 20 g Amberlite IRA-400 anion exchange resin was added 50 mL of aqueous 1 M NaBH$_4$. The mixture was stirred for 15 minutes at ambient temperature. The BER was washed thoroughly with distilled water and dried under vacuum at 60°C for 5 hours. The dried resin was stored under nitrogen atmosphere at 4°C. The BER was assessed qualitatively for its ability to release hydride ion by the addition of 2 N hydrochloric acid (10 mL) to 1.5 g BER. A mildly exothermic reaction (NaBH$_4$ +

HCl + 3H$_2$O → B(OH)$_3$ + NaCl + 4H$_2$) was observed with the release of bubbles of hydrogen gas which continued for approximately 20 minutes.

3.2.4 Radiochemistry

3.2.4.1 Synthesis of 4-[^{18}F]fluorobenzonitrile ([^{18}F]FBN)

Aqueous sodium [^{18}F]fluoride (100 to 200 MBq) was loaded onto a Waters Accell QMA light cartridge which had been preconditioned with 10 mL of 0.5 M potassium carbonate and 10 mL of water. The [^{18}F]fluoride was eluted into a reaction vessel with an eluant consisting of 10 mg of Kryptofix®222 (4,7,13,16,21,24-hexaoxa-1,10-diazabicyclo[8.8.8]hexacosane) and 1.7 mg of potassium carbonate in 0.5 mL in acetonitrile/water (77.5%/22.5%). The solvent was co-evaporated with 3 aliquots of anhydrous acetonitrile (1 mL) at 93°C under a stream of nitrogen followed by an additional 5 min to remove residual water. The precursor, 4-cyano-*N,N,N*-trimethylanilinium trifluoromethanesulfonate (1-3 mg) was transferred to the reaction vessel in 0.3 mL anhydrous DMSO and the reaction proceeded at 93°C for 15 minutes. The mixture was transferred to a preconditioned Sep-Pak Plus® C18 cartridge (Waters Corp, MA, USA) with 10 mL water followed by an additional 10 mL water.

3.2.4.2 Synthesis of 4-[^{18}F]fluorobenzylamine ([^{18}F]FBA) using BER.

The C18 Sep-Pak cartridge containing [^{18}F]FBN was eluted with 5 mL of anhydrous ethanol. BER (200 mg containing approximately 3 mmol borohydride anion (BH$_3$$^-$)/g resin) was combined with 0.06 mmoles of cobalt acetate (Co(CH$_3$CO)$_2$·4H$_2$O), nickel chloride (NiCl$_2$·6H$_2$O) or copper sulphate (CuSO$_4$·5H$_2$O) in 0.5 mL distilled, deionized water. Upon the release of hydride

anion (evident by black discolouration of the resin), 0.5 mL of [^{18}F]FBN was immediately added. TLC was performed at 1, 3, and 5 minutes after addition of the nitrile. Alternately, [^{18}F]FBN was added 1, 3, 5, 10, 15, or 60 minutes *after* the addition of the metal catalyst to the resin, followed by TLC analysis. Finally, 0.5 mL of metal catalyst was mixed with 0.5 mL of [^{18}F]FBN and added to the resin. TLC was performed 1 and 5 minutes after addition to the BER.

3.3 Results

3.3.1 *Synthesis of [^{18}F]FBN*

Radio-TLC analysis of the SepPak purified reaction mixture demonstrated the formation of [^{18}F]FBN with a mean radiochemical purity of 87.0% (n = 12). The reaction was typically performed within 30 minutes using low amounts (1 to 3 mg) of precursor. A decay corrected mean yield of 47.3% was obtained starting with 100 to 200 MBq of [^{18}F]fluoride.

3.3.2 *Assessment of BER/metal catalyst parameters in the synthesis of [^{18}F]FBA*

All metal catalysts used in the BER study were able to activate the BER (as observed by the change in colour of the beads from tan to black). Activation of BER was only observed with NaBH$_4$ impregnated resin prepared in-house: a commercially available borohydride resin was not reactive regardless of the metal catalyst or solvents used. The cause of this failure is not known. Perhaps the BH$_4^-$ anion was not accessible to the metal catalyst, or the resin was exposed to moisture prior to use. The addition of nickel chloride to the BER demonstrated the most rapid activation (within 10 seconds), followed by cobalt acetate (60 seconds) (Figure 3-2). Activation of the resin was observed to occur only after a

prolonged incubation with copper sulphate. The rate of conversion from [^{18}F]FBN to [^{18}F]FBA also varied with the catalyst used. Copper sulphate demonstrated the slowest rate of nitrile reduction with 9.8% conversion at 5 minutes. In contrast 73.9% of [^{18}F]FBN had been converted to [^{18}F]FBA with cobalt acetate by 1 minute, with 92.8% reduction by 3 minutes (Table 3-1). The nickel chloride catalyst demonstrated the most rapid rate of reduction with 93.4% of the nitrile converted to its respective amine after 1 minute of incubation with the BER-metal catalyst mixture (Figure 3-3).

Once the beads were activated with NiCl$_2$, the hydride was rapidly expended: conversion was quantitative if [^{18}F]FBN in ethanol was added within 1 minute (Figure 3-4). Longer wait times before the addition of the nitrile decreased the extent of reduction. For example, 78% conversion to the amine was observed if [^{18}F]FBN was added 3 minutes after bead activation. Only 16% conversion was observed with a wait time of 5 minutes. Combining the catalyst with [^{18}F]FBN prior to addition to the BER demonstrated rapid reduction similar in rate and extent to that observed with sequential addition of the catalyst followed by [^{18}F]FBN within 1 minute of activation.

3.4   Discussion

BER is a quaternary ammonium resin to which the borohydride anion, BH$_4^-$, has been attached. Upon the addition of a transition metal salt, such as copper sulphate, cobalt acetate or nickel chloride, metal boride complexes are formed *in situ*, strongly coordinating nitriles and activating them toward reduction by BH$_4^-$

(20). Production of a black coating of metal on the beads, followed by the release of hydrogen indicates the formation of the metal-boride complex.

Metal-assisted borohydride reactions with nonradioactive nitriles are typically performed under controlled stoichiometric conditions between the nitrile substrate and catalyst, or catalyst and borohydride. For example, Osby *et al* used a benzonitrile:catalyst ratio of 10:1 resulting in 86% conversion of FBN to FBA within 2 h (20). To consume all the reactant, however, a large excess of $NaBH_4$ was required. Caddick *et al* also noted the need for a large excess of $NaBH_4$ to reduce benzyl cyanide derivatives (24). As previously mentioned, it is impossible to achieve a normal stoichiometric relationship between radiolabelled FBN and catalyst or reducing agent as only femtomolar quantities of [^{18}F]-labelled benzonitrile are present. Thus, the borohydride bound to the resin represents a very large excess relative to the radiolabelled reactant.

The reaction solvent also plays an important role in the rate and extent of reduction. Methanol, aqueous tetrahydrofuran (THF:water), and ethanol have all been explored as potential solvents for reduction (20,21). When using $NaBH_4$ powder, methanol offers the fastest rate of reaction as a consequence of rapid $NaBH_4$ decomposition. However, with BH_4^- bound to the resin, the BER decomposes at a much slower rate (25). Others have successfully demonstrated nitrile reduction using ethanol as the reaction solvent (20,21). Ethanol slows the rate of BH_4^- decomposition, and is considered, by some, as the solvent of choice for arylnitrile reductions. Although THF:water 2:1 has been suggested as an optimal solvent for reductions with $NaBH_4$ powder and catalyst, the BER was not

as easily wetted as with alcohols, and the metal salts were not easily dissolved in this solvent combination.

According to Caddick *et al*, the starting nitrile must be present in the reaction mixture before formation of the metal boride (24). We found that the simultaneous addition of metal catalyst and [^{18}F]FBN to BER resulted in 100% conversion to [^{18}F]FBA within 1 min. However, we also demonstrated that a reasonably high yield could be achieved if [^{18}F]FBN was added within 3 minutes following metal catalyst activation of the resin.

While no attempt was made to further optimize the reaction, the relatively rapid reaction and near-quantitative yield for the reduction step resulted in a good overall chemical and radiochemical yield of [^{18}F]FBA. Thus, the LiAlH$_4$ method to reduce [^{18}F]FBN can easily be replaced with the BER-catalyst method: the nitrile is rapidly, and quantitatively, converted to the amine *in the presence of water*, and a cleaner reaction improves the reaction conditions for further syntheses.

3.5   Conclusion

In conclusion, this preliminary work demonstrates the potential of using a metal-assisted BER for the synthesis [^{18}F]FBA. The resin is simple to prepare and the reaction occurs rapidly at room temperature without regard to the presence of water. The reagent and catalyst can be added sequentially or simultaneously through automation and allowed to react on the column. The reaction is quantitative, and upon elution from the BER, the presence of metal-boride precipitate is avoided. Thus, the BER-metal catalyst method of nitrile reduction

lends itself well for the synthesis of [^{18}F]FBA in an automated synthesis unit and would have general application for the reduction of nitriles in small scale reactions.

3.6　References

(1) Wester HJ, Schottelius M. Fluorine-18 labeling of peptides and proteins. Ernst Schering Res.Found.Workshop 2007(62):79-111.

(2) Miller PW, Long NJ, Vilar R, Gee AD. Synthesis of ^{11}C, ^{18}F, ^{15}O, and ^{13}N radiolabels for positron emission tomography. Angew.Chem.Int.Ed Engl. 2008;47(47):8998-9033.

(3) Wuest F, Köhler L, Berndt M, Pietzsch J. Systematic comparison of two novel, thiol-reactive prosthetic groups for ^{18}F labeling of peptides and proteins with the acylation agent succinimidyl-4-[^{18}F]fluorobenzoate ([^{18}F]SFB). Amino Acids 2009;36(2):283-295.

(4) Hedberg E, Långström B. ^{18}F-labelling of oligonucleotides using succinimido 4-[^{18}F]fluorobenzoate. Acta Chem.Scand. 1998;52(8):1034-1039.

(5) Li J, Trent JO, Bates PJ, Ng CK. Labeling G-rich oligonucleotides (GROs) with N-succinimidyl 4-[^{18}F]fluorobenzoate (S^{18}FB). J.Label.Compd.Radiopharm. 2006;49(14):1213-1221.

(6) Lange CW, VanBrocklin HF, Taylor SE. Photoconjugation of 3-azido-5-nitrobenzyl-[^{18}F]fluoride to an oligonucleotide aptamer. J.Label.Compd.Radiopharm. 2002;45(3):257-268.

(7) Kuhnast B, Dolle F, Vaufrey F, Hinnen F, Crouzel C, Tavitian B. Fluorine-18 labeling of oligonucleotides bearing chemically-modified ribose-phosphate backbones. J.Label.Compd.Radiopharm. 2000;43(8):837-848.

(8) Kuhnast B, Hinnen F, Boisgard R, Tavitian B, Dollé F. Fluorine-18 labelling of oligonucleotides: Prosthetic labelling at the 5′-end using the *N*-(4-[^{18}F]fluorobenzyl)-2-bromoacetamide reagent. J.Label.Compd.Radiopharm. 2003;46(12):1093-1103.

(9) de Vries EFJ, Vroegh J, Elsinga PH, Vaalburg W. Evaluation of fluorine-18-labeled alkylating agents as potential synthons for the labeling of oligonucleotides. Appl.Radiat.Isot. 2003;58(4):469-476.

(10) Viel T, Kuhnast B, Hinnen F, Boisgard R, Tavitian B, Dollé F. Fluorine-18 labelling of small interfering RNAs (siRNAs) for PET imaging. J.Label.Compd.Radiopharm. 2007;50(13):1159-1168.

(11) Dollé F. Fluorine-18-labelled fluoropyridines: Advances in radiopharmaceutical design. Curr. Pharm. Des. 2005;11(25):3221-3235.

(12) Kuhnast B, De Bruin B, Hinnen F, Tavitian B, Dollé F. Design and synthesis of a new [^{18}F]fluoropyridine-based haloacetamide reagent for the labeling of oligonucleotides: 2-bromo-*N*-[3-(2-[^{18}F]fluoropyridin-3-yloxy)propyl]acetamide. Bioconjugate Chem. 2004;15(3):617-627.

(13) Haradahira T, Hasegawa Y, Furuta K, Suzuki M, Watanabe Y, Suzuki K. Synthesis of a F-18 labeled analog of antitumor prostaglandin Δ^7- PGA$_1$ methyl ester using *p*-[^{18}F]fluorobenzylamine. Appl.Radiat.Isot. 1998;49(12):1551-1556.

(14) Bettio A, Honer M, Müller C, Brühlmeier M, Müller U, Schibli R, et al. Synthesis and preclinical evaluation of a folic acid derivative labeled with^{18}F for PET imaging of folate receptor-positive tumors. J.Nucl.Med. 2006;47(7):1153-1160.

(15) Kuhnast B, Klussmann S, Hinnen F, Boisgard R, Rousseau B, Fürste JP, et al. Fluorine-18- and iodine-125-labelling of spiegelmers. J.Label.Compd.Radiopharm. 2003;46(13):1205-1219.

(16) Kuhnast B, Hinnen F, Hamzavi R, Boisgard R, Tavitian B, Nielsen PE, et al. Fluorine-18 labelling of PNAs functionalized at their pseudo-peptidic backbone for imaging studies with PET. J.Label.Compd.Radiopharm. 2005;48(1):51-61.

(17) Hamzavi R, Dolle F, Tavitian B, Dahl O, Nielsen PE. Modulation of the pharmacokinetic properties of PNA: Preparation of galactosyl, mannosyl, fucosyl, *N*-acetylgalactosaminyl, and *N*-acetylglucosaminyl derivatives of aminoethylglycine peptide nucleic acid monomers and their incorporation into PNA oligomers. Bioconjugate Chem. 2003;14(5):941-954.

(18) Boisgard R, Kuhnast B, Vonhoff S, Younes C, Hinnen F, Verbavatz J-, et al. In vivo biodistribution and pharmacokinetics of ^{18}F-labelled Spiegelmers: A new class of oligonucleotidic radiopharmaceuticals. Eur.J.Nucl.Med.Mol.Imaging 2005;32(4):470-477.

(19) Koslowsky I, Shahhosseini S, Wilson J, Mercer J. Automated radiosynthesis of *N*-(4-[^{18}F]fluorobenzyl)-2- bromoacetamide: An F-18-labeled reagent for the prosthetic radiolabeling of oligonucleotides. J.Label.Compd.Radiopharm. 2008;51(10):352-356.

(20) Osby JO, Heinzman SW, Ganem B. Studies on the mechanism of transition-metal-assisted sodium borohydride and lithium aluminum hydride reductions. J.Am.Chem.Soc. 1986 01/01;108(1):67-72.

(21) Khurana J, Kukreja G. Rapid reduction of nitriles to primary amines with nickel boride at ambient temperature. Synth.Commun. 2002 04/15;32(8):1265.

(22) Dolle F, Hinnen F, Vaufrey F, Tavitian B, Crouzel C. A general method for labeling oligodeoxynucleotides with ^{18}F for *in vivo* PET imaging. J.Label.Compd.Radiopharm. 1997;39(4):319-330.

(23) Sim TB, Yoon NM. Selective reduction of α,β-unsaturated acid derivatives using borohydride exchange resin-$CuSO_4$ in methanol. Synlett 1995(7):726-728.

(24) Caddick S, Judd DB, Lewis AKDK, Reich MT, Williams MRV. A generic approach for the catalytic reduction of nitriles. Tetrahedron 2003;59(29):5417-5423.

(25) Sim TB, Yoon NM. Reducing characteristics of borohydride exchange resin-$CuSO_4$ in methanol. Bull.Chem.Soc.Jpn 1997;70(5):1101-1107.

Table 3-1   Yield of 4-[^{18}F]fluorobenzylamine using metal-catalyst activated BER*

Metal catalyst	1 min	3 min	5 min
NiCl$_2$	93.4	95.2	92.3
Co(II) acetate	73.9	92.8	94.5

*[^{18}F]FBN was added immediately upon evidence of the release of hydride ion. Radio-TLC was performed at 1, 3, and 5 min after addition of [^{18}F]FBN to the metal catalyst-activated BER
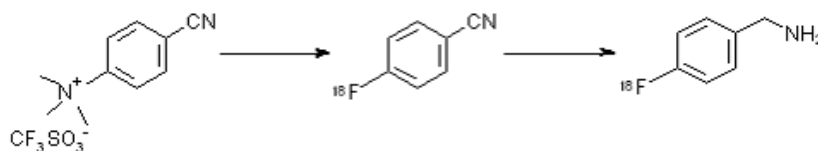
Figure 3-1 Synthesis of 4-[^{18}F]fluorobenzylamine ([^{18}F]FBN)

A   **B**
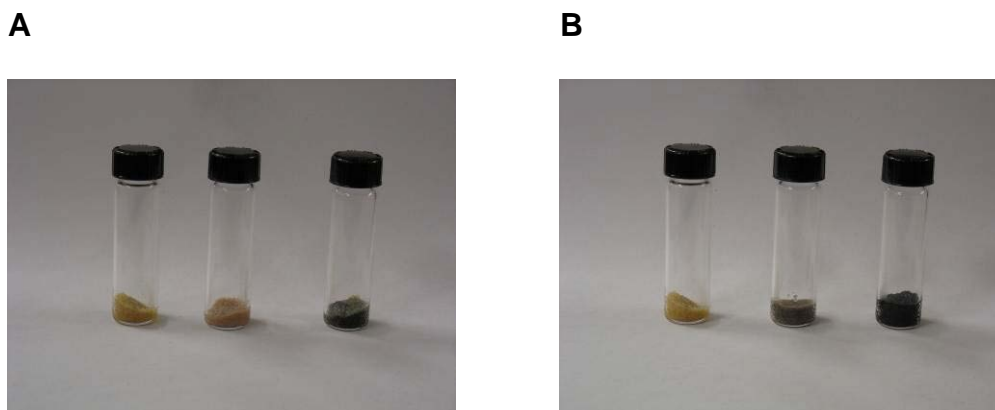
Figure 3-2 Colour change of BER upon addition of metal catalyst. The black colour denotes activation of BER with release of hydride ion. The left vial corresponds to BER wetted with water; the middle vial represents BER wetted with Co(II) acetate; the vial on the right represents BER wetted with NiCl$_2$. A: 10 s after addition of the metal catalyst; B: 60 s after addition of the metal catalyst.
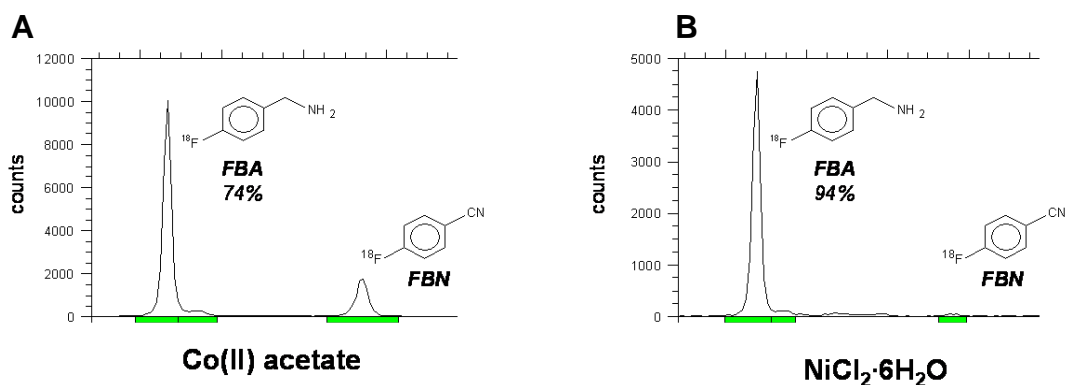
Figure 3-3 Radio-TLC scans of Co(II) acetate- and NiCl$_2$-assisted conversion of [^{18}F]FBN to [^{18}F]FBA 1 min after addition of FBN to the metal catalyst-activated BER
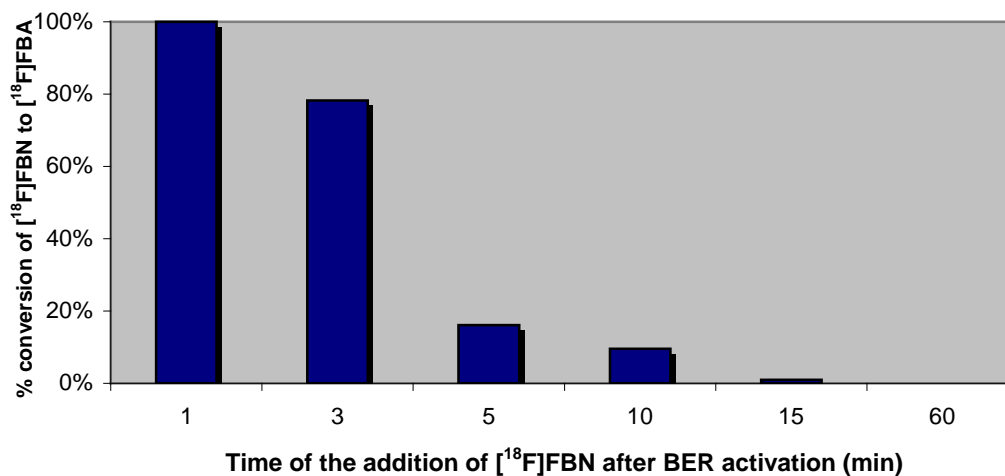
Figure 3-4 Radio-TLC results of the conversion to FBA following addition of the FBN to previously NiCl$_2$-activated BER. FBN was added at various time points after activation of the resin

CHAPTER 4
Validation of an ^{18}F-labelled oligonucleotide probe for imaging $p21^{WAF1}$ transcriptional changes in human tumour cells

This chapter is based on a manuscript submitted for publication and authored by I. Koslowsky, S. Shahhosseini, R. Mirzayans, D. Murray, and J. Mercer.

The work presented in this chapter was carried out by I. Koslowsky with technical assistance from S. Shahhosseini. Cell cultures were prepared by Bonnie Andrais.

4.1 Introduction

The ability to longitudinally image alterations in gene expression in human tumours during a course of radio- or chemo-therapy using sensitive techniques such as positron emission tomography (PET) would have major ramifications for monitoring early tumour responsiveness to treatment. This would, in turn, allow clinicians to optimize treatments to individual patients early in the treatment process. A critical determinant of the cellular response to DNA-damaging agents, such as ionizing radiation, is the stabilization and activation of p53 (1). p53 is a multifunctional protein whose roles in the DNA damage-response pathway include its activity as a nuclear transcription factor that regulates the expression of many downstream genes, including the gene encoding the cyclin dependent kinase inhibitor p21$^{WAF1/CIP1}$ (hereafter called p21) (2). For example, activation of the p53-p21 axis soon after irradiation may promote cell survival by transiently activating cell-cycle checkpoints, allowing the cell to repair DNA damage; it can also promote the loss of clonogenic potential, e.g., by activating p53-directed apoptosis. Furthermore, in some genetic backgrounds exposure to ionizing radiation can cause prolonged p21 up-regulation and p21-directed "permanent" cell cycle arrest (i.e., premature or "accelerated" senescence) (3-7).

Most of our understanding of these events has come from studies using cultured cells exposed to DNA-damaging agents *in vitro*, and little is known about such responses *in vivo*. Imaging changes in *p21* mRNA expression post-irradiation *in vivo* should thus provide important insight into these early tumour responses and their potential impact on the outcome of radio-/chemo-therapy. The objective of

84

the present study is to develop [^{18}F]-labelled antisense oligodeoxynucleotides (asODNs) that will bind to the *p21* mRNA sequence *in vitro* that can ultimately be used as an imaging probe for this transcript *in vivo*. Successful imaging of gene expression requires entry of the probe into the cell and hybridization with its target *p21* transcript.

asODNs have been used in a variety of tumour cell lines to explore the relationship between *p21* expression and cell cycle arrest/apoptosis (8-12). A proof-of-concept for using antisense technology to image *p21* transcripts was provided by Wang *et al* (13), who reported that they were able to image the up-regulation of *p21* expression by epidermal growth factor in a MDA-MB-468 human breast cancer xenograft using an asODN probe labelled with [^{111}In]DTPA. This report, which used single-photon emission computed tomography (SPECT) imaging, encouraged us to investigate the potential of a [^{18}F]-labelled asODN for imaging radiation-induced p21 expression with PET. Thus, this study was designed to validate that an asODN, directed to *p21* mRNA, retains its antisense behaviour after conjugation with a (radio)fluorinated prosthetic group; and to observe the cellular distribution of [^{18}F]asODNs and fluorescent [F]asODNs in irradiated HCT116 human colon carcinoma cells, which are known to up-regulate their expression of p21 after irradiation.

4.2 Materials and Methods

4.2.1 Oligonucleotides

A fully phosphorothioated 20-mer antisense oligodeoxynucleotide (asODN) targeting the 3′-untranslated region of human *p21* mRNA as described by Poluha

et al (11) was synthesized and purified by University Core DNA Services, University of Calgary (Alberta, Canada). A 20-mer random sequence oligonucleotide (rsODN) was used as a control. The sequence of the asODN was 5′-TGTCATGCTGGTCTGCCGCC-3′. The rsODN consisted of the sequence 5′-CCGGTGAACGAGCGAGCACA-3′. For flow cytometry studies, ODNs were tagged with the fluorophore Quasar 570 CPG (Biosearch Technologies, Novato, CA, USA) on thé 3′-end (hereafter designated as asODN-Q or rsODN-Q). Confocal microscopy studies utilized the above ODNs as well as Quasar-labelled ODNs tagged with the nonradioactive prosthetic group *N*-(4-fluorobenzyl)-2-bromoacetamide (FBBA) on the 5′-end ([F]asODN-Q or [F]rsODN-Q).

4.2.1.1 *Radiolabelling of oligodeoxynucleotide (ODN)*

The synthesis of [^{18}F]FBBA was performed as described previously (14) using a TRACERlab Fx$_{FDG}$ automated synthesis unit. Typically, 100 to 200 MBq of purified [^{18}F]FBBA could be obtained for radiolabelling ODNs from 10 GBq of [^{18}F]fluoride. Lyophilized ODN (0.5 or 1 mg) was reconstituted with 1 mL of phosphate buffered saline (PBS) 0.1 M, pH 8, mixed with methanol, 1/1 (v/v), and added to [^{18}F]FBBA. The mixture was heated in a vented vial at 120°C for 30 minutes. Unreacted [^{18}F]FBBA was separated from the radiolabelled ODN with a NAP™-10 column (GE Healthcare, Chalfont St Giles, UK) by elution with PBS 0.01 M, pH 7.2. No further purification was performed. The concentration of ODN in the eluate was determined by u.v. spectroscopy at 260 nm using a DU-7400 spectrophotometer. Analysis of the mixture was performed with reverse-phase HPLC using the following gradient system: triethylammonium

acetate/acetonitrile 95/5 to 90/10 over 3 minutes, followed by 90/10 to 75/25 over 7 minutes, with a washout phase of 50/50 for 10 minutes; flow rate: 6 mL/min; retention time: 14.6 to 14.9 minutes. The [^{18}F]ODNs eluted with the same retention time as the non-radioactive, fluorinated ODNs. The final specific activity of the products ranged from 100 to 1000 MBq/µmol, with a mean of 380 MBq/µmol.

4.2.2   Cells and Cell Culture

HCT116 colon carcinoma cells were purchased from the American Type Culture Collection (Rockville, MD, USA). The cells were cultured as monolayers in Dulbecco's Modified Eagle Medium (Invitrogen, Grand Island, NY, USA) with nutrient mixture F-12 (Ham) (1/1) (DMEM/F12) supplemented with 10% (v/v) fetal bovine serum (FBS), 1 mM L-glutamine, 100 IU/mL penicillin G, and 100 µg/mL streptomycin sulphate. Opti-Mem I Reduced Serum medium (Invitrogen, Grand Island, NY, USA) was used for all transfection studies. All cell cultures were incubated at 37°C in 5% CO_2/air. Lipofectin (Invitrogen, Carlsbad, CA, USA), a liposomal formulation of the cationic lipid N-[1-(2,3-dioleyloxy)propyl]-*N,N,N*-trimethylammonium chloride (DOTMA) and dioleoyl phosphatidylethanolamine (DOPE) (15), was employed as the liposomal transfection agent and prepared as per the manufacturer's instructions. A 10 µg/mL concentration of Lipofectin was employed for *in vitro* studies.

4.2.3 Irradiation

^{60}Co γ-ray exposures were performed in a Gammacell 220 Unit (Atomic Energy of Canada Limited, Ottawa, ON, Canada) at a dose rate of ~5 Gy/min (total dose of 5 Gy). Cells were irradiated 24 hours after seeding.

4.2.4 Protein Immunostaining

Approximately 10^5 cells per 2 mL of medium were plated in 35-mm culture dishes with coverslips and incubated overnight at 37°C. Four hours prior to irradiation, the cells were treated with naked asODN or rsODN (400 nM) i.e. no transfection agent was used; or liposome-transfected asODN or rsODN (hereafter called 'transfected' ODNs). As a control, some cells were treated with the liposomal vector alone. Cell were subsequently irradiated and incubated for 24 hours. Immunofluorescence analysis was performed as described previously (7). Briefly, the cells were permeabilized with 2 mL of 100% methanol for 20 minutes at -10°C and probed with a 1:1000 dilution of primary mouse monoclonal antibody (p21(187), Santa Cruz Biotechnology, Santa Cruz, CA, USA) followed by a 1:250 dilution of AlexaFluor488 goat anti-mouse IgG (Molecular Probes, Eugene, OR, USA). DAPI (4',6-diamidino-2-phenylindole dihydrochloride, Sigma, St. Louis, MO, USA), a nuclear stain, was added prior to imaging. Cells were examined with a Zeiss Axioplan2 microscope (Carl Zeiss, Jena, Germany). Images were captured using the Metamorph program and processed with Adobe Photoshop.

4.2.5 Western Blotting

Approximately 5 x 10^5 cells per 4 mL of medium were plated in 60-mm culture dishes and incubated overnight at 37°C. Four hours prior to irradiation, the cells were treated with 50, 100, 200, or 400 nM of asODN or rsODN, or with the FBBA-labelled oligonucleotides, [F]asODN or [F]rsODN. The ODNs were transfected with or without a liposomal vector. As a control, some cells were treated with the vector alone. Cells were subsequently irradiated and incubated for 24 hours. The cells were lysed with 50 mM Tris buffer, pH 7.4, containing a cocktail of the protease inhibitors aprotinin 10 µg/mL, leupeptin 10 µg/mL, and phenylmethylsulfonyl fluoride 1 mM, and an ATPase inhibitor sodium orthovanadate 2 mM (Sigma, St. Louis, MO, USA). Protein concentration of the cell lysates was determined with the Bradford protein assay kit (Bio-Rad, Hercules, CA, USA) and the concentration measured at 595 nm with a DU-7400 spectrophotometer. Sodium dodecylsulfonate polyacrylamide gel electrophoresis (SDS-PAGE) was performed under reducing conditions on 30 µg of cell lysates in 25 mM Tris buffer, pH 8.3, containing 192 mM glycine and 0.1% w/w SDS. The gel bands were transferred to a polyvinylidene difluoride (PVDF) membrane (Hybond-P, Amersham Bioscience, Baie d'Urfé, QC, Canada), using the semi-dry membrane transfer method. Ponceau S Stain was applied to verify uniform transfer of the protein bands to the membrane. The membranes were probed with a 1:2000 dilution of p21 mouse monoclonal antibody (Sigma, St. Louis, MO, USA) in PBS containing 5% Carnation skim milk (to block non-specific binding of antibody to membrane), washed with PBS containing 0.1% Tween (to remove unbound protein), followed by incubation with a 1:1000 dilution of IgG

polyclonal goat anti-mouse horseradish peroxidase (HRP) IgG (Santa Cruz Biotechnology, Santa Cruz, CA, USA). The membranes were washed with PBS/Tween solution and the protein bands detected using the enhanced chemiluminescence kit (ECL, GE Healthcare, Chalfont St Giles, UK) and exposure to Kodak Imaging film (Kodak, Rochester, NY, USA). The membranes were subsequently stripped of the p21 probe with a 25 mM glycine/1% SDS solution, pH 2, and reprobed for actin (1:5000 goat polyclonal IgG (Sigma, St. Louis, MO, USA)) in PBS/milk. The membranes were then processed as above.

4.2.6 *Flow Cytometry*

Approximately 5 x 10^5 cells per 4 mL of medium were plated in 60-mm culture dishes and incubated overnight at 37°C. The cells were subsequently irradiated and incubated for 24 hours, followed by incubation with 280 nM Quasar-tagged ODNs with or without a vector for 0.5, 1, 2, or 2.5 hours. The cells were washed and resuspended in PBS containing 2 mM ethylenediamine tetraacetic acid (EDTA). One plate was left untreated and acted as a negative control. Cellular uptake of the fluorescent probes was assessed using a FACSCalibur Flow Cytometer (Becton Dickenson, San Jose, CA, USA) with a 488 nm laser and the Cell-Quest Pro analysis package. The data collected included forward scatter, side scatter, and fluorescence-1 (FL-1, Quasar 570). The detected fluorescence was gated to exclude autofluorescence of the untreated control cells. Histograms were recorded showing cell number versus fluorescence intensity in cells corresponding to ODN uptake. The median fluorescence intensity (MFI) ratios of naked asODN-Q to rsODN-Q and transfected asODN-Q to rsODN-Q were

determined to evaluate the differences of cellular uptake and internalization of asODN versus its random sequence control. Studies were performed in triplicate on different days.

4.2.7 Cell Fractionation Studies

Approximately 5×10^5 cells per 4 mL of medium were plated in 60-mm culture dishes and incubated overnight at 37°C. The cells were subsequently irradiated and incubated for 24 hours, followed by incubation with approximately 0.4 nmoles of $[^{18}F]$-labelled asODN or rsODN per 10^6 cells (with or without a vector) for 0.5 to 2.5 hours. A cell fractionation technique described by Eboue *et al* (16) was employed to determine uptake and intracellular compartmentalization of naked or transfected $[^{18}F]$ODNs. All media, washings, and cellular fractions were transferred to counting tubes and counted in a Wizard™ 3" 148 automatic gamma counter (PerkinElmer Life Sciences, Turku, Finland). The data were background corrected and decay corrected to a standard. All analyses were performed at least 3 times on different days. The Student T-test was employed for statistical analysis of the data.

4.2.8 Confocal Microscopy

Approximately 10^5 cells per 2 mL of medium were plated in 35-mm tissue culture dishes with 14-mm microwell (MatTek, Ashland, MA, USA) and incubated overnight at 37°C. Twenty-four hours after irradiation, cells were incubated with [F]asODN-Q, 280 nM, with or without a vector. The cell nuclei were stained with 1 µL of Hoechst 33342 (1 µg/mL) (Molecular Probes, Eugene, OR, USA) 30 min prior to imaging. The intracellular distribution of the probes was visualized

using a Zeiss 510 LSM microscope (Carl Zeiss Microscope Systems, Jena, Germany) at 543 nm ([F]asODN-Q) and 364 nm (nuclear stain) following 2.5 hours of probe incubation. The intensity of the excitation laser, or acousto-optical tunable filter (AOTF), was optimized for each wavelength for each scan to visualize the location of the probe. Differential interference contrast was included in some images for morphological information.

4.3 Results

4.3.1 Radiolabelling of oligonucleotide (ODN)

RP-HPLC analysis of the radiolabelled ODNs demonstrated a single radioactive peak with the same retention time as that of the non-radioactive, fluorinated ODNs (retention time (t_R): 14.6 to 14.9 minutes). The ODNs were not adversely affected by high temperatures if heated in a vented vial: RP-HPLC demonstrated a single peak corresponding to the retention time of an uncooked ODN (t_R: 13.8 min). The final specific activity of the products ranged from 100 to 1000 MBq/μmol, with a mean of 380 MBq/μmol.

4.3.2 Protein Immunostaining

Protein immunostaining was performed to verify upregulated p21 expression post-irradiation and to confirm an antisense effect with the selected asODN. The cells were treated with ODNs for 4 hours prior to irradiation followed by a 24-hour incubation after irradiation to give the ODNs the opportunity to enter the cell and hybridize with both endogenous and ionizing radiation-induced p21 transcripts. Figure 4-1 illustrates the effect of transfected asODN on p21 protein expression in irradiated HCT116 cells. Cells which were not irradiated or treated

with ODNs were used as an endogenous control (Figure 4-1A): minimal constitutive expression of p21 protein was observed in these cells. In contrast, irradiated cells that were not treated with ODNs expressed a high level of p21 protein (Figure 4-1B). The vector alone did not affect p21 expression in irradiated cells, nor did transfected rsODN (Figures 4-1C and 1D, respectively). However, transfected asODN effectively blocked ionizing radiation-induced p21 expression to the level of the non-irradiated control (Figure 4-1E). DAPI staining of intact nuclei showed that treatment with asODNs did not damage the cells at the concentration used over the time period studied (Figure 4-1F).

4.3.3 Western Blot

Western blotting was used to determine antisense activity of asODN as well as its activity after conjugation with a [F]-containing prosthetic group. Figure 4-2 shows p21 protein expression levels in HCT116 cells that have been treated with naked or transfected asODN or rsODN. The non-irradiated control cells exhibited a low level of p21 expression, reflecting the minimal constitutive expression of this gene in an unstressed environment. Following irradiation with 5 Gy, greatly increased p21 expression was observed in cells that were not treated with ODNs. Treatment with 400 nM of transfected asODN inhibited p21 expression to the level of the non-irradiated control cells. In comparison, the naked asODN, naked rsODN, and transfected rsODN had minimal impact on p21 expression at this time point.

The labelling of asODN with FBBA ([F]asODN) did not appear to interfere with its ability to down-regulate p21: treatment with transfected [F]asODN

demonstrated a concentration-dependent inhibition of p21 of similar magnitude to the nonfluorinated transfected asODN, with downregulation of p21 evident at an ODN concentration of 50 nM (Figures 4-3B and 3A, respectively). Again, no change in p21 expression was observed with the transfected rsODN and [F]rsODN as compared to the control cells (Figures 4-3C and 3D, respectively).

4.3.4 Flow Cytometry

The following studies (i.e., flow cytometry, cell fractionation, and confocal microscopy) were designed to evaluate the potential of the asODN as an imaging agent, with respect to its cellular internalization and intracellular localization, following upregulation of *p21* gene expression.

Flow cytometry was performed to observe the uptake and intracellular pattern of distribution of fluorescently-labelled asODNs and rsODNs. Table 4-1 depicts the percent of 5-Gy-irradiated HCT116 cells within a culture that contained the fluorescent probes as a function of incubation time. Irradiated untreated cells were used as a control to exclude autofluorescence; such cells typically represented less than 2% of the gated population. No difference in the number of cells internalizing the probes per unit time period was observed regardless of ODN sequence or whether a transfection agent was used, although more variability was observed in cells incubated with naked ODN versus transfected ODN. At 2.5 h, 53 to 81% of the cells had internalized the naked probes versus 73 to 77% with the transfected ODNs.

Figures 4-4A and 4B compare uptake of asODN-Q and rsODN-Q, respectively, at 1 hour; Figures 4-4C and 4D depict the distribution of asODN-Q and rsODN-Q at

2 hours. M1 represents the gated population and excludes unlabelled cells. A discrete Gaussian-type histogram at low fluorescence intensity was observed in cells treated with naked ODN (dark gray profile). The intensity of the signal did not increase with time, implying little change in uptake and intracellular distribution of the probe over the time period tested. In contrast, a distinct bimodal pattern of signal intensity was evident in cells containing transfected asODN-Q at 1 h (light gray profile), with the fluorescent signal increasing in intensity by 2 h. A similar pattern of uptake and distribution of fluorescent rsODNs was observed (Figures 4-4B and 4D), although the bimodal distribution was less evident at 2 h.

Figure 4-5 illustrates the differences of cellular uptake and internalization of asODN-Q and its random sequence control. A mean naked asODN to naked rsODN MFI ratio of 1 was observed at all time periods, demonstrating that the cells do not differentiate between the naked asODN and rsODN with respect to their uptake or internal distribution. In contrast, transfected asODN demonstrated a 1.8-fold increase in MFI ratio over the transfected rsODN after 2 h of incubation. Therefore, although a similar number of cells were able to internalize the probes in the presence of a vector (see Table 4-1) a higher amount of transfected asODN remained in the cells as opposed to its random sequence control. In other words, once asODN is free from endosome entrapment and released from Lipofectin, it remains within the cell to bind with its target, whereas the rsODN is able to exit the cell as it has no specific target.

4.3.5 Cell Fractionation Studies

Cell fractionation as described by Eboue *et al* [16] provided a means for locating and quantifying the radiolabelled probes in the subcellular fractions. Table 4-2 compares the uptake of radioactivity of naked or transfected [^{18}F]asODN or [^{18}F]rsODN over 2.5 hours whereas Table 4-3 shows transfected [^{18}F]ODN uptake in the cytoplasm, endosomes, and nucleus, as a percentage of the cell-associated radioactivity. Transfected ODNs were superior in their ability to bind to and enter the cells as compared to the naked ODNs, which exhibited <1% mean uptake at each time period tested (Table 4-2). The uptake of the transfected radiolabelled ODNs at 0.5 hours was approximately 2-fold higher than the naked ODNs, and uptake of the transfected antisense and random sequence probe was observed to be similar ([^{18}F]asODN: 1.7% vs. [^{18}F]rsODN: 2.0%). Uptake increased with longer incubation times: at 2.5 h, [^{18}F]rsODN exhibited a higher uptake of 4.8% as compared with [^{18}F]asODN (2.9%), although the difference was not statistically significant.

Subtle differences in the behaviour of the internalized ODNs, on the other hand, were observed, as shown in Table 4-3. Transfected [^{18}F]asODN demonstrated variable uptake; however, increased radioactivity was observed over time in both the cytoplasm and endosomes. Activity in the cytoplasm increased from 8.6% at 30 minutes to 23% at 2.5 h (P <0.05). Endosomal activity was also observed to increase from 9.5% of the cell-associated activity at 1 h to 34.8% at 2.5 h. Radioactivity associated with the nuclear pellet remained constant with 20% of the cell associated activity observed in the nucleus at all time periods tested. Transfected [^{18}F]rsODN also demonstrated wide variability of uptake in the cell

fractions, however no significant difference in [^{18}F]rsODN accumulation was observed over time in the cytoplasm, endosomes and nucleus with this probe. Thus, it appears that the processing of [^{18}F]asODN differs from that of [^{18}F]rsODN once the probes have been internalized.

4.3.6 *Confocal Microscopy*

Figures 4-6A to 6C show the location of fluorescently-labelled [F]asODNs, after a 2.5 h incubation with the probe, in live 5-Gy-irradiated HCT116 cells examined using confocal microscopy. Hoechst 33342 stain (blue) shows the intact nucleus, with uptake of [F]asODN-Q in red. 4-6A represents irradiated untreated cells (i.e., no [F]asODN-Q): a very faint red fluorescent signal at high laser intensity (acousto-optic tunable filter (AOTF): 48.5%) was observed uniformly distributed in the cytoplasm of the cell, and likely represents mitochondrial-associated autofluorescence. Distribution of naked [F]asODN-Q (Figure 4-6B) was observed in the cytoplasm as discrete dense foci of fluorescence located near the nucleus at the same AOTF setting. Figures 4-6C and 4-6D depict uptake of transfected [F]asODN-Q with and without morphology, respectively: at an AOTF setting of 0.9%, large distinct foci of fluorescence were observed in the cytoplasm. The probe was also observed in the nucleus: the distribution appeared uniform within the nucleus, with sporadic smaller fluorescent foci. However, the cell population showed heterogeneous accumulation of [F]asODN with some cells intensely fluorescent while others show minimal to no accumulation. Uniform distribution of the probe was also faintly detected in the cytoplasm. Neither the

autofluorescence in the control cells nor in the cells containing naked [F]asODN-Q were visible at the 0.9% AOTF setting (images not shown).

4.4 Discussion

While pharmacokinetic parameters of various [^{18}F]-labelled ODNs have been assessed (17-19), no literature describes the assessment of [^{18}F]-labelled asODNs directed to a specific mRNA target in cell culture or *in vivo*. Prior to *in vivo* imaging it is important to ascertain, in a suitable *in vitro* model, that the modified asODN is able to gain intracellular access, and discriminately bind to its mRNA transcript. A particularly relevant target transcript in this regard is *p21*, which is one of a large number of genes that are transcriptionally transactivated by p53 in response to DNA damage. It has been shown that p21 can be rapidly induced following γ-radiation in a number of cell lines, and sustained p21 expression was observed in HCT116 (colon carcinoma), A172 (malignant glioma), and SKNSH (neuroblastoma) for at least 6 days (7). We have confirmed the sustained induction of p21 in HCT116 with immunofluorescence and Western blot studies. We were also able to show that the induction of p21 expression following a 5-Gy γ-ray exposure could be effectively blocked with [F]asODN if a delivery vector was used, whereas no inhibition of expression was observed with the similarly transfected [F]rsODN. These observations are in agreement with those reported by Tian *et al* (12) who demonstrated inhibition of p21 expression in HCT116 cells previously irradiated with 10 Gy using the same asODN sequence, but unlabelled asODN. These observations confirm that asODNs modified with a fluorine-containing prosthetic group can target their mRNA transcript as effectively as the

unmodified ODN. This is an important result since the addition of the fluorine containing prosthetic group is a requirement for future PET imaging applications. The naked asODN was not able to block the induction of *p21* mRNA post-irradiation, at the concentrations studied, even with a long incubation time of 24 hours. Cell fractionation studies demonstrated limited uptake (<1%) of naked [^{18}F]asODN and [^{18}F]rsODN, and flow cytometry showed that cells transfected with naked fluorescently-labelled ODNs had a low MFI even though up to 96% of the cells were successfully transfected with the fluorescent probes within 2.5 hours of incubation. Antisense activity with naked probes has been reported, however these studies used saturation concentrations of asODN for prolonged periods of time: upon removal of the medium containing the asODN, the antisense activity was lost (20,21). Uptake of the asODN at saturation levels involves energy-dependent and independent mechanisms of uptake and must allow the probe to avoid entrapment and be available for targeting cytoplasmic mRNA (22). At the lower concentrations proposed for radionuclide imaging studies, energy dependent adsorptive pinocytosis is the most likely mechanism of uptake, resulting in entrapment of the probe within endosomal vesicles (see Chapter 1.6). Others have observed that antisense activity is lost once the oligonucleotides become sequestered in the vesicular compartment (22). The confocal microscopy images of irradiated HCT116 cells confirm that the probe localizes in discrete areas near the nucleus, possibly in vacuoles, granules, or perinuclear organelles. The low cellular uptake of the naked probes and the

consolidation of [F]asODN in cytoplasmic organelles explain the lack of antisense activity observed here with Western blotting.

Results obtained in this study confirm that, in order to enhance uptake and avoid vesicular sequestration, a transfection agent will be required. Lipofectin, the cationic liposome used in this study, increased uptake of the [^{18}F]ODN 3- to 5-fold in irradiated HCT116 cells by 2.5 h. As well, subtle differences in the distribution between [^{18}F]asODN and [^{18}F]rsODN were observed when the liposomal agent was used. Flow cytometry results also provide evidence of differences in the distribution between the two transfected fluorescent probes: both asODN-Q and rsODN-Q showed a higher fluorescence intensity than the naked ODNs. In addition, an approximately 2-fold increase in the MFI of transfected asODN-Q was observed over the similarly transfected rsODN-Q after 1 h of incubation with the cells. These results are in contrast to those observed with the naked probes, where both asODN-Q and rsODN-Q demonstrated equivalent intensity of fluorescence at the time periods tested. Thus, both the naked asODN and rsODN were internalized and processed similarly once inside the cell. The flow cytometry and cell fractionation studies provide a snapshot of the dynamic molecular processes within a population of cells, and reflect not only the uptake of the ODNs but also the efflux. These results suggest that the cell can discriminate between the two probes *if* the probes escape the endosomes and are released from their carrier.

Lipofectin is considered an efficient transfection agent for DNA-type probes and is commonly used in *in vitro* studies; however, cationic liposomes are generally

not considered appropriate vectors for *in vivo* use as they exhibit detergent-like properties as well as nonspecific interactions with serum, both of which can lead to cytotoxicity (23). In addition, the liposome vector enhanced nuclear localization of the probes. The role of the (radio)fluorescent probe in the nucleus is unclear at this time. It has been suggested that the nucleus may serve as a depot for excess ODNs with asODNs shuttling between the nucleus and cytoplasm, hybridizing with mRNA (24,25). Regardless, alternate biocompatible vectors will be required to guide [^{18}F]asODNs to cytoplasmic mRNA transcripts.

4.5   Conclusions

In order to determine whether [^{18}F]-labelled asODNs have the potential for use as imaging probes of gene expression *in vivo*, it is important to confirm that the modified, radiolabelled asODN retain its biological activity, and is able to reach its target *in vitro*. We have demonstrated that the conjugation of a radiofluorine-labelled prosthetic group to an asODN did not interfere with the ODNs ability to block the induction of p21 expression by γ-rays in HCT116 cells. As well, with the aid of a transfection agent, the cells were able to discriminate between [^{18}F]asODN and [^{18}F]rsODN implying recognition of its target mRNA transcript. These results have provided stimulus for further investigation into the cellular distribution and retention of [^{18}F]-labelled antisense oligonucleotides in p21-wild type versus p21-knockout HCT116 human colon carcinoma cell lines using a delivery vector compatible with *in vivo* animal models.

4.6 References

(1) Appella E, Anderson CW. Post-translational modifications and activation of p53 by genotoxic stresses. Eur.J.Biochem. 2001;268(10):2764-2772.

(2) El-Deiry WS, Harper JW, O'Connor PM, Velculescu VE, Canman CE, Jackman J, et al. *WAF1/CIP1* is induced in *p53*-mediated G_1 arrest and apoptosis. Cancer Res. 1994;54(5):1169-1174.

(3) Mazzatti DJ, Lee Y, Helt CE, O'Reilly MA, Keng PC. p53 modulates radiation sensitivity independent of p21 transcriptional activation. Am.J.Clin.Oncol.Cancer Clin.Trials 2005;28(1):43-50.

(4) Jänicke RU, Sohn D, Essmann F, Schulze-Osthoff K. The multiple battles fought by anti-apoptotic p21. Cell Cycle 2007;6(4):407-413.

(5) Belka C. The fate of irradiated tumor cells. Oncogene 2006;25(7):969-971.

(6) Wendt J, Radetzki S, Von Haefen C, Hemmati PG, Güner D, Schulze-Osthoff K, et al. Induction of p21[CIP/WAF-1] and G2 arrest by ionizing irradiation impedes caspase-3-mediated apoptosis in human carcinoma cells. Oncogene 2006;25(7):972-980.

(7) Mirzayans R, Scott A, Cameron M, Murray D. Induction of accelerated senescence by γ radiation in human solid tumor-derived cell lines expressing wild-type TP53. Radiat.Res. 2005;163(1):53-62.

(8) Sak A, Wurm R, Elo B, Grehl S, Pöttgen C, Stüben G, et al. Increased radiation-induced apoptosis and altered cell cycle progression of human lung cancer cell lines by antisense oligodeoxynucleotides targeting p53 and p21[WAF1/CIP1]. Cancer Gene Ther. 2003;10(12):926-934.

(9) Dupont J, Karas M, LeRoith D. The cyclin-dependent kinase inhibitor p21[CIP/WAF] is a positive regulator of insulin-like growth factor I-induced cell proliferation in MCF-7 human breast cancer cells. J.Biol.Chem. 2003;278(39):37256-37264.

(10) Ohtsubo M, Gamou S, Shimizu N. Antisense oligonucleotide of *WAF1* gene prevents EGF-induced cell-cycle arrest in A431 cells. Oncogene 1998;16(6):797-802.

(11) Poluha W, Poluha DK, Chang B, Crosbie NE, Schonhoff CM, Kilpatrick DL, et al. The cyclin-dependent kinase inhibitor p21*[WAF1]* is required for survival of differentiating neuroblastoma cells. Mol.Cell.Biol. 1996;16(4):1335-1341.

(12) Tian H, Wittmack EK, Jorgensen TJ. p21^WAF1/CIP1 antisense therapy radiosensitizes human colon cancer by converting growth arrest to apoptosis. Cancer Res. 2000;60(3):679-684.

(13) Wang J, Chen P, Mrkobrada M, Hu M, Vallis KA, Reilly RM. Antisense imaging of epidermal growth factor-induced p21^WAF-1/CIP-1 gene expression in MDA-MB-468 human breast cancer xenografts. Eur.J.Nucl.Med.Mol.Imaging 2003;30(9):1273-1280.

(14) Koslowsky I, Shahhosseini S, Wilson J, Mercer J. Automated radiosynthesis of *N*-(4-[^18F]fluorobenzyl)-2- bromoacetamide: An F-18-labeled reagent for the prosthetic radiolabeling of oligonucleotides. J.Label.Compd.Radiopharm. 2008;51(10):352-356.

(15) Felgner PL, Gadek TR, Holm M, Roman R, Chan HW, Wenz M, et al. Lipofection: a highly efficient, lipid-mediated DNA-transfection procedure. Proc.Natl.Acad.Sci.U.S.A. 1987;84(21):7413-7417.

(16) Eboue D, Auger R, Angiari C, Le Doan T, Tenu JP. Use of a simple fractionation method to evaluate binding, internalization and intracellular distribution of oligonucleotides in vascular smooth muscle cells. Arch. Physiol. Biochem. 2003;111(3):265-272.

(17) Boisgard R, Kuhnast B, Vonhoff S, Younes C, Hinnen F, Verbavatz J-, et al. In vivo biodistribution and pharmacokinetics of ^18F-labelled Spiegelmers: A new class of oligonucleotidic radiopharmaceuticals. Eur.J.Nucl.Med.Mol.Imaging 2005;32(4):470-477.

(18) Marzabal S, Terrazzino S, Kühnast B, Dollé F, Deverre JR, Jobert A, et al. In vivo imaging and pharmacokinetics of oligonucleotides. Nucleosides Nucleotides 1999;18(6-7):1731-1733.

(19) Tavitian B, Terrazzino S, Kühnast B, Marzabal S, Stettler O, Dollé F, et al. In vivo imaging of oligonucleotides with positron emission tomography. Nat.Med. 1998;4(4):467-470.

(20) Li B, Hughes JA, Phillips MI. Uptake and efflux of intact antisense phosphorothioate deoxyoligonucleotide directed against angiotensin receptors in bovine adrenal cells. Neurochem.Int. 1997;31(3):393-403.

(21) Galderisi U, Di Bernardo G, Melone MAB, Galano G, Cascino A, Giordano A, et al. Antisense inhibitory effect: A comparison between 3'-partial and full phosphorothioate antisense oligonucleotides. J.Cell.Biochem. 1999;74(1):31-37.

(22) Lebedeva I, Benimetskaya L, Stein CA, Vilenchik M. Cellular delivery of antisense oligonucleotides. Eur.J.Pharm.Biopharm. 2000;50(1):101-119.

(23) Zelphati O, Szoka Jr. FC. Liposomes as a carrier for intracellular delivery of antisense oligonucleotides: A real or magic bullet? J.Control.Release 1996;41(1-2):99-119.

(24) Lorenz P, Baker BF, Bennett CF, Spector DL. Phosphorothioate antisense oligonucleotides induce the formation of nuclear bodies. Mol.Biol.Cell 1998;9(5):1007-1023.

(25) Lorenz P, Misteli T, Baker BF, Bennett CF, Spector DL. Nucleocytoplasmic shuttling: A novel in vivo property of antisense phosphorothioate oligodeoxynucleotides. Nucleic Acids Res. 2000;28(2):582-592.

Table 4-1 Percent of HCT116 cells containing ODN labelled with Quasar-570*

Time (h)	% cells containing fluorescent probe		
	0.5	1	2.5
Naked asODN	42.4 (25.3 – 61.8)	54.2 (21.4 – 89.3)	81.4 (73.2 – 96.7)
Naked rsODN	40.0 (13.1 – 60.4)	55.0 (13.8 – 88.2)	52.5 (19.9 – 96.3)
Transfected asODN	31.0 (29.1 – 33.7)	50.8 (31.1 – 64.9)	72.9 (66.1 – 83.6)
Transfected rsODN	42.5 (35.3 – 50.4)	53.9 (36.0 – 65.0)	77.1 (60.2 – 85.6)

*emission: 566 nm
Results are given as mean of at least 3 replicates (plus range). A total of 10,000 cells were counted per sample

Table 4-2 Uptake of $[^{18}F]$ODNs expressed as percent of the total radioactivity added to the cells

Time (h)	% total radioactivity			
	0.5	1	2	2.5
Naked asODN	0.8 (0.2 – 2.0)	0.4 (0.3 – 0.7)	0.5 (0.3 – 0.8)	0.5 (0.3 – 0.7)
Naked rsODN	0.8 (0.3 – 1.7)	0.5 (0.5 – 0.6)	0.5 (0.4 – 0.6)	0.6 (0.3 – 1.0)
Transfected asODN	1.7 (0.5 – 3.2)	2.0 (1.6 – 2.4)	2.8 (2.0 – 3.9)	2.9 (2.0 – 4.0)
Transfected rsODN	2.0 (1.6 – 2.6)	3.0 (2.4 – 3.3)	4.1 (2.8 – 5.4)	4.8 (3.1 – 5.7)

Results are given as the mean of at least 3 replicates (plus range)

Table 4-3 Uptake of transfected [^{18}F]ODN in HCT116 cells expressed as percent of cell-associated radioactivity

Time (h)	% cell-associated radioactivity			
	0.5	1	2	2.5
Cytoplasm				
asODN	8.6 (1.4)*	10.1 (2.0)	12.7 (6.8)	23.0 (8.6)*
rsODN	15.6 (4.6)	12.1 (1.2)	17.6 (4.4)	12.0 (3.8)
Endosomes				
asODN	20.0 (10.2)	9.5 (9.2)	29.4 (19.8)	34.8 (13.4)
rsODN	16.1 (4.2)	18.7 (8.6)	32.1 (20.6)	17.8 (3.8)
Nucleus				
asODN	21.8 (17.1)	25.1 (15.0)	23.1 (14.9)	19.8 (8.4)
rsODN	17.3 (6.6)	18.5 (8.8)	18.5 (10.7)	23.4 (8.5)

Results are given as the mean of at least 3 replicates ($\pm$ 1 standard deviation).
*p <0.05 for [^{18}F]asODN in cytoplasm at 0.5 h and 2.5 h
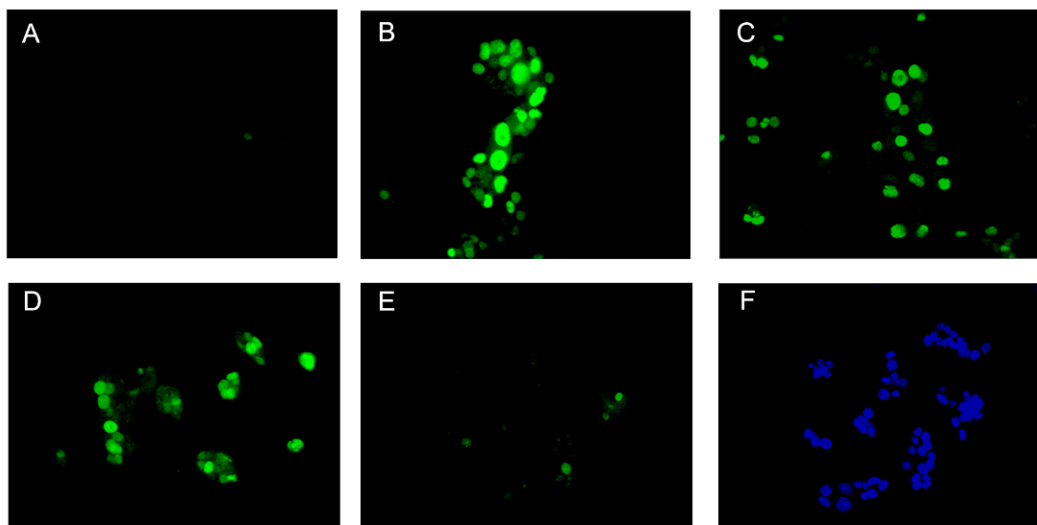
Figure 4-1 Immunofluorescence analysis of p21 protein expression in HCT116 cells. **A**: Before ionizing radiation exposure or ODN treatment. **B**: 24 h post-irradiation (5 Gy); no ODN treatment. **C**: 24 h post-irradiation and treatment with the liposome transfection agent; no ODN. **D**: 24 h after irradiation and incubation with transfected rsODN (400 nM). **E**: 24 h after irradiation and incubation with transfected asODN (400 nM). **F**. DAPI staining of nuclei of asODN-treated cells in panel E
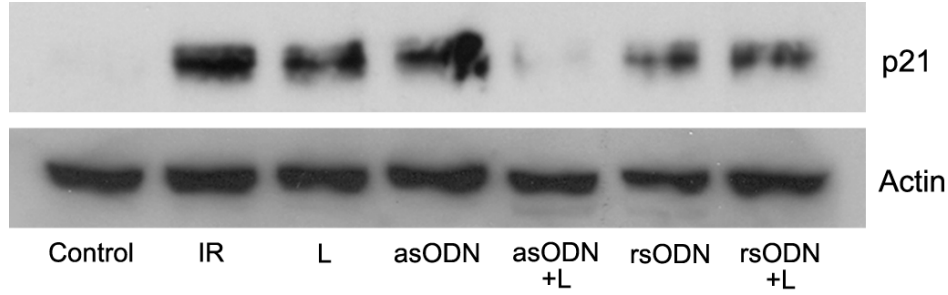
Figure 4-2 Western blot analysis of p21 protein expression in HCT116 cells after incubation for 24 h with asODN or rsODN (400 nM). Control: p21 expression in cells not exposed to ionizing radiation or treated with ODN. IR: p21 expression in cells 24 h after irradiation with 5 Gy. L: liposome treatment (no ODN) for 24 h after irradiation. asODN and rsODN: naked (no transfection agent); asODN + L and rsODN + L: liposome transfected ODNs
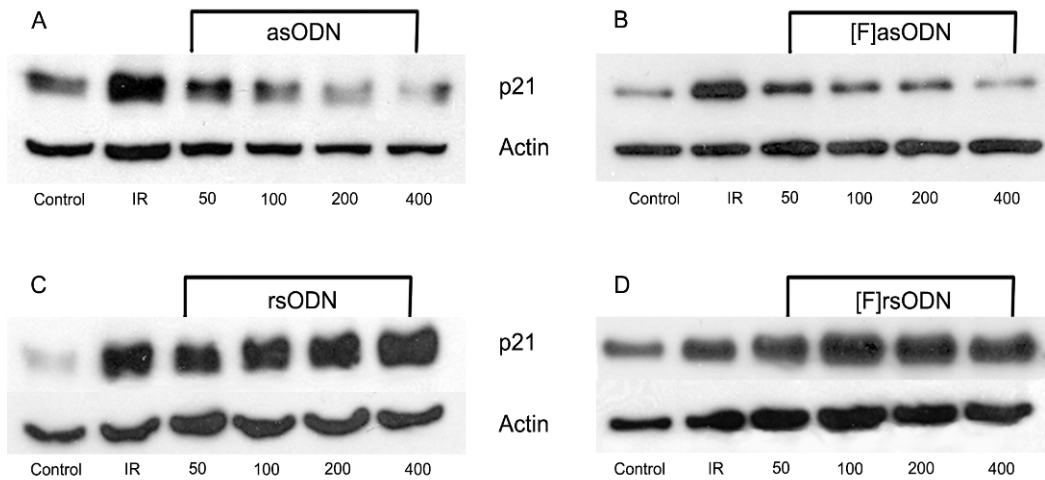
Figure 4-3 Western blot analysis of p21 protein expression in HCT116 cells after incubation for 24 h with 50 to 400 nM of transfected ODNs. **A**: asODN, **B**: nonradioactive [F]asODN, **C**: rsODN, and **D**: nonradioactive [F]rsODN. Control: p21 expression in cells not exposed to ionizing radiation or treated with ODN. IR: p21 expression in cells 24 h after irradiation with 5 Gy
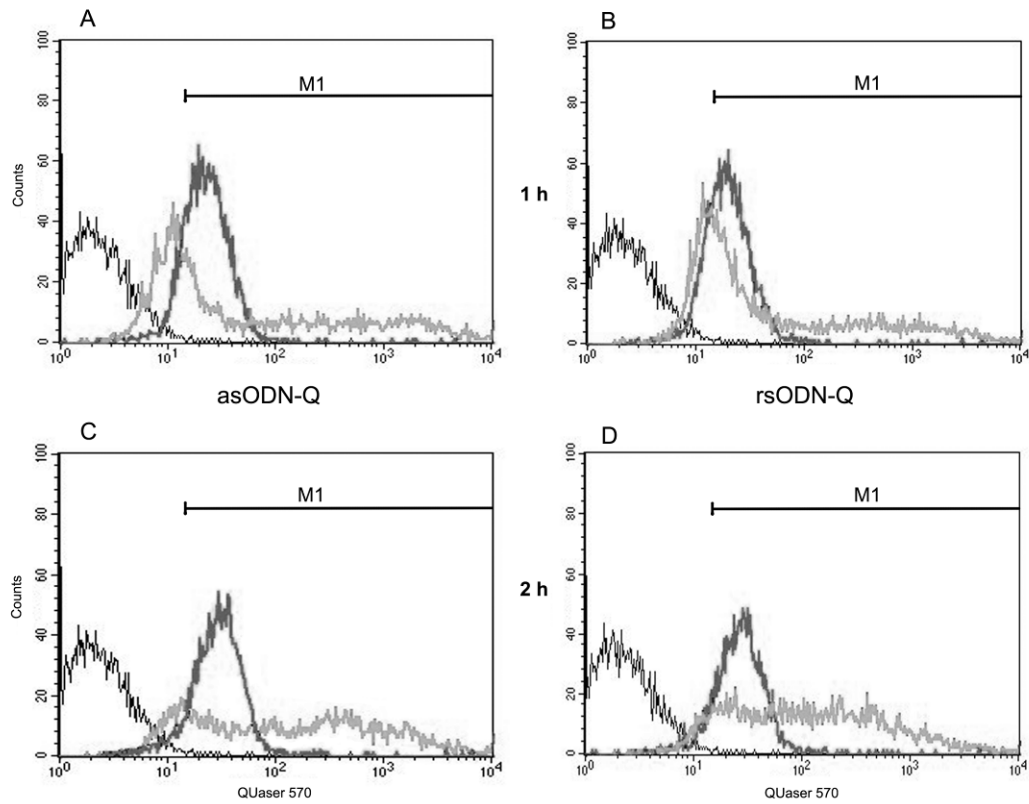
Figure 4-4 Flow cytometry histograms of cell counts vs. fluorescence intensity (Quasar 570) for 5-Gy-irradiated HCT116 cells treated with 280 nM asODN-Q (**A** and **C**) or rsODN-Q (**B** and **D**). Panels A and B represent uptake of ODNs at 1 h; panels C and D uptake at 2 h. The dark gray profile depicts naked ODN; the light gray curve shows uptake of transfected ODNs. The black profiles correspond to untreated, irradiated cells. M1 represents the region associated with cells that have internalized the ODN
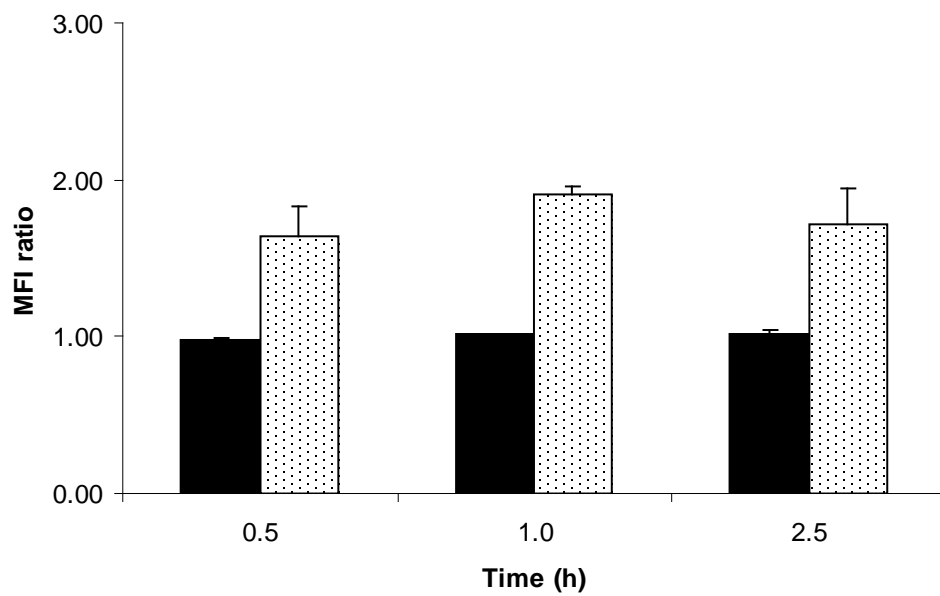
Figure 4-5 Ratio of the median fluorescence intensity (MFI) of ODNs in irradiated HCT116 cells over time. Naked asODN:rsODN ratios are shown as black bars; the transfected asODN:rsODN ratios are shown as speckled bars. Results are based on at least 3 replicates performed on different days. Error bars represent 1 standard deviation
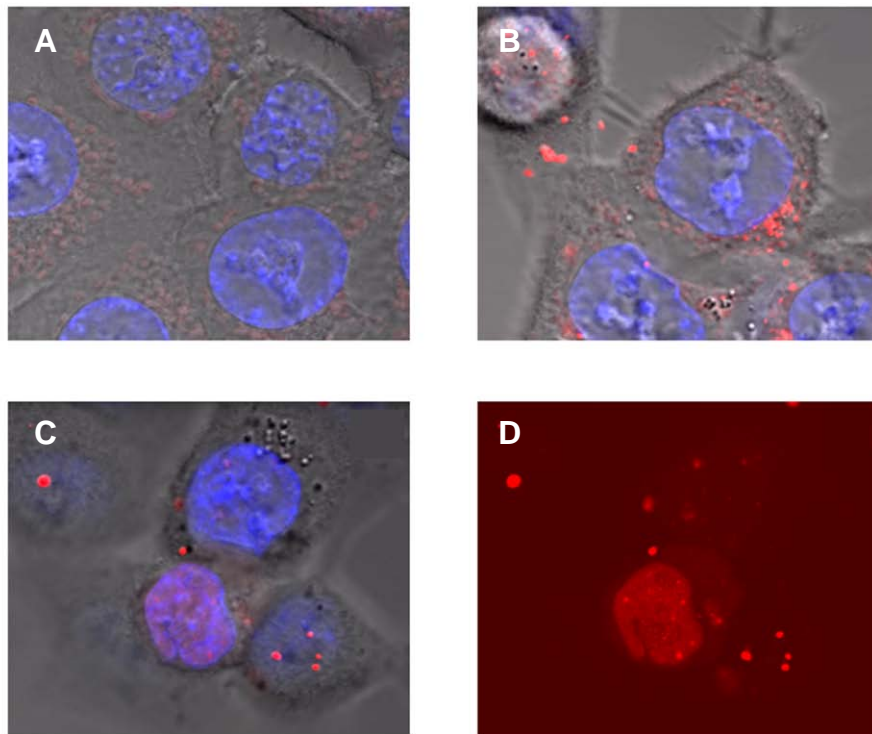
Figure 4-6 Confocal images of live, 5-Gy-irradiated HCT116 cells after 2.5 h incubation with Quasar-tagged [F]asODN.   Hoechst 33342 blue stain represents intact nuclei (364 nm).   Red signal represents [F]asODN-Q (543 nm). **A**: irradiated cells, no ODN treatment. **B**: naked [F]asODN-Q. **C**: liposome-transfected [F]asODN-Q. **D**: liposome-transfected [F]asODN-Q (red signal only)

CHAPTER 5

Evaluation of a block copolymer based nanocarrier for the delivery of [^{18}F]-labelled oligonucleotides

This chapter is based on a manuscript submitted for publication and authored by I. Koslowsky, S. Shahhosseini, E. von Guggenberg, X-B. Xiong, D. Murray, A. Lavasanifar, J. Mercer

The work presented in this chapter was carried out by I. Koslowsky with technical assistance from S. Shahhosseini. X-B. Xiong synthesized the spermine grafted polyamine block copolymer, SP. Cell cultures were prepared by Bonnie Andrais.

5.1 Introduction

Positron emission tomography (PET) is a non-invasive medical imaging technique using compounds labelled with short-lived positron emitting radionuclides for quantitative investigations of molecular and cellular structures and processes *in vivo* (1-4). In this context, the imaging of gene expression using biomarkers such as antisense oligodeoxynucleotides (asODNs) labelled with PET radionuclides can be an invaluable clinical tool for studying disease progression and early response to treatment with radio- or chemotherapy in animal models of cancer and in cancer patients. A number of PET radionuclides have been employed to radiolabel asODNs and their modified congeners for imaging gene expression. (5-9). ^{18}F is the most common positron emitter explored in this regard due to its relatively favourable physical characteristics (i.e. β^+ E_{max} of 0.633 MeV; half-life of 109.6 minutes).

The challenges associated with imaging gene expression *in vivo* overlap with those of asODN-based gene therapy and include the need to deliver the (radiolabelled) probe to the affected tissue, followed by cellular internalization and release of the probe into the cytoplasm and/or nucleus, depending on the target site. However, this is where the similarity ends. Whereas the goal of asODN-based gene therapy is to affect a therapeutic antisense response through the downregulation of the expressed gene, the goal of imaging is to visualize the current state of gene expression without perturbation of ongoing biochemical processes. The requirements for delivery of the probe to the target tissue also differ: gene therapy typically requires prolonged plasma clearance using

micromolar (µM) concentrations of probe to ensure the affected cells receive a therapeutic dose. Saturation of the target cells with µM concentrations of asODN promotes intracellular uptake using energy-dependant and independent mechanisms (10) with some of the probe escaping endosomal encapsulation and reaching its target mRNA. In contrast, PET imaging of gene expression uses submicromolar concentrations of [^{18}F]-labelled asODN which must be rapidly delivered to the target tissue before the isotope has decayed. Energy-dependent adsorptive pinocytosis prevails at low concentrations of radiolabelled asODN and therefore few molecules will elude encapsulation (10). Finally, the clearance of unbound or metabolized probe must be rapid to improve visualization of [^{18}F]-labelled asODN hybridization to its target.

In order to address these challenges, a large number of modified ODNs have been developed, many of which show promising improvement in probe stability and/or cellular accumulation (11,12). However, intracellular access to target mRNA remains a significant hurdle for gene expression imaging or gene therapy, and it is generally recognized that, in most cases, a delivery vector will be required to improve cellular accumulation of the asODN (13). While transfection agents have been well studied for *in vitro* use, these agents are generally not considered safe for use *in vivo*. There have been a few reports of *in vivo* imaging in animal tumour models with vector-assisted radiolabelled asODNs: some reports are promising (14); however, in general, results generally describe low accumulation of the radiolabelled probe in the tumour (15-17). A biocompatible delivery vector which can improve cellular uptake and release of [^{18}F]-labelled asODNs into the

target cell/tissue would clearly be advantageous for molecular imaging of gene expression.

Our interest in gene expression involves imaging changes in *p21* mRNA expression following radiation therapy. The gene encoding the cyclin dependent kinase inhibitor p21$^{WAF1/CIP1}$ (hereafter called p21) is regulated by p53, a multifunctional protein whose roles in the DNA damage-response pathway include activation of the p53-p21 axis (18). Activation of this axis soon after irradiation may promote cell survival by transiently activating cell-cycle checkpoints, allowing the cell to repair DNA damage; it can also promote the loss of clonogenic potential, e.g., by activating p53-directed apoptosis. Furthermore, in some genetic backgrounds exposure to ionizing radiation can cause prolonged p21 up-regulation and p21-directed "permanent" cell cycle arrest (i.e., premature or "accelerated" senescence) (19-23). Imaging changes in *p21* mRNA expression post-irradiation *in vivo* should thus provide important insight into these early tumour responses and their potential impact on the outcome of radio-/chemo-therapy. Based on this long term goal, we have radiolabelled an asODN, directed toward *p21* mRNA, with an [^{18}F]-labelled prosthetic group and have demonstrated that this modification does not interfere with its antisense ability in p21-expressing (p21$^{+/+}$) human colon carcinoma cells. We have also demonstrated that an antisense effect was only observed in cells transfected with asODN bound to a liposomal carrier as opposed to cells incubated with naked asODN for 24 h (see Chapter 4). However, the traditional cationic liposomal preparations used for *in vitro* transfection experiments, as was used in this work,

are not compatible with *in vivo* use due to cytotoxicity, inhibition of the delivery in the presence of serum and size limiting cellular membrane permeability (24).

We are currently investigating the use of block copolymers as delivery vectors for radiolabelled asODN. These agents act through the formation of polymeric micelles capable of encapsulating ODNs and this appears to be a promising approach for both gene therapy and imaging. Amphiphilic copolymers, consisting of blocks of polyethylene oxide (PEO) and polyamine-functionalized polycaprolactone (PCL), rapidly condense DNA via electrostatic forces to form self-assembling micelles (25,26). Inside the cell, release of the asODN from endosomes is proposed to occur via the 'proton sponge effect' whereby the acidic endosomal environment creates a charge gradient across the endosomal membrane due to the increased protonation of the polymer. This process provokes counterion and water influx and results in endosomal swelling and rupture (27,28). The effectiveness of polyamine polymeric micelles as delivery vectors was demonstrated by Xiong *et al* who were able to inhibit p-glycoprotein expression using a spermine (SP)- or tetraethylenepentamine (TP)-functionalized block copolymer carrying MDR-1 siRNA in MDR-1-transfected MDA435/LCC6 cells (29). With 1 h of incubation, confocal microscopy demonstrated accumulation of the fluorescently-tagged siRNA in the endosomal compartments; with 3 h of incubation, the probe was clearly visible in the cytoplasm, suggesting the successful release of the siRNA from the vesicles. Based on this evidence, we chose to evaluate this class of vector for the delivery of [^{18}F]-labelled asODNs. Our aim was to study the cellular accumulation and efflux/retention of

(radio)fluorinated asODN transfected with the spermine-functionalized polymer, SP, in p21$^{+/+}$ and p21$^{-/-}$ expressing human cancer cells.

5.2   Materials and Methods

5.2.1   Materials

Chemicals were purchased from Sigma-Aldrich (St. Louis, MO, USA) or Caledon Lab (Georgetown, ON, Canada) and were used without further purification. [^{18}F]fluoride was produced with a TR19/9 cyclotron (Advanced Cyclotron Systems, BC, Canada) via the ^{18}O(p,n)^{18}F nuclear reaction using enriched [^{18}O]water (Rotem Inc, Topsfield, MA, USA). The prosthetic group precursor, 4-cyano-*N,N,N*-trimethylanilinium trifluoromethanesulfonate, and the nonradioactive prosthetic group reference compound, *N*-(4-fluorobenzyl)-2-bromoacetamide, were synthesized as described by Dollé *et al* (30). The media used for cell culture and transfection studies were purchased from Invitrogen, Grand Island, NY, USA. The cellular markers used in confocal microscopy were purchased from Molecular Probes Inc, Eugene, OR, USA.

5.2.1.1   Oligonucleotides

A fully phosphorothioated 20-mer antisense oligodeoxynucleotide (asODN) targeting the 3′-untranslated region of human *p21* mRNA as described by Poluha *et al* (31) was synthesized and purified by University Core DNA Services, University of Calgary (Calgary, AB, Canada). A 20-mer random sequence oligodeoxynucleotide (rsODN) was used as a control. The sequence of the asODN was 5′-TGTCATGCTGGTCTGCCGCC-3′. The rsODN consisted of the sequence 5 -CCGGTGAACGAGCGAGCACA-3′.   For confocal microscopy

studies ODNs were synthesized with Quasar 570 CPG (Biosearch Technologies, Inc, Novato, CA, USA) on the 3′-end and the nonradioactive prosthetic group *N*-(4-fluorobenzyl)-2-bromoacetamide on the 5′-end ([F]asODN-Q or [F]rsODN-Q) (University Core DNA Services, Calgary, AB, Canada).

5.2.1.2   Transfection Agents

The block copolymer poly(ethylene oxide)-*block*-poly(ε-caprolactone) with a spermine-grafted side chain (SP) (Figure 5-1) was kindly provided by Dr. Afsaneh Lavasanifar (University of Alberta, Edmonton, Alberta).   SP was reconstituted in water at a concentration of 2 µg/mL. ODNs were reconstituted with serum followed by incubation with SP at a SP:ODN ratio of 16:1 (w/w) for 30 min at 37°C prior to addition to the cells. Lipofectin was employed as the liposomal transfection agent and was prepared as per the manufacturer's instructions (Invitrogen, Carlsbad, CA, USA). A 3 µg/mL concentration of Lipofectin was employed for *in vitro* studies.

5.2.1.3   Cells and Cell Culture

The human colon carcinoma cell lines HCT116($p21^{+/+}$), and its p21 knockout version, 80S4, were purchased from the American Type Culture Collection (Rockville, MD, USA). The cells were cultured as monolayers in Dulbecco's Modified Eagle Medium with nutrient mixture F-12 (Ham) (1/1) (DMEM/F12) supplemented with 10% (v/v) fetal bovine serum, 1 mM L-glutamine, 100 IU/mL penicillin G, and 100 µg/mL streptomycin sulphate. Opti-Mem I Reduced Serum media was used for all transfection studies. For studies utilizing the [^{18}F]-labelled probes, 5 x 10^5 cells per 4 mL were plated in 60 mm dishes. For confocal

microscopy studies with fluorescently-tagged probes, 10^5 cells per 2 mL of medium were plated in 35-mm culture dishes with 14-mm microwell (MatTek Corp, Ashland, MA, USA). All cultures were incubated at 37°C and 5% CO_2 in air.

5.2.2 Analytical methods

Analysis of the radiolabelled ODN was performed with reverse phase (RP)-HPLC using a Beckman Coulter Inc system consisting of a Model 168 Diode Array u.v. module, 260 nm; a Model 126 analytical dual pump; a radioactivity detector (Ortec, TN, USA): ACE *Mate*™ Single Channel Analyzer; and a Phenomenex Luna, 10 µm, 10 x 250 mm, C18 column (Torrance, CA, USA) with guard column. A gradient mobile phase was employed: triethylammonium acetate 100 mM, pH 7.0 (*aq*)/acetonitrile 90/10 to 60/40 over 30 minutes, followed by a washout phase of 30/70 for 5 minutes at a flow rate of 3 mL/min. The concentration of [^{18}F]-labelled ODNs was determined by u.v. spectroscopy at 260 nm using a Beckman DU 7400 spectrophotometer.

5.2.3 Irradiation

^{60}Co γ-ray exposures were performed in a Gammacell 220 Unit (Atomic Energy of Canada Limited, Ottawa, ON, Canada) at a dose rate of ~5 Gy/min (total dose of 5 Gy). Cells were irradiated 24 hours after seeding

5.2.4 Radiolabelling of ODNs

Synthesis of the prosthetic group, *N*-(4-[^{18}F]fluorobenzyl)-2-bromoacetamide ([^{18}F]FBBA, was performed in a GE TRACERlab FX$_{FDG}$ automated synthesis unit (GE Healthcare, WS, USA) as described in Chapter 2 (8). Typically, 150 to

460 MBq of purified [^{18}F]FBBA was collected for radiolabelling ODNs from starting [^{18}F]fluoride of 11 to 22 GBq.

Lyophilized ODN, 0.25 mg, was reconstituted with 0.5 mL of phosphate buffered saline (PBS) 0.1 M, pH 8, mixed with methanol, 1:1 (v/v), and added to [^{18}F]FBBA. The mixture was heated in a vented vial at 120°C for 30 minutes. Methanol 50%, 0.5 mL, was added midway through the reaction to maintain volume. Unreacted [^{18}F]FBBA was separated from the [^{18}F]-labelled ODN using a NAP™-10 column (GE Healthcare, Chalfont St Giles, UK) by eluting [^{18}F]ODN with 1.5 mL PBS 0.01 M, pH 7.2. No further purification was performed.

5.2.5   *In vitro cellular accumulation and retention studies*

Twenty-four hours after a 5 Gy exposure to radiation, the cells were transfected with (radio)fluorinated ODNs encapsulated in Lipofectin, SP, or with no transfection agent (naked). The cells were incubated with [^{18}F]asODN or [^{18}F]rsODN (collectively described as [^{18}F]ODN), or the corresponding nonradioactive fluorescent [F]ODN-Q, for 2.5 hours at a concentration of 50 nM (0.1 nmoles ODN per 1 million cells). The cellular uptake of the probes was subsequently assessed, or the medium was refreshed and the cells were incubated a further 6 hours at 37°C to evaluate cellular retention of the probes. Those cells which had been incubated with [^{18}F]-labelled ODNs were trypsinized, washed, and the cell pellet separated from the media. All media, cell washings and pellets were transferred to counting tubes and counted in a Wizard™ 3" 148 automatic gamma counter (PerkinElmer Life Sciences, Turku, Finland). The data were

background corrected and decay corrected to a standard. All accumulation and retention experiments were performed at least 3 times on different days. The Student T-test was employed for statistical analysis of the data.

Cells which had been incubated with the fluorescent probes [F]asODN-Q and [F]rsODN-Q, were prepared as follows for imaging with confocal microscopy. Thirty minutes prior to live imaging, Hoechst-33342 (1 µL, 1 µg/mL) and LysoTracker® Green DND-26 (50 nM) were added to the cells to stain cell nuclei and acidic organelles respectively. To stain the membrane, 10 µL (1 mg/mL) Alexa Fluor® 488 wheat germ agglutinin conjugate (WGA) was added 10 minutes prior to imaging. The intracellular distribution of the probes was visualized using a Zeiss 510 LSM fluorescence microscope (Carl Zeiss Microscope Systems, Jena, Germany) at an emission wavelength of 543 nm ([F]ODN-Q), 364 nm (nuclear stain), and 511 nm (endosomes) or 519 nm (membrane). The intensity of the excitation laser was optimized for each emission wavelength for each scan to visualize the location of the probe. Differential interference contrast was included in some images for morphological information.

5.3 Results and Discussion

The intent of this study was to evaluate the spermine-grafted PEO-*b*-PCL block copolymer as a potential delivery vector of [^{18}F]-labelled asODN for the purpose of imaging gene expression. SP rapidly forms micelles, when simply mixed with anionic biomolecules such as ODNs, through electrostatic interaction with the nitrogenous spermine functional group. von Guggenberg *et al* previously demonstrated that [^{18}F]-labelled ODNs were completely complexed with SP at a

SP:ODN ratio of 16:1 (w:w) (32). The complex was stable in serum and able to release its cargo when challenged with the competing polyanion, heparin. As well, cytotoxic effects were not observed at this SP:ODN ratio. Cellular accumulation and efflux of SP-transfected [F]ODNs were compared with Lipofectin, a liposomal transfection agent which has been previously used to successfully transfect asODNs directed to *p21* mRNA (33,34). Naked ODNs were also used to provide a baseline level of uptake and efflux in the absence of a carrier.

5.3.1 *Induction of p21 expression in human colon carcinoma cells*

Two human colon carcinoma cell lines were chosen for this study: the wild-type HCT116 containing intact $p21^{+/+}$ alleles, and its corresponding $p21^{-/-}$ knockout version, 80S4, which acted as a negative control for p21 expression. In HCT116 cells, *p21* mRNA has been shown to increase approximately 6-fold 4 hours after a radiation dose of 5 Gy (23). Upregulated p21 expression was still observed 24 hours after exposure, and accelerated senescence was observed 6 days after irradiation. Others have also demonstrated increased p21 expression in HCT116 cells after exposure to larger doses of radiation, with subsequent loss of clonogenic potential due to the induction of cellular senescence (34,35). As 5 Gy has been reported as the approximate apoptotic threshold for HCT116 cells (36) this dose was used for the induction of p21 expression.

5.3.2 *Radiolabelling of ODNs*

Conjugation of the [^{18}F]FBBA prosthetic group to the ODNs resulted in a mean radiochemical yield of 40% (as determined by the fraction of the reaction mixture

which eluted from the NAP™-10 column as [18F]-labelled ODN). Analysis by RP-HPLC demonstrated minimal degradation of the ODN after heating at 120°C in a vented vial. As well, similar HPLC retention times of unlabelled ODNs were observed before and after treatment at 120°C (t_R: 13.8 min). Attempts to use milder reaction temperatures resulted in lower yields. [18F]ODNs eluted as a single radioactive peak using RP-HPLC which corresponded to the retention time of the nonradioactive fluorinated ODNs (t_R: 14.9 min ([18F]rsODN; 15.4 min ([18F]asODN). A mean specific activity of 3.2 GBq/µmol (n=14) was achieved at the end of the reaction. Others have reported similar yields at 120°C but with a shorter reaction time (37,38). However we found that ODNs which were refluxed with [18F]FBBA at 120°C produced degradation products which could be avoided by venting the reaction vessel.

5.3.3 Cellular Accumulation and Retention of [18F]-labelled ODNs within cell lines

The uptake and retention of SP-transfected [18F]asODN and [18F]rsODN were evaluated against the cellular accumulation and retention of Lipofectin-transfected and naked ODNs in both cell lines. In HCT116 cells, the naked [18F]ODNs showed the lowest uptake of 1.5 to 1.6% at 2.5 h, with only 0.4 to 0.5% of the added radioactivity retained after 6 hours (Table 5-1). [18F]ODNs incubated with the liposomal vector showed a much higher uptake at 12 to 13% which was retained in the cells 6 h post wash i.e. radioactivity was not observed to elute from the cells. The SP-incubated [18F]ODNs exhibited an intermediate uptake of 5 to 7 % at 2.5 h, with 2% of the total activity retained 6 h later. Uptake of the probes was in agreement with preliminary work performed in our laboratory where 4 to

5% of the total SP-[^{18}F]asODN activity was associated with the cells in comparison to 15% for Lipofectin-transfected cells after 2 h of incubation (32). The characteristics of uptake and retention of [^{18}F]ODNs in 80S4 cells were similar to that observed in HCT116 cells except that values were lower than those observed in the p21$^{+/+}$ cells (Table 5-2).

No significant difference in uptake or retention was observed between [^{18}F]asODN and [^{18}F]rsODN within each cell line regardless of the delivery vector. Specificity of liposome-transfected [F]-labelled asODN to *p21* mRNA was previously demonstrated using western blot and protein immunofluorescence analyses by effectively inhibiting p21 protein expression in HCT116 cells exposed to radiation. [F]rsODN, on the other hand, did not influence p21 expression (see Chapter 4). Therefore, accumulation of [^{18}F]asODN may be due to specific targeting, as opposed to the accumulation of [^{18}F]rsODN which may be from non-specific targeting due to the capacity of nucleic acid polymers to display an aptameric effect (13). Another possibility for the lack of difference observed between the accumulation of [^{18}F]asODN and [^{18}F]rsODN is due to the short (2.5 h) incubation period of the probes with the cells. Hnatowich *et al* showed significantly higher accumulations of ^{35}S-labelled antisense ODNs directed against the RIα in ACHN cells as compared to control ODNs over time with twice the accumulation of the antisense ODN versus control ODN by 24 hours (13). However, no apparent statistical difference between the antisense ODN and its control ODN was observed with an incubation period of 5 h or less of incubation. Therefore, uptake studies appear to require longer incubation times, even when a

delivery vector is used, in order to visualize differences in uptake between antisense and control probes.

5.3.4 Cellular Uptake and Retention of [^{18}F]-labelled ODNs between cell lines

A difference in uptake of naked [^{18}F]asODN between the two cell lines was observed to approach significance (HCT116: 1.5%; 80S4: 0.9%, p=0.05). Although such a low level of accumulation of naked [^{18}F]asODN may be ineffective from an imaging perspective, the results imply that p21$^{+/+}$ expressing cells exhibit selectivity for the antisense probe.

[^{18}F]-labelled ODNs exhibited higher uptake and retention when transfected with Lipofectin, ([^{18}F]asODN uptake in HCT116: 13.4%; in 80S4: 6.8%; retention in HCT116: 12.2%; in 80S4: 5.7%), (Figure 5-2), however, no statistical difference was observed between the two cell lines. In contrast, SP-transfected [^{18}F]asODN demonstrated statistically higher uptake in the HCT116 cells versus 80S4 cells at both 2.5 h of incubation (4.7% vs. 1.4%, respectively; p< 0.05), and 6 h after a media change (1.8% vs. 0.3%, respectively; p<0.01). The higher cellular accumulation of both naked and SP-transfected [^{18}F]asODN in p21$^{+/+}$ cells versus p21$^{-/-}$ cells strongly suggests specificity of the antisense probes to its target. The higher variability in cellular uptake and retention of the [^{18}F]rsODN suggests that the random sequence probe has no specific target. Approximately 10% more SP-transfected [^{18}F]rsODN was observed to efflux from HCT116 cells over 6 h as opposed to the SP-transfected [^{18}F]asODN; whereas, similar efflux was observed with both probes in p21$^{-/-}$ cells. Although these observations are not statistically

significant, the results reinforce the suggestion of specificity of the antisense probe to *p21* mRNA.

5.3.5 *Confocal Microscopy*

Confocal microscopy was used to ascertain the intracellular location of fluorescently tagged [F]ODNs. Figure 5-3A illustrates uptake of the SP-transfected [F]asODN-Q 2.5 h after incubation with HCT116 cells. A uniform distribution of red probe is clearly evident in the cytoplasm with no evidence of binding to the cell membrane (green) or internalization into nucleus (blue). At 6 h post wash, 'free' red fluorescent probe was observed near acidic organelles (green), with some of the probe trapped within the vesicles (yellow) (Figures 5-3B and 3C). These results are in agreement with those observed by Xiong *et al* using siRNA transfected with SP/siRNA complexes (29) and demonstrate that the SP-transfected [F]asODN-Q continues to be released from these organelles into the cytoplasm.

[F]ODN-Q transfected with Lipofectin showed highly intense uptake in the nucleus and lower accumulation in the cytoplasm (Figure 5-4A). The nuclei remained intensely fluorescent 6 h after a media change, with faint evidence of fluorescent probe in the cytoplasm. Lipofectin-transfected [F]ODN-Q were observed to distribute in a heterogenous pattern in the cell population with highly intense fluorescence in the nuclei of a small number of cells. In comparison, SP-transfected [F]ODN-Q appeared homogeneously distributed throughout the cell population.

The naked and SP-transfected probes were only dimly visible in 80S4 cells due to the very low fluorescence emitted. Figure 5-4B shows the localization of naked [F]asODN-Q in the endosomes of 80S4 (yellow), a pattern that was typically observed with naked [F]asODN-Q and [F]rsODN-Q in both cell lines. These images confirm the similar, low retention observed with the naked [^{18}F]-labelled asODN and rsODN probes 6 h after wash out, and demonstrate that the probes remain trapped within vesicles for prolonged periods.

From an imaging perspective, the rapid efflux of the excess/unbound probe is generally considered a desirable feature and should improve the target signal within the cells. However, the modest cellular accumulation and low retention of SP-transfected [^{18}F]asODNs are a concern as there may be insufficient signal to visually detect targeted mRNA with PET. Modification of the polymer through conjugation of functional groups targeting tumour-associated epitopes overexpressed on cancer cells could improve uptake, and ultimately, retention of the probe. For example, block copolymers can be modified with epidermal growth factor (EGF) for increased specificity to HCT116 cells, which are known to express the EGF receptor (39,40) Lee *et al* have reported on the effectiveness of using an EGF-conjugated PEO-*b*-PCL block copolymers for targeted therapy of EGF receptor positive tumours: EGF-conjugated micelles were more potent than free EGF in inhibiting EGFR expression in MDA-MB-468 breast cancer cells (41).

There are methods, apart from modifications to the transfection agent, which could improve the signal. For instance, high specific activity (i.e. the measure of

the radioactivity per unit mass of the labelled and unlabelled compound) is considered a prerequisite for successful *in vivo* imaging of gene expression (42). Methods to optimize the yield and specific activity of [^{18}F]-labelled ODNs include modification to the synthesis of [^{18}F]FBBA (Chapter 3) (43), reducing the ODN starting material, and further purification of the [^{18}F]-labelled probes by HPLC.

Another factor which may impact the uptake and retention of the [^{18}F]asODN is the turnover rate of the upregulated target mRNA. It is been suggested that for successful imaging of gene expression, a rapid turnover of the target mRNA is required thus providing 'fresh' target to which the incoming [^{18}F]asODN can bind (13). The *p21* mRNA used as the target in our study has previously been shown to become rapidly induced after exposure to radiation with peak production of mRNA at 4 h and 24 h (23). In our study, cells were transfected with the probes 20 to 24 h post cellular exposure to radiation, i.e. near the peak of *p21* mRNA transcription. It may be necessary to study cellular accumulation and retention of [^{18}F]-labelled probes at an alternate time point after radiation to benefit from rapid expression of *p21* mRNA.

5.4   Conclusion

Selective uptake and retention of SP-transfected [^{18}F]asODN was demonstrated in the p21$^{+/+}$-expressing HCT116 cells as opposed to the p21 knock-out cell line. Although cellular accumulation at 2.5 h remained lower than that observed with liposome-transfected [^{18}F]asODN, SP-transfected fluorinated probes were found uniformly distributed within the cytoplasm with evidence of unsequestered probe

in the cytoplasm 6 h later. In contrast, liposome-transfected [F]ODNs exhibited a heterogeneous pattern of distribution with predominant localization in the nuclei, and naked probes remained sequestered in acidic vesicles. Neither the liposome-transfected nor naked probes demonstrated selectivity between $p21^{+/+}$ and $p21^{-/-}$ cell lines.

Overall these results demonstrate the potential of polyamine PEO-*b*-PCL block copolymers as vehicles for the delivery of radiolabelled antisense ODNs for noninvasive antisense imaging, or for the delivery of radiotherapeutic ODNs.

5.5   References

(1) Antoni G, Langstrom B. Radiopharmaceuticals: molecular imaging using positron emission tomography. Handb.Exp.Pharmacol. 2008;(185 Pt 1)(185 Pt 1):177-201.

(2) Wester HJ. Nuclear imaging probes: from bench to bedside. Clin.Cancer Res. 2007 Jun 15;13(12):3470-3481.

(3) Mukherjee A, Wickstrom E, Thakur ML. Imaging oncogene expression. Eur.J.Radiol. 2009;70(2):265-273.

(4) Wiebe LI. Applications of nucleoside-based molecular probes for the in vivo assessment of tumour biochemistry using positron emission tomography (PET). Braz. Arch. Biol. Technol. 2007;50(3):445-459.

(5) Wu F, Lendvai G, Yngve U, Eriksson B, Långström B, Bergström M. Hybridisation of [^{76}Br]-labelled antisense oligonucleotides to Chromogranin A mRNA verified by RT-PCR. Nucl.Med.Biol. 2004;31(8):1073-1078.

(6) Roivainen A, Tolvanen T, Salomäki S, Lendvai G, Velikyan I, Numminen P, et al. ^{68}Ga-labeled oligonucleotides for in vivo imaging with PET. J.Nucl.Med. 2004;45(2):347-355.

(7) Lendvai G, Velikyan I, Estrada S, Eriksson B, Långström B, Bergström M. Biodistribution of ^{68}Ga-labeled LNA-DNA mixmer antisense oligonucleotides for rat chromogranin-A. Oligonucleotides 2008;18(1):33-49.

(8) Koslowsky I, Shahhosseini S, Wilson J, Mercer J. Automated radiosynthesis of N-(4-[^{18}F]fluorobenzyl)-2- bromoacetamide: An F-18-labeled reagent for the prosthetic radiolabeling of oligonucleotides. J.Label.Compd.Radiopharm. 2008;51(10):352-356.

(9) Kuhnast B, De Bruin B, Hinnen F, Tavitian B, Dollé F. Design and synthesis of a new [^{18}F]fluoropyridine-based haloacetamide reagent for the labeling of oligonucleotides: 2-bromo-N-[3-(2-[^{18}F]fluoropyridin-3-yloxy)propyl]acetamide. Bioconjugate Chem. 2004;15(3):617-627.

(10) Yakubov LA, Deeva EA, Zarytova VF, Ivanova EM, Ryte AS, Yurchenko LV, et al. Mechanism of oligonucleotide uptake by cells: involvement of specific receptors? Proc.Natl.Acad.Sci.U.S.A. 1989 Sep;86(17):6454-6458.

(11) Haberkorn U, Mier W, Eisenhut M. Scintigraphic imaging of gene expression and gene transfer. Curr.Med.Chem. 2005;12(7):779-794.

(12) Duatti A. In vivo imaging of oligonucleotides with nuclear tomography. Curr. Drug Targets 2004;5(8):753-760.

(13) Hnatowich DJ, Nakamura K. Antisense targeting in cell culture with radiolabeled DNAs - A brief review of recent progress. Ann.Nucl.Med. 2004;18(5):363-368.

(14) Nakamura K, Wang Y, Liu X, Kubo A, Hnatowich DJ. Cell culture and xenograft-bearing animal studies of radiolabeled antisense DNA-carrier nanoparticles with streptavidin as a linker. J.Nucl.Med. 2007;48(11):1845-1852.

(15) Zhang Y, He J, Liu G, Venderheyden J, Gupta S, Rusckowski M, et al. Initial observations of ^{99m}Tc labbelled locked nucleic acids for antisense targeting. Nucl.Med.Commun. 2004;25(11):1113-1118.

(16) Nakamura K, Wang Y, Liu X, Kubo A, Hnatowich DJ. Influence of two transfectors on delivery of ^{99m}Tc antisense DNA in tumor-bearing mice. Mol.Imaging Biol. 2006;8(3):188-192.

(17) Zheng J, Tan T. Antisense imaging of colon cancer-bearing nude mice with liposome-entrapped 99m-technetium-labeled antisense oligonucleotides of *c-myc* mRNA. World J.Gastroenterol. 2004;10(17):2563-2566.

(18) El-Deiry WS, Harper JW, O'Connor PM, Velculescu VE, Canman CE, Jackman J, et al. *WAF1/CIP1* is induced in *p53*-mediated G$_1$ arrest and apoptosis. Cancer Res. 1994;54(5):1169-1174.

(19) Mazzatti DJ, Lee Y, Helt CE, O'Reilly MA, Keng PC. p53 modulates radiation sensitivity independent of p21 transcriptional activation. Am.J.Clin.Oncol.Cancer Clin.Trials 2005;28(1):43-50.

(20) Jänicke RU, Sohn D, Essmann F, Schulze-Osthoff K. The multiple battles fought by anti-apoptotic p21. Cell Cycle 2007;6(4):407-413.

(21) Belka C. The fate of irradiated tumor cells. Oncogene 2006;25(7):969-971.

(22) Wendt J, Radetzki S, Von Haefen C, Hemmati PG, Güner D, Schulze-Osthoff K, et al. Induction of p21$^{CIP/WAF-1}$ and G2 arrest by ionizing irradiation impedes caspase-3-mediated apoptosis in human carcinoma cells. Oncogene 2006;25(7):972-980.

(23) Mirzayans R, Scott A, Cameron M, Murray D. Induction of accelerated senescence by γ radiation in human solid tumor-derived cell lines expressing wild-type TP53. Radiat.Res. 2005;163(1):53-62.

(24) Zelphati O, Szoka Jr. FC. Liposomes as a carrier for intracellular delivery of antisense oligonucleotides: A real or magic bullet? J.Control.Release 1996;41(1-2):99-119.

(25) Gaucher G, Dufresne M, Sant VP, Kang N, Maysinger D, Leroux J. Block copolymer micelles: preparation, characterization and application in drug delivery. J.Control.Release 2005 12/5;109(1-3):169-188.

(26) Dufresne M, Elsabahy M, Leroux J. Characterization of polyion complex micelles designed to address the challenges of oligonucleotide delivery. Pharm.Res. 2008;25(9):2083-2093.

(27) Kakizawa Y, Kataoka K. Block copolymer micelles for delivery of gene and related compounds. Adv.Drug Deliv.Rev. 2002 2/21;54(2):203-222.

(28) Boussif O, Lezoualc'h F, Zanta MA, Mergny MD, Scherman D, Demeneix B, et al. A versatile vector for gene and oligonucleotide transfer into cells in culture and in vivo: polyethylenimine. Proc.Natl.Acad.Sci.U.S.A. 1995 08/01;92(16):7297-7301.

(29) Xiong X, Uludağ H, Lavasanifar A. Biodegradable amphiphilic poly(ethylene oxide)-block-polyesters with grafted polyamines as supramolecular nanocarriers for efficient siRNA delivery. Biomaterials 2009 1;30(2):242-253.

(30) Dolle F, Hinnen F, Vaufrey F, Tavitian B, Crouzel C. A general method for labeling oligodeoxynucleotides with ^{18}F for *in vivo* PET imaging. J.Label.Compd.Radiopharm. 1997;39(4):319-330.

(31) Poluha W, Poluha DK, Chang B, Crosbie NE, Schonhoff CM, Kilpatrick DL, et al. The cyclin-dependent kinase inhibitor p21^{WAF1} is required for survival of differentiating neuroblastoma cells. Mol.Cell.Biol. 1996;16(4):1335-1341.

(32) von Guggenberg E, Shahhosseini S, Koslowsky I, Lavasanifar A, Murray D, Mercer J. Evaluation of novel biodegradable vectors for improved cellular uptake of radiolabeled oligonucleotides. J.Label.Comp.Radiopharm. 2009;52:S324.

(33) Wang J, Chen P, Mrkobrada M, Hu M, Vallis KA, Reilly RM. Antisense imaging of epidermal growth factor-induced p21 WAF-1/CIP-1 gene expression in MDA-MB-468 human breast cancer xenografts. Eur.J.Nucl.Med.Mol.Imaging 2003;30(9):1273-1280.

(34) Tian H, Wittmack EK, Jorgensen TJ. p21$^{WAF1/CIP1}$ antisense therapy radiosensitizes human colon cancer by converting growth arrest to apoptosis. Cancer Res. 2000 Feb 1;60(3):679-684.

(35) Waldman T, Zhang Y, Dillehay L, Yu J, Kinzler K, Vogelstein B, et al. Cell-cycle arrest versus cell death in cancer therapy. Nat.Med. 1997;3(9):1034-1036.

(36) Mirzayans R, Murray D. Cellular senescence: implications for cancer therapy. In: Garvey RB, editor. New research on cell aging Hauppauge, NY: Nova Science Publishers, Inc; 2007. p. 1-64.

(37) Kuhnast B, Klussmann S, Hinnen F, Boisgard R, Rousseau B, Fürste JP, et al. Fluorine-18- and iodine-125-labelling of spiegelmers. J.Label.Compd.Radiopharm. 2003;46(13):1205-1219.

(38) Kuhnast B, Dolle F, Vaufrey F, Hinnen F, Crouzel C, Tavitian B. Fluorine-18 labeling of oligonucleotides bearing chemically-modified ribose-phosphate backbones. J.Label.Compd.Radiopharm. 2000;43(8):837-848.

(39) Rajagopal S, Huang S, Moskal TL, Lee B-, El-Naggar AK, Chakrabarty S. Epidermal growth factor expression in human colon and colon carcinomas: Anti-sense epidermal growth factor receptor RNA down-regulates the proliferation of human colon cancer cells. INT. J. CANCER 1995;62(6):661-667.

(40) Wang HM, Rajagopal S, Chakrabarty S. Inhibition of human colon cancer malignant cell behavior and growth by antisense epidermal growth factor receptor expression vector. Anticancer Res. 1998;18(4 A):2297-2300.

(41) Lee H, Hu M, Reilly RM, Allen C. Apoptotic epidermal growth factor (EGF)-conjugated block copolymer micelles as a nanotechnology platform for targeted combination therapy. Mol.Pharm. 2007;4(5):769-781.

(42) Lewis MR, Jia F. Antisense imaging: And miles to go before we sleep? J.Cell.Biochem. 2003;90(3):464-472.

(43) Koslowsky I, Mercer J, Wuest F. Improved synthesis of 4-[^{18}F]fluorobenzylamine: a useful building block in ^{18}F chemistry. J.Label.Comp.Radiopharm. 2009;52:S175.

Table 5-1 Cellular accumulation and retention of [^{18}F]ODNs in irradiated HCT116 cells

	% Uptake			% Retention		
	Naked	**Liposome**	**SP**	**Naked**	**Liposome**	**SP**
[^{18}F]asODN	1.5 (0.3)	13.4 (7.8)	4.7 (2.0)	0.5 (0.3)	12.2 (10.3)	1.8 (0.4)
[^{18}F]rsODN	1.6 (0.7)	12.2 (4.7)	7.1 (5.0)	0.4 (0.2)	12.4 (6.1)	2.0 (1.7)

Uptake of [^{18}F]-labeled ODN in previously irradiated HCT116 (p21$^{+/+}$) cells was determined after 2.5 h incubation of the probe with the cells. Retention was determine 6 h after a media change at 2.5 h. The data represent the mean ($\pm$ 1 standard deviation) of 3 experiments performed on different days.

Table 5-2 Cellular accumulation and retention of [^{18}F]ODNs in irradiated 80S4 cells

	% Uptake			% Retention		
	Naked	**Liposome**	**SP**	**Naked**	**Liposome**	**SP**
[^{18}F]asODN	0.9 (0.3)	6.8 (2.4)	1.4 (0.5)	0.4 (0.3)	5.7 (4.0)	0.3 (0.2)
[^{18}F]rsODN	0.9 (0.4)	10.9 (7.0)	2.1 (1.5)	0.3 (0.2)	10.7 (8.1)	0.4 (0.2)

Uptake of [^{18}F]-labeled ODN in previously irradiated 80S4 (p21$^{-/-}$) cells was determined after 2.5 h incubation of the probe with the cells. Retention was determine 6 h after a media change at 2.5 h. The data represent the mean ($\pm$ 1 standard deviation) of 3 experiments performed on different days.
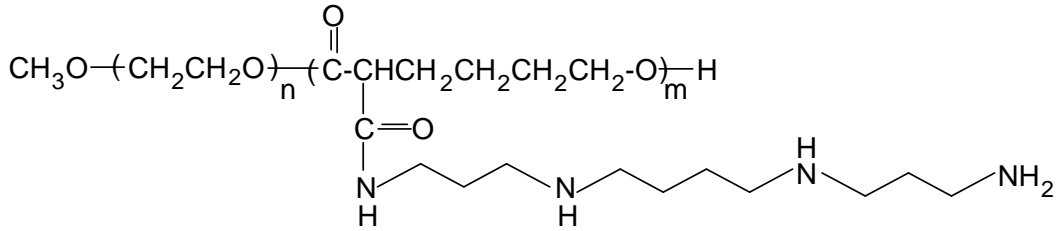
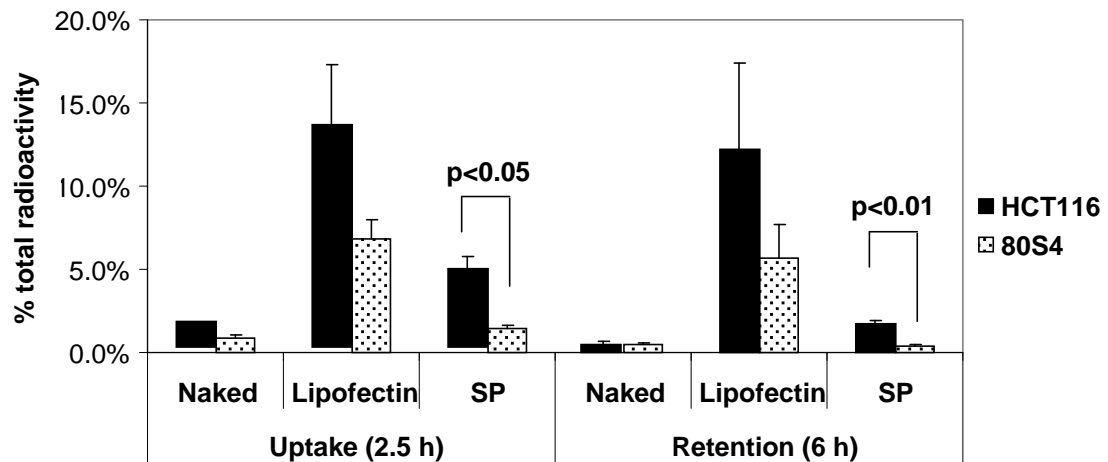Figure 5-1 Chemical structure of poly(ethylene oxide)-poly(ε-caprolactone) spermine (SP)

Figure 5-2 Cellular accumulation and retention of [^{18}F]asODN in irradiated HCT116 (p21$^{+/+}$) and 80S4 (p21$^{-/-}$) cells. The data represent the mean of 3 experiments performed on different days. Error bars represent 1 standard deviation.
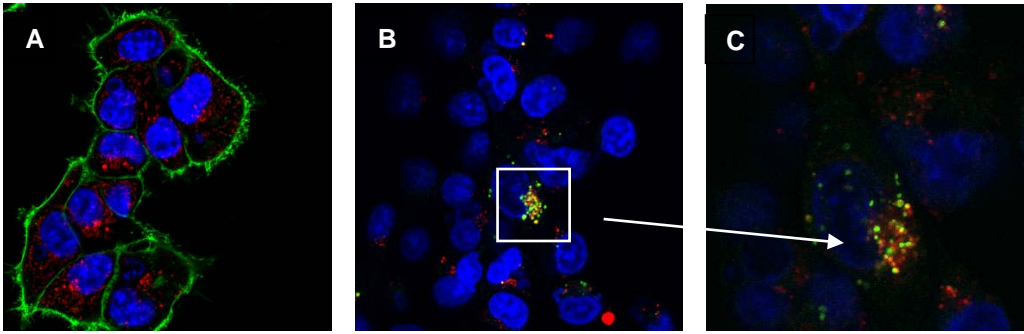
Figure 5-3 SP transfection of [F]asODN-Q in HCT116 cells. Uptake at 2.5 h is shown in A: [F]asODN-Q (red) in cytoplasm; nuclei (blue); cell membrane (green).   Panels B and C display retention of the probe at 6 h post wash. [F]asODN (red); acid organelles (green); [F]asODNin endosomes (yellow). Panel C is an enlargement of Panel B
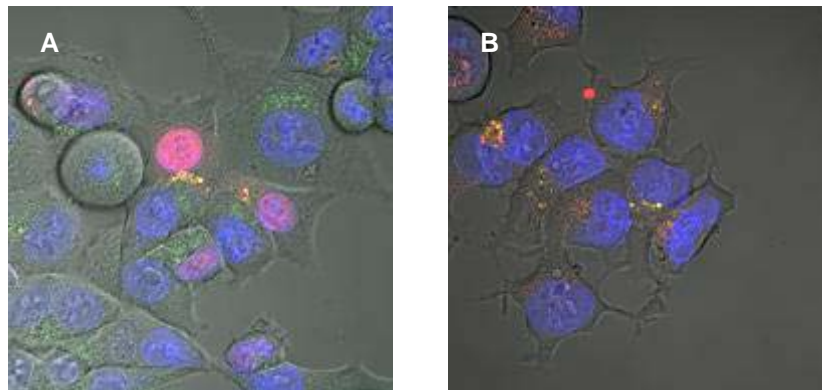

Figure 5-4 Retention of liposome-transfected and naked [F]asODN-Q in HCT116 and 80S4 cells, respectively. Panel A shows high uptake of [F]asODN-Q in nucleus (pink/purple) of HCT116 cells 6 hours post wash with some accumulation in endosomes (yellow); 'empty' endosomes are depicted in green.   Panel B depicts naked [F]asODN-Q in 80S4 cells 6 h post wash with evidence of probe accumulation in endosomes (yellow). Morphologic background is included to assist in determining the location of the probes within the cellular structure.

CHAPTER 6

To Summarize and Philosophize

In this research work oligonucleotides (ODNs), biologically stabilized by phosphorothioate linkages, were successfully radiolabelled with [^{18}F] by attachment of the prosthetic group, [^{18}F]FBBA. Using automated synthesis [^{18}F]FBBA could be synthesized in sufficient yield, and [^{18}F]-labelled ODNs could be produced with suitable specific activity to perform cell culture studies. Using techniques employed in molecular biology, such as Western blot, fluorinated antisense (as) ODN was shown to exhibit specificity toward complimentary *p21* mRNA in the cell population in comparison to random sequence ODN. Flow cytometry and confocal microscopy offered a visual perspective of the distribution of the fluorinated asODNs within individual cells. Together with results of *in vitro* cellular accumulation and retention studies with [^{18}F]-labelled ODN, it can be concluded that [^{18}F]-labelled asODNs do demonstrate selective uptake in p21$^{+/+}$ cells, and that the magnitude of the uptake and the specificity are dependent on the delivery vector used. Lipofectin, a liposome frequently employed to improve cellular transfection efficiency *in vitro*, allowed us to demonstrate that (radio)fluorinated asODN retained its antisense effect after labelling with FBBA. Because of its known biological incompatibility, Lipofectin was not evaluated *per se* as a potential vector for *in vivo* use; however, the heterogeneous intracellular distribution of the fluorescent probes, upon transfection with Lipofectin, and its predilection to indiscriminately concentrate ODNs in the nucleus, implies that this particular liposome would not

be considered an ideal delivery vector of [^{18}F]asODN for imaging. In contrast, the studies with polyamine-grafted block copolymer (SP-transfected) probes demonstrated intracellular distribution that is more likely to represent delivery of the [^{18}F]asODN to mRNA in the cytoplasm. Although uptake and retention of SP-transfected [^{18}F]asODN was lower than with Lipofectin, selective accumulation and retention of SP-transfected [^{18}F]asODN was observed in p21$^{+/+}$ expressing cells. Therefore, SP exhibits favourable cellular kinetics to be considered suitable as a delivery vector for radiolabelled probes. As well, SP can be modified to include receptor-targeting functional groups thus improving tumour cell targeting, and ultimately improving uptake and target specificity.

A limitation of this work is that *in vivo* imaging with [^{18}F]-labelled ODN was not performed. With the promising *in vitro* results observed using SP as a vector for [^{18}F]-labelled ODNs, a preliminary *in vivo* pharmacokinetic study in an appropriate animal model would have been a meaningful addition to this work. The availability of both the p21$^{+/+}$ human colon carcinoma cell line and a corresponding knock-out (p21$^{-/-}$) cell line offers a unique opportunity to, simultaneously, evaluate the specificity of [^{18}F]asODN in the corresponding solid tumours *in vivo*.

Further *in vitro* studies, using Western blot, would complement *in vivo* imaging. Validation that SP-transfected [F]asODN can inhibit p21 expression would confirm that the ODN is being released from SP and available to hybridize with its target mRNA. These studies would add credibility to tumour uptake observed in *in vivo* studies.

Further work is required to improve the uptake and selectivity of [^{18}F]asODNs in p21$^{+/+}$ cells. Specifically, improving the yield and specific activity of [^{18}F]FBBA and [^{18}F]ODNs, respectively, should increase the ability to discriminate between 'directed' and non-specific cellular uptake.

The reduction of [^{18}F]FBN to [^{18}F]FBA is a critical step in the synthesis of [^{18}F]FBBA. Incomplete reduction of [^{18}F]FBN to [^{18}F]FBA reduces the yield of [^{18}F]FBBA and thus, the specific activity of [^{18}F]ODNs. The presence of residual water in ASUs, in which common transfer lines are used, is the main cause for the incomplete conversion to the amine with LiAlH$_4$. Preliminary work, described in Chapter 3, demonstrates that quantitative reduction of [^{18}F]FBN can be achieved by utilizing a solid-phase, water-tolerant approach of nitrile conversion. Through activation of a borohydride exchange resin (BER) with transition-metal catalysts, [^{18}F]FBN was observed to be converted to [^{18}F]FBA within 1 min. As opposed to the necessity of an anhydrous environment with LiAlH$_4$, an aqueous environment is necessary for the BER for improved solubility of the metal catalysts, and improved wetting of the resin. A limitation of this work is that this method has not yet been tested in an ASU. However, the potential application of BER in radiochemistry justifies the need to investigate this method further, not only to improve the yield of [^{18}F]FBBA, a probe useful for labelling a variety of biomolecules, but also to improve the yield of other [^{18}F]FBA-derived prosthetic groups.

The hypothesis of this research work is that [^{18}F]-labelled asODNs (a) retain their specificity towards an mRNA target and (b) have the potential to visualize and

quantify upregulated p21 gene expression following radiation treatment. We have demonstrated that the first part of the hypothesis is true, based on the conclusions mentioned above. The ability of [^{18}F]-labelled asODNs to visualize and quantify upregulated p21 expression *in vivo* has yet to be determined, and there have been no reports in the literature demonstrating specific uptake *in vivo* of [^{18}F]-labelled ODNs in an animal tumour model. The cell culture studies, described in this work, demonstrate that [^{18}F]-labelled asODNs have the *potential* to image gene expression. However, perhaps the question should be: Is [^{18}F] the *most appropriate* radionuclide for imaging gene expression? The answer is dependent on the interplay between a number of factors. From a radiochemistry perspective, factors include the length and complexity of radiolabelling, and the specific activity of the radiolabelled ODN, and hinge on the physical half life of the radionuclide. From a biological perspective, a rapid plasma clearance rate and rapid transport into the cell are the key factors if [^{18}F] is to be considered as an appropriate radionuclide for radiolabelling ODNs.

The multi-step synthesis of [^{18}F]FBBA is challenging, however [^{18}F]FBBA can be produced in sufficient yields within 1 h. With appropriate improvements in synthesis, such as use of BER for nitrile reduction and automated transfer of the reaction mixture for purification by normal phase HPLC, losses of radioactivity can be controlled and [^{18}F]FBBA can be prepared in higher yields. Higher yields of [^{18}F]FBBA should translate to a higher yield of [^{18}F]-labelled ODN. Further purification of [^{18}F]ODN by RP-HPLC can also improve specific activity but adds additional time to the procedure and results in more losses due to decay.

Regardless, the synthesis of high-yielding [^{18}F]FBBA is achievable within a time frame suitable for using [^{18}F].

The general consensus in the molecular imaging community is that the most significant barrier to gene expression imaging is transport of the probe across the cell membrane, and that a delivery vector will be required for visualizing upregulated gene expression with radiolabelled antisense probes in diseased tissue, regardless of the type of modified ODN used (1-4). Thus it will be the pharmacokinetics of the delivery vector *in vivo* which determines effectiveness and efficiency of probe delivery. Several groups are diligently exploring methods to improve the delivery of radiolabelled antisense probes for imaging and for radiotherapeutic use. The more promising reports are those involving the Tat cell penetrating peptides, and the peptide nucleic acid (PNA) chimeras. The cell culture results reported by Zhang *et al* demonstrating rapid uptake of the Tat-directed PNAs are remarkable (5), and other Tat-peptide carrying antisense probes have demonstrated selective uptake in animal tumour models (6,7). The PNA chimeras labelled with ^{99m}Tc or ^{64}Cu show promising uptake *in vivo* in animal tumour models with tumour uptake observed 12 and 24 h after i.v. injection of ^{99m}Tc-labelled PNA probes (8). Higher uptake of ^{64}Cu-labelled PNA was observed at 4 h post injection with improved tumour-to-background ratio at 24 h post injection (9). Probes labelled with ^{99m}Tc, with a physical half-life of 6 h, or ^{64}Cu, with a 12.7 h half-life, can provide information of uptake and retention at later time periods than probes labelled with relatively short half-life

radionuclides. Based on these reports, employing a radionuclide with a longer physical half-life may be a 'better fit' for imaging gene expression.

The polymer based vectors have not been extensively evaluated for delivery of radiolabelled antisense probes. Generally, the uptake of the ODN-polymer complex was no better than that observed with the naked ODN (10). However, many advances have been made in polymer design, and block copolymers, specifically, continue to be investigated as potential drug delivery agents (11). Pharmacokinetic investigations of PEGylated copolymeric micelles have shown that drug-loaded micelles prolong circulation in the blood and reduce hepatic and kidney uptake (12). Another report of ^{111}In-labelled copolymeric micelles also showed prolonged circulation in the blood, but with higher hepatic and splenic retention between 8 and 24 h post injection (13). No specific functional groups were used to improve targeting to tumour tissue. However, it is realistic to believe that the 'fine-tuning' of polymeric design using a targeted approach would improve the rate of uptake into target tissue and, depending on clearance, offer imaging times the same day of injection. If this can be achieved, ODNs labelled with short-lived radionuclides, such as [^{18}F], may remain a viable option for imaging gene expression using PET.

References

(1) Hnatowich DJ, Nakamura K. Antisense targeting in cell culture with radiolabeled DNAs - A brief review of recent progress. Ann.Nucl.Med. 2004;18(5):363-368.

(2) Lendvai G, Estrada S, Bergström M. Radiolabelled oligonucleotides for imaging of gene expression with PET. Curr.Med.Chem. 2009;16(33):4445-4461.

(3) Lewis MR, Jia F. Antisense imaging: And miles to go before we sleep? J.Cell.Biochem. 2003;90(3):464-472.

(4) Hnatowich DJ, Nakamura K. The influence of chemical structure of DNA and other oligomer radiopharmaceuticals on tumor delivery. Curr.Opin.Mol.Ther. 2006 Apr;8(2):136-143.

(5) Zhang YM, Tung CH, He J, Liu N, Yanachkov I, Liu G, et al. Construction of a novel chimera consisting of a chelator-containing Tat peptide conjugated to a morpholino antisense oligomer for technetium-99m labeling and accelerating cellular kinetics. Nucl.Med.Biol. 2006 Feb;33(2):263-269.

(6) Nakamura K, Wang Y, Liu X, Kubo A, Hnatowich DJ. Cell culture and xenograft-bearing animal studies of radiolabeled antisense DNA-carrier nanoparticles with streptavidin as a linker. J.Nucl.Med. 2007;48(11):1845-1852.

(7) Wang Y, Liu X, Nakamura K, Chen L, Rusckowski M, Hnatowich DJ. In vivo delivery of antisense MORF oligomer by MORF/carrier streptavidin nanoparticles. Cancer Biother.Radiopharm. 2009 Oct;24(5):573-578.

(8) Tian X, Aruva MR, Qin W, Zhu W, Sauter ER, Thakur ML, et al. Noninvasive molecular imaging of MYC mRNA expression in human breast cancer xenografts with a [^{99m}Tc]peptide-peptide nucleic acid-peptide chimera. Bioconjug.Chem. 2005 Jan-Feb;16(1):70-79.

(9) Tian X, Aruva MR, Zhang K, Shanthly N, Cardi CA, Thakur ML, et al. PET imaging of *CCND1* mRNA in human MCF7 estrogen receptor positive breast cancer xenografts with oncogene-specific [^{64}Cu]chelator-peptide nucleic acid-IGF1 analog radiohybridization probes. J.Nucl.Med. 2007;48(10):1699-1707.

(10) Nakamura K, Wang Y, Liu X, Kubo A, Hnatowich DJ. Influence of two transfectors on delivery of ^{99m}Tc antisense DNA in tumor-bearing mice. Mol.Imaging Biol. 2006;8(3):188-192.

(11) Wei X, Gong C, Gou M, Fu S, Guo Q, Shi S, et al. Biodegradable poly(ε-caprolactone)–poly(ethylene glycol) copolymers as drug delivery system. Int.J.Pharm. 2009 10/20;381(1):1-18.

(12) Lin WJ, Chen YC, Lin CC, Chen CF, Chen JW. Characterization of pegylated copolymeric micelles and in vivo pharmacokinetics and biodistribution studies. J.Biomed.Mater.Res.B.Appl.Biomater. 2006 Apr;77(1):188-194.

(13) Hoang B, Lee H, Reilly RM, Allen C. Noninvasive monitoring of the fate of ^{111}In-labeled block copolymer micelles by high resolution and high sensitivity microSPECT/CT imaging. Mol.Pharm. 2009;6(2):581-592.